Investigation of the Mechanical Response of Monolithic Shearwalls with Openings

by

Mohammadreza Khajehpour

Thesis submitted to the University of Ottawa

in partial fulfillment of the requirements for the degree of

Doctor of Philosophy

in Civil Engineering

Under the auspices of the Ottawa-Carleton Institute for Civil Engineering

Department of Civil Engineering

Faculty of Engineering

University of Ottawa

Abstract

The current research project presents a study combining numerical analyses and experimental campaigns to evaluate the structural performance of cross-laminated timber (CLT) shearwalls with openings.

The results of an extensive numerical analysis using a validated Finite Element model is presented with the aim to investigate the influence of the geometrical and mechanical properties of lintel beams and parapets on the stiffness and strength of multi-storey CLT shearwalls with symmetric door or window openings. The influence of construction techniques, where the opening is cut out of the panel or constructed using separate elements is investigated. The results of the analysis show that in general, monolithic models resulted in significantly higher strength and stiffness values compared to those obtained from models assuming segmented shearwalls. The study particularly highlights the importance of the parapet in the overall behaviour and failure mechanism, even though no structural function is typically associated with it.

A comprehensive experimental campaign involving 36 beams with vertical outer layers and two different lay-ups was conducted to evaluate the applicability of analytical models originally developed for beams with horizontal outer layers. The experimental results reveal significant differences between 3-ply and 5-ply specimens, indicating an inverse correlation between bending strength and lamination thickness, and successfully verifying the adapted analytical models against both newly obtained data and existing literature.

Furthermore, the study addresses an identified gap in the literature regarding panel failure modes in monolithic CLT shearwalls with cut-out openings. An experimental investigation on 12 full-scale shearwalls designed to reach failure within the CLT panel showed that all tested specimens initiated cracking in the lintel or parapet, with ultimate failure occurring at the hold-downs.

The numerical predictions corresponded well with the experimental load-displacement curves and the observed failure patterns, underscoring the models' capacity to capture the complex failure mechanisms of CLT shearwalls.

This study advances the understanding of how construction methodology interacts to influence the kinematic behaviour and failure modes in CLT shearwalls with openings, providing valuable insights for both the design and analysis of such structural elements.

Acknowledgements

This study would not have been possible without the support and contributions of many individuals who have remained encouraging and helpful throughout the course of my Ph.D. program.

First and foremost, I would like to express my deepest gratitude to my supervisor, Dr. Ghasan Doudak, for his unwavering guidance and support over the past several years. His encouragement, insightful ideas, and expert knowledge helped me navigate numerous challenges and taught me how to lead this research process with confidence and efficiency.

I would also like to extend my sincere thanks to my co-supervisor, Dr. Daniele Casagrande. His continuous supervision, thoughtful feedback, and steadfast support were instrumental to the successful completion of this study.

I am especially grateful to Dr. Muslim Majeed and Dr. Gamal Elnabelsya, technical officers in the structural laboratory at the University of Ottawa, for their invaluable assistance, constructive insights, and technical advice during the experimental phase of my research. I also wish to thank Mr. Luc Cloutier and his colleagues in the Department of Civil Engineering for their generous support and collaboration.

It has been a privilege to work with an outstanding research team in the field of timber engineering. I deeply appreciate the efforts of everyone who assisted me in achieving the highest standards of accuracy in the laboratory.

I gratefully acknowledge the support of Nordic Structures (Montreal, Canada) and Rothoblaas (Italy) for providing the CLT panels, steel connections, and fasteners used in the connection and shearwall-level experimental testing.

Finally, I extend my heartfelt thanks to my family for their unwavering support and encouragement. Most of all, I am profoundly grateful to my beloved mother and wife for their patience, love, and strength during the most challenging moments of this journey. Their support has been my greatest source of light and motivation, and this accomplishment would not have been possible without them.

Table of Contents

List of Tables

Table of Figures

List of symbols and abbreviations

AB	Angle Bracket
AB-S	Angle Bracket failure in net shear
AB-T	Angle Bracket failure in torsional shear
CLT	Cross Laminated Timber
FE	Finite Element
HD	Hold-Down
L-A	Lintel failure due to bending
MSW	Monolithic Shear-Wall
P-A	Parapet failure due to bending
P-S	Parapet failure due to shear
RVE	Representative Volume Element
RVSE	Representative Volume Sub Element
SSW	Segmented Shear-Wall
a	Distance between the loading point and the nearest support
H	Height of CLT panel
$E_{m,loc,eff}$	The effective local modulus of elasticity
f_m	bending strength
$f_{v,gross}$	gross shear strength
$f_{v,net}$	net shear strength
h	Depth of CLT beam
l_{led}	ledger of length
l_1	ledger length for the local deflection measuring
m	Number of horizontal laminations along the depth
M_R	bending moment resistance
n	*n.of layers*
$n_{CA,p}$	number of crossing areas
n_H	n. of horizontal layers
t_{net}	effective beam thickness

$t_{v,1}$ thickness of the first vertical layer

$t_{v,2}$ thickness of the second vertical layer

$t_{v,p}$ thickness of the *p-th* vertical layer

$\tau_{tor,i,k}$ Torsional shear stress components acting on the crossing areas between the *i-th* horizontal lamination of the *k-th* horizontal layer

V_R shear load resistance

$W_{L,10}$ *Local displacement at 10% F_{max}*

$W_{L,40}$ *Local displacement at 40% F_{max}*

ΔF increase in load and deflection in the linear elastic range between 10% and 40% of maximum load

Δw increase in deflection in the linear elastic range between 10% and 40% of maximum load

J_{eff} effective modulus of inertia

$f_{v,rol}$ rolling shear strengths

$f_{v,tor}$ torsional shear strengths

$E_{m,loc}$ elastic modulus

n Number of storeys

w_S length of the two wall segments

h_L Lintel’s height

w_L Lintel’s length

h_P Parapet’s height

q Vertical load

E_0 Modulus of Elasticity parallel to the grain

G_0 In-plane shear modulus

E_{90} Modulus of elasticity perpendicular to the grain

f_t Mean value of tensile strength

f_C Mean value of compressive strength

$f_{v,r}$ Mean value of in-plane net-shear strength

$\tau_{T,r}$ Mean value of torsional strength

$E_{eff,v}$ Effective values of the modulus of elasticity along vertical direction

$E_{eff,h}$ Effective values of the modulus of elasticity along horizontal direction

G_{eff}	Effective values of the in-plane shear modulus
t_{CLT}	Total thickness of the CLT panel
t_v	Total thickness of the vertical layers
t_h	Total thickness of the horizontal layers
w	Width of the laminations
t_{mean}	Mean value of the thickness of laminations
$\sigma_{h\ or\ x}$	Axial stress along horizontal-x direction
$\sigma_{v\ or\ z}$	Axial stress along vertical-z direction
T	Shear stress
$t_{RVSE,i}$	Ideal thickness for each RVSE layer
t_i	Thickness for the i-th layer in the panel
n_x	In-plane internal force per unit length along horizontal-x direction
n_z	In-plane internal force per unit length along vertical-z direction
F_{max}	Maximum strength of the shear-wall
K	Stiffness of the shear-wall
l_{wall}	Length of the shear-wall
R_K	Ratio of stiffness between the MSW and SSW cases
R_F	Ratio of peak load between the MSW and SSW cases
$F_{max,SSW}$	Value of peak load for the SSW models
K_{SSW}	Value of stiffness for the SSW models

CHAPTER 1- INTRODUCTION

1.1 Timber in Modern Construction

Mass timber, particularly Cross Laminated Timber (CLT), is at the forefront of a construction revolution, offering innovative solutions for lateral load resisting systems (LLRSs). CLT panels are manufactured off-site using advanced CNC technology, ensuring large, precise, and high-quality components that can be used to form shearwalls and diaphragms. These elements are crucial for transferring wind and seismic forces safely down to the foundation. Metal connectors such as hold-downs, angle brackets, and fasteners not only join the panels together but also play a significant role in the strength, stiffness and energy dissipation of the building.

In addition to its structural benefits, mass timber offers significant environmental and economic advantages. Timber naturally stores carbon, leading to a lower carbon footprint compared to materials like steel or concrete, and its renewable nature supports sustainable building practices. Moreover, the lightweight nature of CLT panels, combined with efficient off-site production, reduces construction costs, waste, and transportation challenges.

Ongoing advances in experimental testing and numerical modeling continue to refine understanding of how CLT systems perform under real-world conditions. These developments are critical for updating design guidelines and ensuring that mass timber structures can safely meet the demands of tall and complex buildings. Overall, mass timber is not only redefining modern construction with its strength and versatility but is also paving the way for a greener, more resilient built environment.

1.2 Emergence of Cross Laminated Timber

Cross Laminated Timber is a modern engineered wood product made by bonding several layers of lumber boards so that each layer is oriented at a right angle (orthogonal) to the one below it (Figure 1.1), using high-performance structural adhesives. This crosswise arrangement produces large, robust panels that offer enhanced stiffness, dimensional stability, and load distribution compared to conventional timber elements. By alternating the grain direction in each layer, CLT effectively minimizes the effects of natural expansion and contraction caused by moisture changes, which are common challenges in traditional wood construction. The result is a material that not only harnesses the aesthetic and environmental benefits of timber but also meets the rigorous demands of modern structural applications.

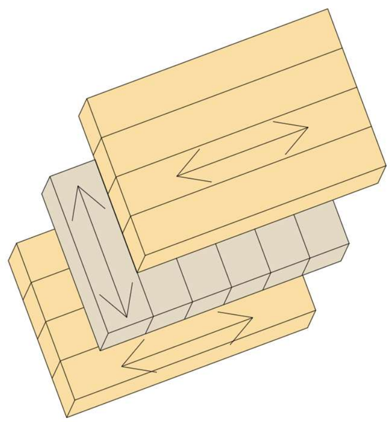

Figure 1.1*: CLT layout*

CLT panels are produced allowing for the creation of large-format elements that serve as effective structural components. Their high in-plane stiffness makes them ideal for use as shear walls, floor diaphragms, and roof systems, while their two-way load distribution stemming from the cross-laminated arrangement ensures that forces are evenly dispersed. This structural efficiency, coupled with the material's natural ability to sequester carbon and reduce greenhouse gas emissions, has driven the widespread adoption of CLT in multi-storey and tall timber buildings. Landmark projects, such as the 14-storey "Treet" in Norway and the 18-storey "Brock Commons" in Canada, underscore CLT's capacity to compete with traditional steel and concrete systems (Pei et al., 2016).

1.3 Lateral Load-Resisting Systems in CLT Constructions

The suitability of using cross-laminated timber shearwalls to resist lateral loading has been extensively investigated in recent years, mainly due to the high in-plane stiffness of the panels and the wall's capability to dissipate energy through controlled yielding mechanisms in the mechanical fasteners joining the CLT panels together and to their base (Pei et al., 2016; Izzi et al.,2018). Adequate behaviour and energy dissipative capabilities are generally achieved through over-designing the CLT panels, while controlling the behaviour and sequence of yielding of the connections by employing appropriate capacity-based design rules (Zarnani et al.,2015; Sharnewaz et al.,2017a; Tannert et al.,2018; Casagrande et al.,2019). For CLT shearwalls without openings, the dissipative connections generally comprise of mechanical anchors connecting the CLT panels to the foundation or floor below, when the CLT shearwall consists of a single panel (Figure 1.2a). Significantly higher level of energy-dissipation can be obtained in the case of multi-panel CLT shearwalls, when the panel-to-panel vertical joints are engaged (Figure 1.2b), due to the inherent ductility found in the connections (Gavric et al.,2013; Li et al.,2015; Nolet et al.,2019).

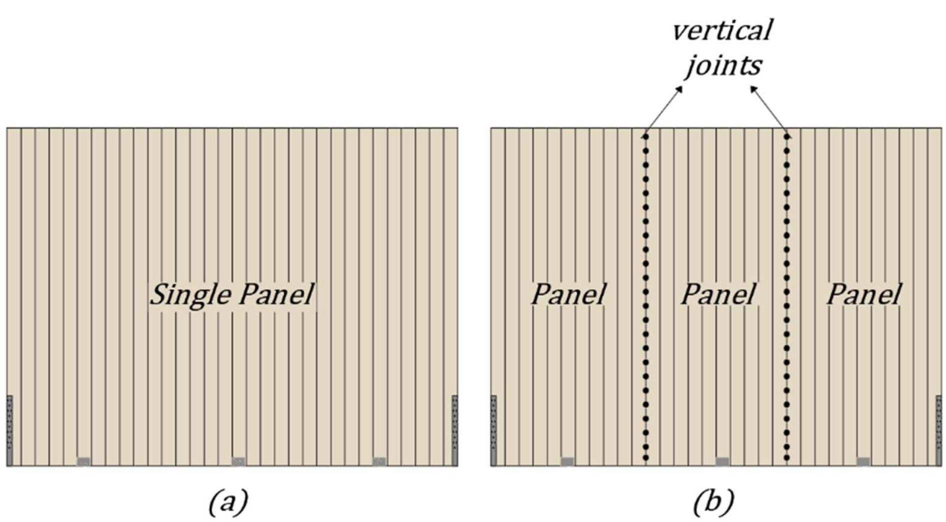

Figure 1.2: *Single- (a) and multi-panel (b) CLT shearwall*

A considerably different behaviour and failure mechanisms are expected when window and door openings are incorporated into the shearwall. The opening may result in the deformation contribution of the CLT panel being quite significant and possibly comparable to that obtained from the mechanical anchors. Also, high stress levels around the corners of the opening may develop and possibly lead to undesired and premature brittle failure mode in the CLT panel (Yasumura et al.,2015). This is particularly critical in the case where the opening is directly cut out of the wooden panel which called monolithic shearwall (MSW) as may be seen in Figure 1.3a, allowing for structural continuity between the wall segments and lintel beam element or parapet. In this construction technique, the geometrical dimensions of the lintel beam and parapet may strongly influence the kinematic behaviour and failure mode of the CLT shearwall and the interaction between the various shearwall components may be the governing factor in establishing the mechanical behaviour of the shearwall (Mestar et al.,2021). The overall behaviour of such system closely resembles that of a frame rather than a shearwall and the impact of this change in behaviour cannot be ignored during analysis and design. An alternative way to introduce openings in a CLT shearwall is by joining separate lintel and parapet elements to the wall segments using connections which called segmented shearwall (SSW) that usually do not allow for any moment continuity between those timber elements (Figure 1.3b). Using this construction method, the wall segments are usually considered as two separate cantilevers and the lintel beam is assumed to only support gravity loads, while the contribution of the parapet is assumed to be insignificant and limited to framing the opening.

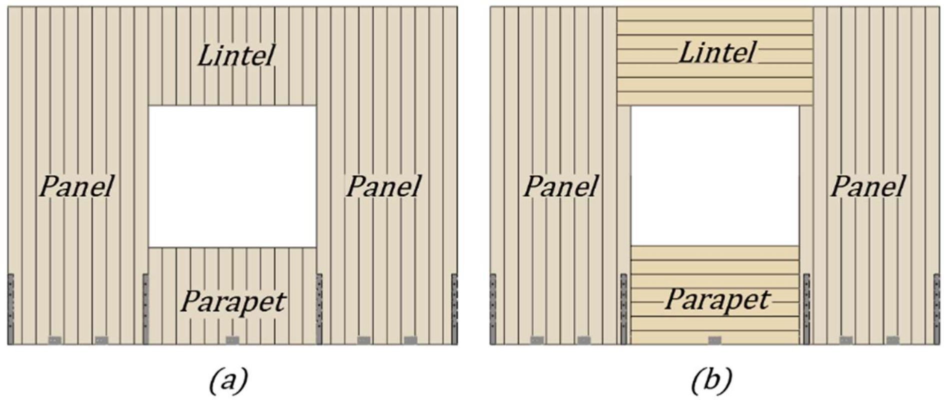

Figure 1.3: *CLT shearwall with opening cut out of the panel (a); CLT shearwall with assembled elements (b)*

1.4 Problem Statement

The majority of the research studies conducted on CLT shearwalls have been focused on the role of the mechanical anchors (Shen et al.,2013; Gavric et al.,2015a; Tomasi et al.,2015; Lium et al.,2018;Yinlan et al.,2019) and CLT shearwalls with no opening (Ceccoti et al.,2006; Popovski et al.,2010; Gavric et al.,2015b; Flatscheer et al.,2015; D'Arenzo et al.,2021). The outcomes from these studies have made it clear that the wooden panels behave mostly like rigid bodies, whereas the main deformation contributions and energy dissipation of the shearwall are chiefly related to the non-linear behaviour of mechanical anchors (i.e. hold-down and angle brackets).

Research on the behaviour of CLT shearwalls, where openings are cut out of the panel, has been quite limited, and mainly focused on determining reduction factors that take into account the effects of openings on the stiffness of the CLT panels.

Review of the available literature in chapter 2, especially that on CLT shearwalls with openings, highlights the potential for brittle failure modes in the CLT panels, particularly lintel beam and parapet sections. There is a need to establish better understanding of the conditions in which such failure mechanisms can occur and the contribution of lintels and parapets to the mechanical behaviour of the CLT shearwall assembly. Parametric studies and sensitivity analyses concerning the influence of the geometrical and mechanical properties of lintel beams and parapets as well as of the mechanical anchors on the overall behaviour of CLT shearwalls with openings have been scarce and limited to the elastic region and single-storey configurations. Moreover, an in-depth investigation of the construction process of the openings on the overall non-linear response of multi-storey CLT shearwalls in terms of lateral stiffness and strength has not yet been undertaken.

The current study presents the results of an extensive experimental study on single-storey platform-type CLT shearwall with opening and numerical analysis using a validated Finite Element (FE) model with the aim to investigate the influence of the geometrical and mechanical properties of lintel beams and parapets on the stiffness and strength of multi-storey symmetric platform-type CLT shearwalls with either door or window openings. It is noteworthy to mention that this investigation is strictly limited to platform-type construction systems and does not address balloon-type CLT shearwalls, is expected to be significantly different. The influence of construction techniques, where the opening is cut out of the panel or constructed using separate elements is also investigated. To the author's knowledge, no other studies have previously investigated the potential benefit that could be achieved in design by cutting the openings into the CLT panel during the manufacturing process rather than using separate elements. Providing structural continuity between wall segments and parapet or lintel beam, while carefully selecting a sequence of failure mechanisms, is expected to lead to a building performance that is dominated by ductile behaviour, with the additional benefit of loads on anchors being significantly reduced.

This approach is typically ignored by designers and replaced by analysis models that assume the CLT shearwall as cantilevered beams, ignoring the interaction between the wall segments and lintels beams even in cases where the panels are cut out of the wall panel.

1.5 Research Objectives

To address the research gaps and fulfill the aims of this work, the main objectives of the study are outlined below:

- To investigate the structural behaviour and failure mechanisms of cross-laminated timber shearwalls with door and window openings.
- To evaluate the influence of construction methods specifically, Monolithic Shearwalls versus Segmented Shearwalls on stiffness, strength, peak load, and failure modes.
- To assess the structural role of lintel beams and parapet sections, and how they affect overall wall behaviour in the shearwalls with opening.
- To conduct extensive parametric studies using the FE model to analyze the effects of varying storey numbers, opening sizes, wall segment widths, lintel and parapet dimensions, hold-down arrangements, and gravity loads on structural performance.
- To evaluate existing analytical models initially developed for beams with horizontal laminations for their applicability to vertical lay-up configurations.

1.6 Methodological Overview

This thesis combines complementary experimental campaigns and validated numerical modelling to investigate the influence of openings, lintel beams, and parapets on the performance of symmetric platform-type CLT shearwalls. The methodological framework follows a progressive sequence in which experimental results provide the foundation for model development, calibration, and validation.

The validated model is then used to conduct extensive sensitivity and parametric analyses. This structure ensures that the numerical outcomes are supported by physical evidence and that the conclusions of the study are both scientifically reliable and practically relevant.

The experimental programme was designed with two main objectives. The first was to provide benchmark data on the mechanical behaviour of CLT beams with vertically oriented laminations, representative of lintel regions in monolithic panels. The second was to generate full-scale evidence on the global behaviour of CLT shearwalls with openings and varied anchorage systems.

The first campaign consisted of four-point bending tests on 3-ply and 5-ply CLT beams with different depths, with the aim of quantifying bending strength, stiffness, and failure modes such as net shear, torsional shear, and flexural rupture. These results were used to calibrate the finite element model at the component level, particularly for lintel behaviour.

The second campaign involved full-scale monotonic shearwall tests under displacement-controlled loading protocols, where variables such as lintel depth, parapet height, wall segment width, and hold-down configuration were systematically studied.

These wall-level experiments captured system behaviours including rocking mechanisms, shifts in rotation centres, load redistribution, and anchorage force demands. Together, the two campaigns produced the experimental dataset required to validate the finite element model at both the component and the system scales.

Once validated against both beam-level and wall-level experimental results, the finite element model was used to perform a wide range of sensitivity and parametric studies. The variables investigated included the number of storeys, opening size and location, wall segment dimensions, lintel and parapet continuity, different hold-down arrangements including mid-panel placements, and the influence of gravity loading. By systematically altering these factors, the model made it possible to evaluate how design choices influence global performance metrics such as stiffness, ultimate strength, ductility, and anchorage demands. The numerical findings were interpreted in the context of the experimental results, which ensured consistency and reinforced confidence in the modelling approach.

In addition to the experimental and numerical work, the methodology incorporated an evaluation of existing analytical models that were originally developed for beams with horizontal laminations. These models were examined for their applicability to vertically laminated CLT elements, with emphasis on lintel behaviour and structural continuity at the wall level.

This step provided a link between simplified analytical formulations, detailed experimental evidence, and the advanced numerical simulations. The overall methodological sequence, beginning with experimental benchmarking, continuing through model validation, and concluding with parametric and analytical studies, provides a clear and coherent framework for addressing the research objectives and generating results that are relevant for both design practice and future code development.

1.7 Thesis Organization

The thesis is structured into six chapters, each progressing from context and background to experimental and numerical investigations, followed by synthesis and conclusions.

Chapter 1 introduces the motivation for the study, highlighting the increasing use of cross-laminated timber (CLT) in modern construction and the challenges associated with incorporating openings into shearwall systems. The problem statement is defined, the objectives are established, and the scope of the work is clarified as being restricted to platform-type CLT shearwalls with openings.

Chapter 2 provides a review of the literature, synthesising prior research on the mechanical behaviour of CLT components, the performance of connections, and the influence of openings on shearwall behaviour. Knowledge gaps are identified, particularly the limited research on platform-type shearwalls with cut-out openings and the lack of understanding regarding lintel and parapet contributions.

Chapter 3 describes the development of the finite element (FE) model used in this research. Details are given on the selection of material properties, mesh refinement, and connection modelling. The model is validated against experimental results, establishing its reliability for subsequent parametric studies.

Chapter 4 presents the first experimental campaign at the component scale. CLT beams with vertical outer laminations, representing lintels in monolithic wall panels, are tested under four-point bending. Their strength, stiffness, and failure modes are analysed and compared with analytical predictions for horizontally laminated beams, providing essential calibration data for later modelling.

Chapter 5 focuses on the second experimental campaign at the system scale. Full-scale shearwalls with cut-out openings are tested under monotonic lateral loading. Variations in lintel depth, parapet continuity, wall segment width, and anchorage configuration are examined. Results highlight how these parameters influence global stiffness, strength, rocking behaviour, and the sequence of failure mechanisms.

Chapter 6 synthesises the findings through an extended programme of parametric and analytical studies using the validated FE model. The influence of storey number, opening size and location, wall geometry, anchorage arrangements, and gravity loading are systematically evaluated.

Analytical models originally developed for horizontal laminations are also assessed for their applicability to vertical laminations and monolithic assemblies.

This chapter provides the most comprehensive understanding of parameter sensitivities and identifies areas where current design codes may overestimate or underestimate actual performance. The thesis concludes within this chapter by summarising the principal findings from both experimental and numerical investigations, acknowledging limitations, and outlining directions for future research. By retaining the conclusions within Chapter 6 rather than creating a separate chapter, the thesis maintains coherence while ensuring that synthesis and forward-looking recommendations are clearly outlined.

CHAPTER 2- LITERATURE REVIEW

2.1 Introduction and Background

This chapter explores the literature on the behaviour of Cross-Laminated Timber shearwalls subjected to lateral loading, with focus on how openings (i.e., doors and windows) affect structural performance. Emphasis is placed on the roles of mechanical connectors as well as on the effects of structural details like lintels, parapets, and the orientation of laminations.

The advent of engineered wood products such as CLT has enabled the creation of structural panels with excellent dimensional stability, enhanced stiffness, and superior in-plane strength. These characteristics have paved the way for CLT's use in walls, floors, and roofs. At the same time, environmental considerations and a drive toward carbon-neutral construction have accelerated interest in timber in general and CLT in particular as an alternative to more energy-intensive materials.

2.2 Background on CLT Shearwalls

Cross-laminated timber has rapidly gained popularity as a viable, sustainable material in mid-rise and tall building construction. The basic CLT panel comprises multiple layers of lumber boards, each oriented perpendicular to the one adjacent and bonded with structural adhesives, thus creating a product with enhanced dimensional and mechanical stability. This lay-up produces high in-plane stiffness and strength characteristics, enabling CLT to be used for walls, floors, roofs, and diaphragms. Researchers have established that CLT walls can dissipate energy through ductile yielding of panel-to-panel fasteners and, to a lesser degree, mechanical connections (i.e., hold-downs, angle brackets), provided that the timber panels are designed to remain elastic (Pei et al., 2016; Izzi M et al.,2018). Such connections allow localized yielding during seismic or wind events, permitting the structure to sustain large lateral deformations without significant reduction in the load-bearing capacity.

Over the past two decades, numerous experimental programs and analytical studies have demonstrated the ability of CLT elements to contribute significantly to building resiliency, particularly in seismic regions.

The underlying design philosophy for CLT shearwalls often follows capacity-based principles, where the connectors are deliberately weaker than the panel itself so that ductile metal yielding governs the global response (Zarrnani P et al.,2015; Shahnewaz Md et al.,2017a; Casagrande D et al.,2019). This ensures that any inelastic action localizes in steel components, which can exhibit relatively predictable hysteretic loops. Single-panel shear walls (Figure 2.1a) will exhibit rocking or sliding behaviour with limited possibility for energy dissipation. In multi-panel walls (Figure 2.1b), vertical panel-to-panel joints can also yield, further enhancing energy dissipation (Gavric I et al.,2013; Li M et al.,2015; Nolet V et al.,2019).

Experimental work has shown that, in the absence of openings, the wood panels typically behave as a rigid bodies while the connections provide most of the non-linear response (Shen Y et al.,2013., Gavrric I et al.,2015a; Tomasi R et al.,2015; Lium J et al.,2018).

2.3 Effects of Openings on the Structural Behaviour of CLT Shearwalls

Doors and windows are essential in buildings for functional and aesthetic reasons, but their presence in shearwalls can significantly alter how loads are transferred. When openings interrupt what would otherwise be continuous wall panels, they often introduce stress concentrations and reduce overall stiffness. To address these challenges, engineers typically add boundary elements like chord studs and hold-down anchors or segment the wall so that each portion between openings acts as a separate shear element. Numerous investigations have addressed how openings reduce the effective stiffness and influence local stress concentrations in CLT panels (Dujic B et al.,2015; Pai S et al.,2016; Shahneawz M et alk., 2017b). When an opening is cut into the panel, the deformation contribution of the wood may increase, especially if the anchors are strong enough to keep the base relatively rigid. In such cases, bending and shear deformations in the timber around the opening can dominate the lateral displacement profile (Yasumura M et al.,2015; Pai S et al.,2016; Shahnewaz M et al.,2017b).

The introduction of openings may follow one of two primary construction methods. In a monolithic shearwall, the opening is cut directly from a single CLT panel, preserving continuity between the lintel, parapet, and wall segments (Figure 1.3a). This continuity can lead to a frame-like behaviour, with significant bending or shear in the lintel beam and parapet (Awad V et al.,2017). If the connectors are designed with high strength, stresses may in the timber element may increase, potentially causing brittle failures around the opening corners (Yasumura M et al.,2015; Mestar M et al.,2021).

An alternative is the segmented shearwall, where separate lintel and parapet elements are attached to each vertical wall segment with minimal moment continuity (Figure 1.3b). Each vertical wall segment typically behaves as a cantilever, and the lintel provides mostly gravity load support. Segmented designs often simplify analysis by confining major inelastic actions to the hold-downs, although this can sacrifice any advantage that might be gained by a continuous lintel beam. Studies confirm that many segmented walls fail in the mechanical anchors, leaving the panels largely elastic (Ceccotti A et al.,2006; Flatscher G et al., 2015). However, engineers may choose segmentation for its simplicity, knowing that the risk of brittle panel failures at opening corners diminishes if the lintel does not carry significant in-plane moment (Mestarr M et al., 2020).

Monolithic and segmented approaches reflect different philosophies: one tries to exploit potential continuity in the timber to redistribute forces, while the other isolates wall segments to ensure that ductile anchors remain the only critical components in the in-plane load path.

Although several experimental studies have explored single-story configurations, real buildings can have multiple floors with aligned openings. In such multi-story scenarios, cumulative lateral forces can impose significant demands on the lintels or parapets at lower levels (Yasumura M et al.,2015; Izzi M et al.,2018). Even if small cracks in openings do not immediately reduce capacity, repeated cycles of loading in a major seismic event may propagate these cracks, eventually weakening the panel. Literature on multi-story CLT shearwalls with monolithic openings is relatively limited, and researchers note that more data from full-scale multi-story tests would be beneficial for clarifying how to design lintels and anchors for complex load-sharing behaviour (Yasumura M et al.,2015; Mestar M et al.,2021; Casagrande D et al., 2021a).

The established literature shows that panel failure modes have only been observed in a limited number of studies. At the building level, Yasumura et al. 2015 investigated the mechanical behaviour of a 2-storey CLT structure with monolithic panels including cut-out openings subjected to cyclic loads. Uplift of the U-shaped connectors, adopted to limit the rocking behaviour of the panels, was observed. Some cracks were detected around the openings, propagating either vertically along the direction of outer lamination or diagonally, but no global strength reduction of the tested structure was observed.

Similarly, local cracks around some door openings in the 2-storey CLT building tested by Popovoski M et al.,2010 and Gavric I et al.,2015b did not influence the global response of structure, since the ultimate failure was primarily related to the mechanical anchors.

Zhang et al. 2021 tested a 3-storey platform-type CLT shearwall comprised of a single panel and a large door opening. Tension cracks were reported at the corners of the CLT panel opening.

2.4 Influence of Lintels and Parapets

When openings are cut out of a single panel, the overall kinematics may resemble that of a frame (Mestar M et al.,2021; Awad V et al.,2017). The wall can exhibit either one or multiple centers of rotation, depending on anchor layout and stiffness. High bending moments can develop in the lintel, with the parapet also contributing to local stress distributions. Some experimental studies have shown that relatively large openings induce severe stress concentrations at lintel corners, occasionally causing panel failure (Yasumura M et al.,2015; Awad V et al.,2017; Casagrande D et al.,2021a). Parametric numerical studies, typically employing finite element models, further reveal that the geometry of the lintel (depth, thickness) and the stiffness of hold-down connections dictate whether the wall fails in a ductile or brittle manner (Mestar M et al.,2021; Dujic B et al.,2015; Pai S et al.,2016; Shahnewaz M et al.,2017b).

In contrast, segmented shearwalls treat the lintel and parapet as separate pieces connected to each vertical segment, limiting any flexural continuity. Several experimental studies have confirmed that in such cases, failure tends to occur in the mechanical anchors, and the panel itself rarely exhibits high bending demands (Ceccotti A et al.,2006; Popovski M et al.,2010; Flatscher G et al.,2015).

2.5 Timber Failure Modes Around Openings

Crack initiation and development often materializes at the corners of door or window openings (Yasumurra et al.,2015; Dujic B et al., 2015; Shahnewaz M et al.,2017b; Awad V et al.,2017). Depending on the global system stiffness, these cracks may not immediately reduce capacity, or they may propagate until they compromise the lintel or parapet entirely. A number of experiments, including full-scale tests, have documented brittle lintel failures in bending or net shear when large openings and strong anchors are combined (Mestar M et al.,2021; Casagrande D et al.,2021a).

Cyclic tests on four single-storey CLT shearwalls with either single or double openings were conducted by Awad et al. 2017. A brittle failure in the wooden panels, initiated by cracks around the opening corners, was observed for three specimens. Mestar et al. 2021 tested five shearwalls with openings under a monotonic load procedure to explore shearwall rocking kinematic behaviour. Cracks around the openings were observed only in one configuration with a door opening. Casagrande et al. 2021a performed monotonic tests on six CLT monolithic shearwalls with openings in order to study the geometrical and mechanical parameters influencing brittle failure in CLT panels. Two of the six specimens showed crack development around the corners of openings.

Crack propagation around the opening corners were also observed in three shearwall tests conducted by Zhang et al.2021. Aljuhmani et al.2022 conducted diagonal compression tests on 24 CLT panels with various sizes and orientations of openings to determine the panel in-plane shear strength and stiffness as well as to assess the reduction of stiffness in the panel due to the presence of openings. Isoda et al.2023 explored crack propagation on L- and T-shaped CLT specimens, observing bending and rolling shear failures in the lintel beam and highlighting the limitations of beam theory for analysing such elements

2.6 Experimental Investigations on CLT Components

Experimental research on CLT beams has primarily been focused on members with horizontal outer laminations (Jobstl et al., 2008; Andreolli et al., 2012; Flaig & Blaß.,2014. Different geometrical dimensions and lamination lay-ups have been investigated with the aim to study different failure modes and the influence of geometrical and mechanical parameters (e.g. thickness and orientation of layers, width of boards etc.) on the overall beam behaviour.

In general, four different failure modes can be identified, one of which involved bending and three were related to shear failures. The bending failure mode occurs when the axial longitudinal stress, σ_m, in the horizontal layers reaches the bending strength f_m. Crack development involves horizontal layers only and is typically initiated at the tensile edge of the beam, where the maximum bending moment occurs. Shear failure modes are distinguished as gross-section shear failure, cross-section net-shear failure and torsional shear failure within the crossing-areas between orthogonally glued laminations (Flaig & Blaß .,2013). Gross-section shear failure is characterised by longitudinal (i.e. parallel to the grain) shear stresses, $\tau_{v,gross}$, causing sliding of the wooden fibres. It is typically observed in beams with glued board edges. Net-shear failure is caused by shear stresses, $\tau_{v,net}$, acting perpendicular to the grain in the net cross section of the beam. Torsional failure is caused by torsional stresses, $\tau_{v,tor}$, and rolling shear stresses, $\tau_{v,rol}$, due to shear force transfer between the orthogonally glued adjacent laminations (Brandner R et al.,2017). The following present the experimental campaigns conducted on CLT beams with horizontal outer laminations.

Jöbstl et al.2008 investigated a total of 90 CLT beams, all of which were reported to fail in bending. Andreolli et al.2012 tested a total of 10 CLT beams, using elements with either edge-glued or non edge-glued laminations. In eight specimens a torsional shear failure mode was observed while two specimens failed in bending. Bending failure was also reached in 59 of the 60 beams tested by Flaig & Blaß.,2014 while only one beam failed under torsional shear.

Flaig and Blaß.,2013 conducted experimental tests on twelve 3-ply 80 mm thick specimens with two different lay-ups to induce torsional failure in CLT beams. A smaller lamination width (75 mm) than those used in their previous studies (Flaig & Blaß.,2014) (150 mm) was adopted for all specimens to promote torsional failure. Gagnon et al.2014 investigated 27 CLT beams, where span length was selected to promote shear rather than bending failure mode. Sikora et al.2016 presented the results obtained from experimental testing on six CLT beams, all of which were reported to fail in bending. Jaleč et al.2019 investigated the mechanical behaviour of 12 CLT beams with different widths of laminations. Four of the twelve specimens, consisting of 3-ply CLT elements, failed due to torsional shear, while eight specimens with 5-ply elements failed due to bending. Daneshvar et al.2021 tested two 7-ply deep CLT beams and reported that they failed due to bending in both tests. Li et al.2022 investigated six CLT beams with two different spans, where long span beams were dominated by bending failure while short span beams failed due to torsional shear.

While CLT beams with horizontal outer laminations are prevalent in research and are common in floor or roof applications (Jöbstl R et al.,2008; Amdreoli M et al.,2012; Flaig & Blaß.,2014; Gagnon S et al.,2014; Sikora K et al.,2016; Jelec M et al.,2019; Daneshvar H et al.,2021; Li Z et al.,2022), monolithic shearwalls contain a lintel beam with vertical outer laminations; an orientation typically unfavorable for bending about the horizontal axis.

When these vertically laminated lintels form part of a monolithic shearwall opening, boundary conditions become more complex. Rather than acting as a simple beam, the lintel undergoes partial fixity with the adjacent wall segments and parapet, intensifying local stresses around opening corners. If the lintel's design does not account for the vertical grain orientation as outer layers, brittle failures can arise at relatively low bending moments. Several authors emphasize that standard design procedures, often calibrated for horizontally oriented layers, might not fully apply to lintels with vertical outer laminations as part of monolithic shearwalls (Casagrande D et al.,2021; Yamagata K et al.,2023).

To the authors' knowledge, only two studies have been conducted on CLT beams with vertical outer laminations. Ten CLT beams were investigated by Casagrande et al.2021 to obtain the input parameters for the numerical models adopted for tested CLT shear walls with cut-out openings. The span length was changed while the beam depth was maintained to promote either bending or shear failure. Six specimens failed in bending, while four failed in shear. Yamagata et al.2023 conducted an experimental campaign on 72 CLT beams with both horizontal and vertical outer laminations. Bending, torsional shear and gross-section shear failure modes were observed.

A summary of the conducted tests available in the literature for CLT beams with horizontal and vertical outer lamination is provided in Tables 2.1 and 2.2, respectively. Indicated in the tables are the name of the test series provided in the original publication, number of tests, total thickness of the beam, t_{CLT}, ratio between the total thickness of the horizontal layers t_H to the beam thickness, lamination lay-up, width of laminations *b*, as well as the failure modes reported. As mentioned earlier and clearly demonstrated in the table 2.1, great efforts have been made to investigate the mechanical behaviour of CLT beams with horizontal outer lamination whereas the information on CLT beams with vertical outer layers is still scarce.

Table 2.1: *Tests available in literature for CLT beams with horizontal outer lamination*

Authors	Series	n. of tests	t_{CLT} [mm]	n. of layer	t_H/t_{CLT}	b [mm]	failure mode
Jöbstl et al. (2008)	1	16	125	5	0.60	130	bending
	2	14	125	3	0.80	150	
	3	10	134	5	0.71	146	
	4	10	158	5	0.76	146	
	5	10	99	3	0.81	146	
	6	15	114	3	0.65	200	
	7	15	98	3	0.66	200	
Andreolli et al. (2012)	A-3	4	90	3	0.67	100	torsional shear
	A-5	2	130	5	0.67	100	torsional shear
	B-5	2	135	5	0.60	80	torsional shear
	C-5	2	144	5	0.71	150	bending
Flaig & Blaß (2013)	27-27-27	6	84	3	0.67	75	torsional shear
	30-20-30	6	80	3	0,75	75	
Flaig & Blaß (2014)	2-1_1	6	100	3	0.80	150	bending
	3-1_1	6	160	5	0.75		

	4-1_1	5	200	6	0.80		
	6-1_1	5	300	9	0.80		
	2-2_1	5	100	3	0.80		
	3-2_1	5	160	5	0.75		
	2-1_2	4	100	3	0.80		
	3-1_2	4	160	5	0.75		
	4-1_1	5	200	6	0.80		
	6-1_1	5	300	9	0.80		
	2-2_2	5	100	3	0.80		
	3-2_2	5	160	5	0.75		
Gagnon et al. (2014)	A	12	105	3	0.67	89	torsional shear
	B	15					
Sikora et al. (2016)	I-3-40	3	120	3	0.67	146	bending
	I-5-20	3	100	5	0.60	96	
Jaleč et al. (2019)	1	4	160	5	0.75	172	bending
	2	4	160	5	0.75	172	bending
	3	4	100	3	0.80	198	torsional shear
Daneshvar et al. (2021)	CL-C	2	191	7	0.73	140	bending
Li et al. (2022)	CEB	3	105	3	0.67	140	bending
	CES	3		3			torsional shear
Yamagata et al. (2023)	3-90x240-Major	6	90	3	0.66	N.A.	gross shear
	5-150x120-Major	15	150	5	0.60		bending/shear
	5-150x360-Major	15	150	5	0.60		bending/shear

Table 2.2: Tests available in literature for CLT beams with vertical outer lamination

Authors	Series	n. of tests	t_{CLT} [mm]	n. of layer	t_H/t_{CLT}	b [mm]	failure mode
Casagrande et al. (2021)	B 01	3	100	5	0.40	170	bending
	B 02	3	90	3	0.33		bending
	B 03	2	100	5	0.40		net shear
	B 04	2	90	3	0.33		net shear
Yamagata et al. (2023)	3-90x240-Minor	6	90	3	0.33	N.A.	torsional shear
	5-150x120-Minor	15	150	5	0.40		bending/shear
	5-150x360-Minor	15	150	5	0.40		bending/shear

2.7 Numerical Modeling Efforts

A large body of research employs finite element analyses to investigate the behaviour of CLT shearwalls. In many studies, the CLT panel is modeled using two-dimensional shell or plate elements, while the mechanical connectors such as hold-downs, angle brackets, and panel-to-panel fasteners are represented by nonlinear springs or links (Dujic B et al.,2015; Pai S et al.,2016; Shahnewaz M et al.,2017b; Mestar M et al.,2020). These FE models capture global load-displacement trends effectively and can pinpoint regions of high stress, particularly near the corners of openings. Researchers often use these models to conduct parametric studies, varying parameters like opening sizes, lintel depths, or anchor stiffness. These models generally treat the timber as an orthotropic, elastic material, and the connectors are assigned bilinear or nonlinear curves.

In contrast, the literature that focuses on crack propagation and failure mechanisms in CLT panels within shearwalls is comparatively scarce. For example, numerical methods to examine the stresses around openings in CLT shearwalls were implemented by Pai et al..2017 Similarly, Ruggeri et al.2023 numerically investigated the interaction between floor-to-wall connections and lintels in shearwalls with openings, while Sciomenta et al.2024 proposed two modeling techniques, a concentrated plastic hinge model and a continuous post-elastic model to address crack propagation around openings. Their analysis, conducted on a multi-story shear wall with multiple openings, underscored the importance and benefits of accurately predicting the nonlinear behaviour and failure modes of the CLT panels.

Despite significant efforts to establish the behaviour of monolithic CLT shearwalls with openings, a notable gap remains regarding the failure modes of the CLT panel itself. Only a very limited number of shearwall specimens have exhibited failure originating within the CLT panel and understanding how such failure mechanisms impact overall behaviour is yet to be fully established.

Some studies incorporate contact or gap elements at boundaries to simulate rocking, while others explicitly model each lamination in the panel. Although these basic approaches serve as cost-effective tools for predicting peak load and drift capacity, they may lack the sophistication needed to capture crack propagation fully when a timber failure mode emerges.

2.8 Knowledge Gaps and Future Research Directions

There is broad agreement that more experiments on CLT shearwalls with monolithic opening would help clarify how lintels and parapets behave under lateral loads. In particular, full-scale tests designed specifically to promote failure in the panel are valuable, given that many existing campaigns observe only anchor-driven failures. Additional parametric studies on hold-down configurations, lintel stiffness, and corner reinforcement strategies could yield refined design provisions for monolithic shearwalls with openings.

The existing literature emphasizes that geometry, lamination orientation, and connection detailing are critical when introducing openings into CLT shearwalls. To address the remaining knowledge gaps, this study experimentally investigated twelve monolithic CLT shearwalls with door and window openings, enabling a detailed assessment of their structural response and providing validation data for the numerical model introduced in the following chapter. Furthermore, to quantify the influence of vertical outer laminations in lintel beams, thirty-six CLT beam specimens were tested; the outcomes of these tests are discussed in Chapter 4.

CHAPTER 3- NUMERICAL ANALYSIS OF MULTI-STOREY CLT SHEARWALLS WITH OPENINGS

Following the foundational context established in Chapter 2, which provided an introduction and a thorough literature review on cross-laminated timber shearwalls with openings (Popovski et al., 2014; Frangi et al., 2012), this chapter shifts focus to numerical modeling to deepen the understanding of their structural behaviour. While experimental investigations, detailed in Chapters 4 and 5, offer critical empirical insights, physical testing alone cannot encompass the full spectrum of design scenarios (Casagrande et al., 2020; Gavric et al., 2015). This chapter addresses this limitation through finite element analysis, employing SAP2000 to explore the mechanics of multi-storey CLT shearwalls with openings (Tannert et al., 2013; Serrano, 2016). By developing a model that captures the orthotropic nature of CLT panels and the non-linear behaviour of mechanical connectors, validated against existing experimental data (Pei et al., 2016; Boccadoro et al., 2019), this study conducts extensive parametric analyses. These analyses can then assess the impact of variables such as the number of storeys, opening sizes, lintel and parapet dimensions, wall segment widths, hold-down configurations, and gravity load intensities on structural performance. A key emphasis is placed on comparing monolithic shearwalls, where openings are cut from continuous panels, with segmented shearwalls assembled from separate elements as discussed in prior comparative studies (Popovski and Gavric, 2016; Ceccotti et al., 2013).

3.1 Description of the shearwall configurations

The current study addresses cases of two-, four- and six-storey CLT shearwalls with symmetric single door or window opening, centrally placed within the panel at each level. The geometrical dimensions and types of mechanical anchors were chosen based on practical sizes that are commercially available and used in CLT constructions.

The height of the CLT panel, H, is assumed to be the same for all storeys, while different values were selected for the width of the two wall segments, w_S, the dimensions of the lintel (height h_L and length w_L) and the height of the parapet, h_P, as reported in Table 3.1. Three values of uniformly distributed gravity load, q, applied at the top of each storey, were considered in the analysis.

Table 3.1: *Values of geometrical dimensions adopted in the analyses*

Parameter	Symbol	Values
Height of CLT panel	H [m]	3.2
Number of storeys	n [-]	2; 4; 6
Width of the two wall segments	w_S [m]	0.6; 1.2; 2.4
Lintel’s height	h_L [m]	0.0; 0.2; 0.4; 0.6; 0.8
Lintel's width	w_L [m]	1.6; 2.4
Parapet’s height	h_P [m]	0.0; 0.2; 0.4; 0.8; 1.2
Vertical load	q [kN/m]	0.0; 15.0; 30.0

The angle brackets used in this study are assumed to be of type AE116 and they were connected to the panel by means of 18 16d x 3 ½ spiral nails. The angle bracket spacing is equal to 0.6 m and as such a wall segment with width equal to 2.4 m contains three angle brackets, while only one angle bracket is provided for wall segments with widths equal to 0.6 m and 1.2 m. An additional angle bracket was placed at the bottom centre of the parapet in shearwalls with window openings.

As outlined in Figure 3.1, two different hold-down configurations are investigated, including double (cases A, B, D, E) or single (for cases C, F) hold-down, representing cases where hold-down is placed either at the extremities of each wall segment or the entire wall, respectively. Double hold-down configurations are used for shearwalls with wall segment widths equal to 2.4 m (cases A and D) and 1.2 m (cases B and E), whereas for wall segment widths equal to 0.6 m (cases C and F), single hold-down configuration is adopted.

In addition to the conventional placement of hold-downs at wall ends, cases with hold-downs located in the middle of the panel were also included. This was done to investigate their role in transferring uplift forces between adjacent wall segments and maintaining equilibrium in panels interrupted by openings, where relying solely on end hold-downs may not accurately capture the load distribution.

For each configuration, three different types of hold-downs are investigated, including single hold-down device (HD1), two hold-down devices (HD2) or replacing the hold-down with an angle bracket (AB) similar to those used in the rest of the shearwall, as shown in Figure 3.2. Although the latter configuration is not typical when traditional devices are adopted, recent products have made the replacement of hold-down devices with such type of angle brackets a possible alternative to traditional configurations. The type of hold-down device used is assumed to be WHT 620, and it is connected to the CLT panels by means of 55 4.0x60 mm annular-ringed shank nails.

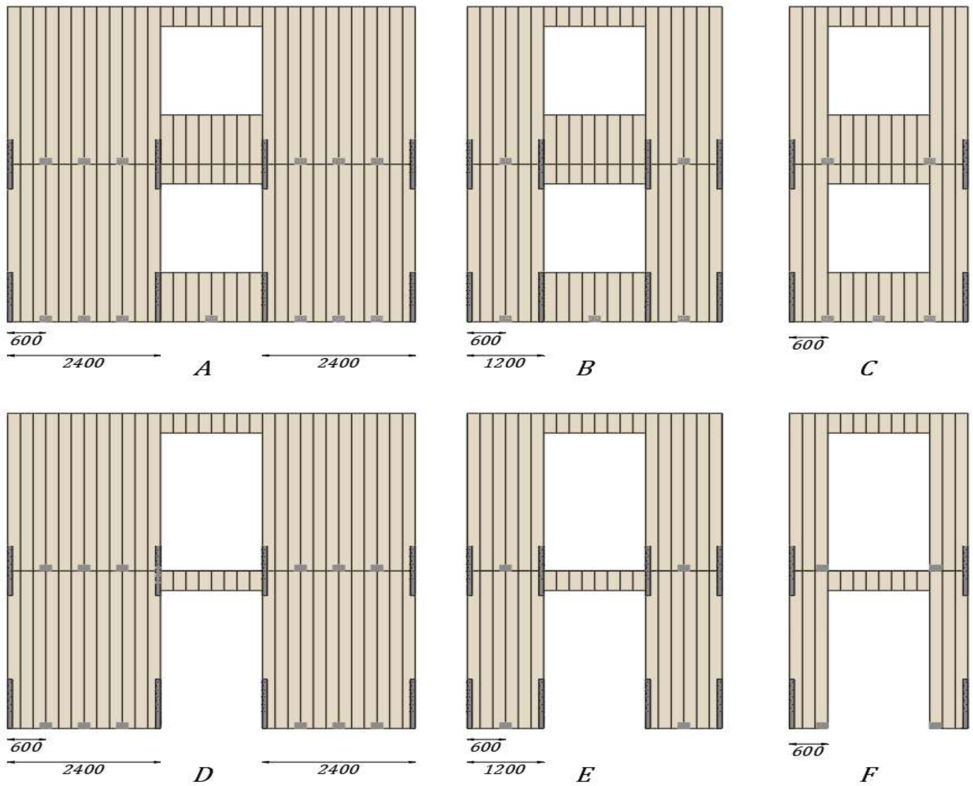

Figure 3.1: *Hold-down configurations for two-storey shear walls*

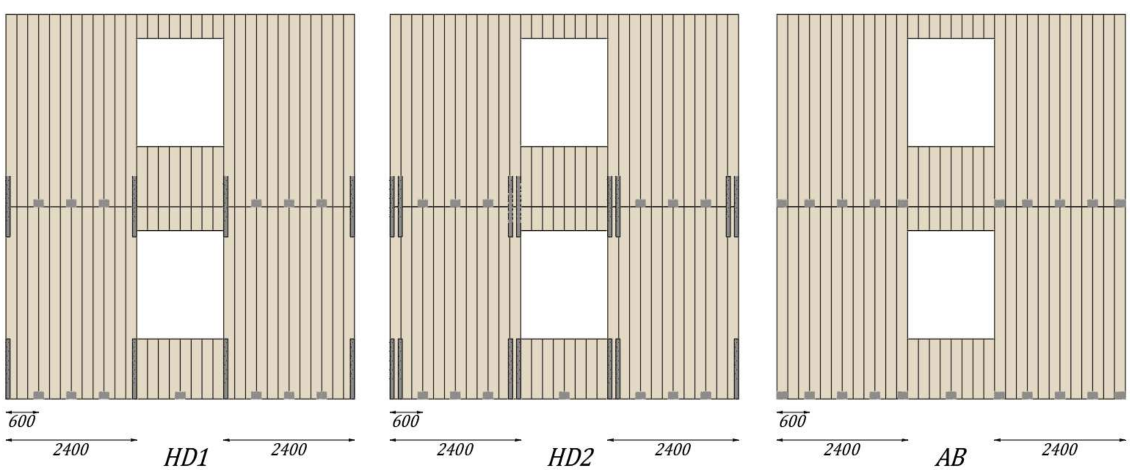

Figure 3.2: *Single hold-down device (HD1), two hold-down devices (HD2) and hold-down replaced by an angle bracket (AB)*

The orientation of the outer laminates of CLT panels is assumed parallel to the vertical direction for all configurations. The thickness and layout of the CLT panels varied along the height of the building to reflect realistic choices in the building design, where lower storey shearwalls were assigned thicker panels due to the cumulative gravity and lateral shear force, as presented in Table 3.2. Three different values of thickness and laminate layouts were selected for the CLT panels, namely 105 (35-35-35) mm, 143 (35-19-35-19-35) mm and 175 (35-35-35-35-35) mm.

Table 3.2: *CLT panel thickness at different storeys*

Storey	Thickness of the panel [mm] Two-Storey	Four-Storey	Six-Storey
1st	105	143	175
2nd	105	143	175
3rd	-	105	143
4th	-	105	143
5th	-	-	105
6th	-	-	105

Laminates layout: 105 (35-35-35) mm, 143 (35-19-35-19-35) mm and 175 (35-35-35-35-35) mm

Values for the modulus of elasticity parallel to the grain, E_0, and the in-plane shear modulus G_0 of the CLT lamination, equal to 11700 MPa and 730 MPa, respectively, were assumed according to NS-GT6. The modulus of elasticity perpendicular to the grain, E_{90}, was taken equal to $E_{90} = \frac{E_0}{30}$, as indicated in the Canadian timber design Standard. The mean value of tensile, f_t, and compressive, f_c, strength parallel to grain was assumed equal to 26.6 MPa and 33.2MPa, respectively, whereas values equal to 11.1 MPa, and 3.5 MPa, were chosen for the mean in-plane net-shear strength, $f_{v,r}$, and torsional strength, $\tau_{T,r}$, respectively (Casagrande et al.,2021b). The mean values of strength from Casagrande et al.2021b were calculated from the 5th percentile values reported in ETA 12/0362 assuming a log-normal distribution of the strength properties with a coefficient of variation (CoV) equal to 20%.

In addition to end hold-downs, mid-panel hold-downs were studied to quantify their role in transferring uplift between adjacent segments and enforcing equilibrium in monolithic panels interrupted by openings, where relying solely on end anchors can misrepresent load paths.

3.2 Mesh size refinement analysis

The mesh size refinement analysis was based on considering a two-storey shearwall with door opening (case #1a with 0.4m lintel height, see Table 3.8) with mesh sizes of 100 mm, 50 mm and 25 mm. The push-over curves and the failure loads of the investigated models with three different mesh sizes are illustrated and reported in Figure 3.3 and Table 3.3, respectively. The refinement criterion adopted in this study was that further mesh reduction should not produce changes greater than 5% in key global response parameters such as ultimate lateral resistance and overall load-displacement behaviour.

It can be observed that decreasing the mesh size from 50mm to 25mm, resulted in a 1% error in the failure force, while the difference between 100 mm and 50 mm meshes was approximately 6%. Since the 50 mm mesh provided results within the defined convergence threshold while maintaining computational efficiency, it was selected as the standard element size for all subsequent modelling.

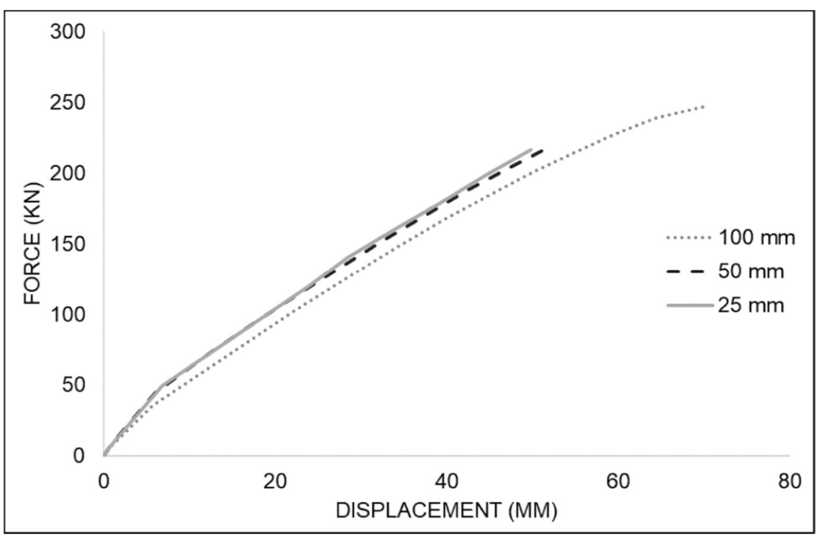

Figure 3.3: *Push-Over curve comparison for different mesh size*

__Table 3.3:__ Failure force comparison for different mesh size

Meshing size (mm)	Failure force [KN] (VAR)
100	247 (13%)
50	**219**
25	216 (-1%)

A comparison in terms of the distribution of internal forces (shear and axial) at the end section of the lintels at the first storey was also carried out. As shown in Figures 3.4, it was observed that the discrepancies in the obtained internal forces between 50 mm and 25mm meshing are relatively small. This further confirmed that the 50 mm mesh size was sufficiently refined to capture local stress distributions while avoiding unnecessary computational cost. For this purpose, 50 mm meshing size was considered for modelling of shearwalls in this study.

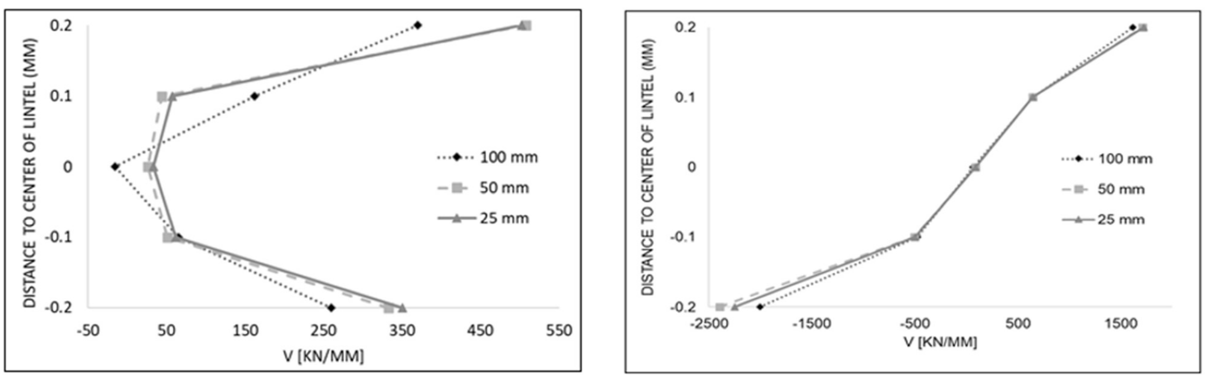

a) b)

__Figure 3.4:__ comparison of shear (a) and axial forces (b) of end section of lintel beam at the first storey for the models with having 25mm, 50mm and 100 mm mesh size [KN/m]

3.3 Description of the FE model

Four-node quadrilateral homogenous area elements were used to model the CLT panels. The 2-D area elements were selected because they represent a reasonable balance between accuracy and modelling efficiency, as demonstrated in published literature. Other studies have also successfully used shell elements to represent the CLT panels. A 50 mm meshing size was adopted based on a mesh analysis, representing a reasonable balance between accuracy and computation time. Elastic orthotropic material properties, characterized by effective values of the modulus of elasticity along the vertical, $E_{eff,v}$, and horizontal, $E_{eff,h}$, directions (Equation 1) as well as the in-plane shear modulus, G_{eff}, (Equations 2) were adopted, to represent the orientation of the different layers, as outlined in Bogensperger et al.2010 and Brandner et al.2017.

$$E_{eff,v} = \frac{E_0 \cdot t_v + E_{90} \cdot t_h}{t_{CLT}}$$
$$E_{eff,h} = \frac{E_0 \cdot t_h + E_{90} \cdot t_v}{t_{CLT}} \quad (1)$$

$$G_{eff} = \frac{G_0}{1 + 6 \cdot \alpha \cdot \left(\frac{t_{mean}}{w}\right)^2} \quad (2)$$

where t_{CLT} is the total thickness of the CLT panel, t_v and t_h are the total thickness of the vertical and horizontal layers, respectively, w is the width of the laminations equal to 150 mm, t_{mean} is the mean value of the thickness of laminations and α is calculated as shown in Equation 3.

$$\alpha = p \cdot \left(\frac{t_{mean}}{w}\right)^{-0.795} \quad (3)$$

where values of p are taken equal to 0.535 and 0.425 for a three- and five-layer panel, respectively (Bogensperger et al.,2010).

For the numerical models representing segmented shearwalls, the two wall segments were modelled as two separated cantilevered shearwalls, connected by means of a truss element, which only ensures the transfer of the vertical load to the wall segments, as shown in Figure 3.5b. In order to reproduce the typical modelling strategy that is adopted by designers when lintels and parapets are made with separate elements and hence are not able to transfer bending moments to the adjacent wall segments, the lintels and parapets were not modelled by means of area elements. Either a diaphragm constraint at the floor level or a truss element connecting the wall segments is adopted in order to ensure the same lateral displacements of wall segments at the different storeys.

The mechanical anchors at the ground and upper storeys were modelled by means of one-joint and two-joint multi-linear link elements, respectively. A uni-directional behaviour along the vertical-tensile direction was assumed for the hold-downs, while a bi-directional behaviour along the vertical-tensile and horizontal-shear directions was assumed for the angle brackets. The mechanical behaviour of hold-downs and angle brackets was represented by a tri-linear curve, obtained from Casagrande et al.2016 and Yinlan et al.2019, respectively, based on experimental testing (Figure 3.6). Rigid compression-only (i.e. gap) elements were adopted to simulate the contact between the CLT panels and the ground at the first storey and between the CLT panel and the floor below at higher storey levels.

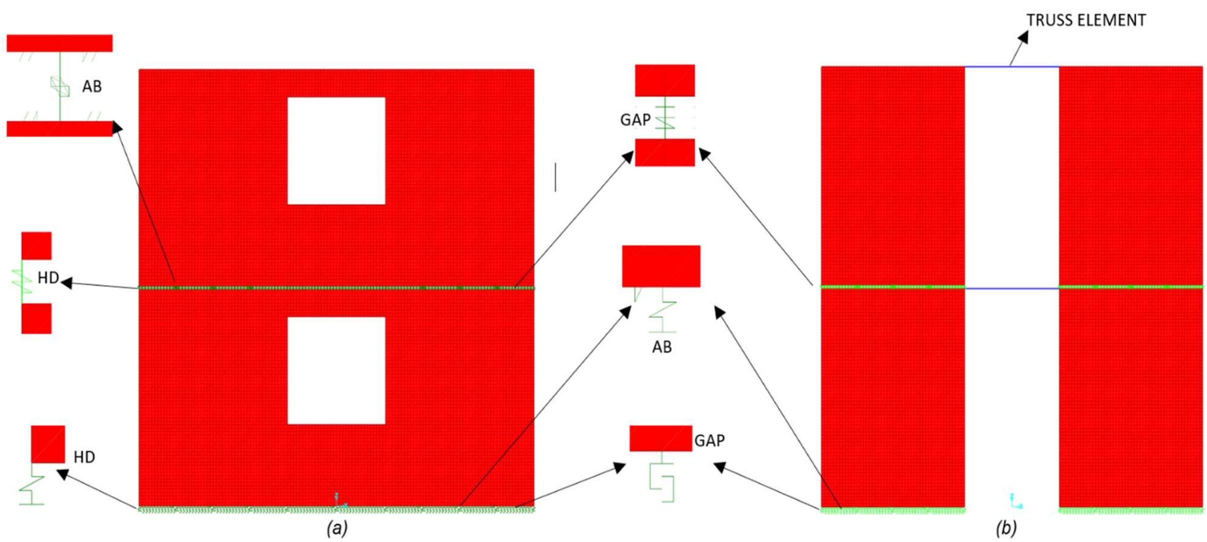

Figure 3.5: *Numerical model for a two-storey CLT shearwall with window opening for MSW (a) and SSW shearwall (b)*

In order to mimic the diaphragm behaviour of the floor assemblies, a horizontal constraint was applied at each level at the top of the wall segments. A push-over analysis was conducted by increasing the lateral loads which were applied at each storey, based on triangular load distribution.

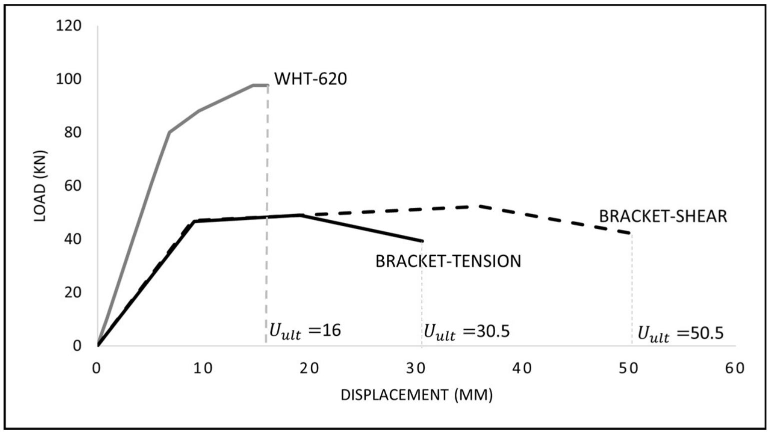

Figure 3.6: N*on-linear behaviour of hold-down and angle bracket*

The failure condition related to the CLT panels was determined by means of a step-by-step verification of the axial, σ_h and σ_v, and shear, τ, stresses in all area elements used in the modelling of the CLT panels.

The representative volume element (RVE) method, presented by Bogensperger et al.2010, was adopted for the calculation of the in-plane axial and shear strength of the panels through the definition of Representative Volume Sub Elements (RVSEs). RVE represents the smallest volume of the CLT shearwall which can be used for the static verification and determining of mechanical properties. The width and height of the RVE are taken as the width of the board and the total thickness of the CLT, respectively. The part between two adjacent planes of symmetry is the smallest possible element and is called RVSE. The ideal thicknesses $t_{RVSE,i}$ for each RVSE is reported in Table 3.4 for three- and five-layer CLT panels, where t_i is the thickness of the *i-th* layer in the panel.

The ideal nominal shear stress τ_0, acting on each RVSE, was calculated using the expression presented in Equation 4.

$$\tau_0 = \frac{v}{\sum_{i=1}^{n} t_{RVSE,i}} \tag{4}$$

where v is the in-plane internal shear force per unit length, determined from the area elements, $t_{RVSE,i}$ is the thickness of the i^{th} RVSE and n is the number of the RVSE layers equal to 2 and 4 for a three- and five-layer CLT panel, respectively.

***Table 3.4:** Ideal thickness of RVSEs for three- and five-layer CLT panel*

3-layer panel	
RVSE	Thickness
#1	$t_{RVSE,1} = Min(2t_1, t_2)$
#2	$t_{RVSE,2} = Min(t_2, 2t_3)$
5-layer panel	
RVSE	Thickness
#1	$t_{RVSE,1} = Min(2t_1, t_2)$
#2	$t_{RVSE,2} = Min(t_2, t_3)$
#3	$t_{RVSE,3} = Min(t_3, t_4)$
#4	$t_{RVSE,4} = Min(t_4, 2t_5)$

The verification in terms of effective shear stress, τ_V, and maximum torsional stresses, τ_T, in the glue interface of RVSEs was undertaken using Equation 5.

$$\begin{cases} \tau_V = 2 \cdot \tau_0 \leq f_{v,r} \\ \tau_T = 3 \cdot \tau_0 \cdot \frac{\max(t_{RVSE,i})}{w} \leq \tau_{T,r} \end{cases} \tag{5}$$

where $f_{v,r}$ and $\tau_{T,r}$ are effective shear strength and torsional strength, respectively, and w is the width of wooden boards.

The verification in terms of horizontal, σ_x, and vertical, σ_z, axial stresses is conducted according to Equation 6.

$$\sigma_x = \frac{n_x}{t_x} \leq \begin{matrix} f_t \; if \; \sigma_x \geq 0 \\ f_c \; if \; \sigma_x < 0 \end{matrix}; \quad \sigma_z = \frac{n_z}{t_z} \leq \begin{matrix} f_t \; if \; \sigma_z \geq 0 \\ f_c \; if \; \sigma_x < 0 \end{matrix} \tag{6}$$

where n_x and n_z are in-plane axial internal force per unit length along the horizontal-x and vertical-z direction, respectively, t_x and t_z are the total thickness of laminations along the horizontal and vertical direction, respectively, and f_t and f_c are the tensile and compressive axial strength of the laminations, respectively.

Failure in the connections is assumed to occur when the mechanical anchors reach their ultimate displacement.

As outlined in Figure 3.6, the ultimate displacement for the hold-down was 16 mm, while the value obtained for tension and shear failure of angle bracket was equal to 30.5 and 50.5 mm, respectively.

It should be emphasized that the present FE formulation does not explicitly incorporate torsional shear mechanisms within the crossing areas of laminations. Consequently, while the model is able to capture axial and net shear failures with good accuracy, torsional shear failures could not be reproduced.

This limitation explains occasional misclassification between net shear and torsional shear observed when comparing model predictions with experimental outcomes.

The adoption of simplified orthotropic elasticity for the CLT panels was appropriate for global response but inherently restricts the model's ability to represent local fracture processes or lamination separation phenomena.

Future refinement of the model should therefore include constitutive laws capable of representing torsional shear interaction and nonlinear fracture propagation in CLT panels.

3.4 Validation of the model

Prior to conducting the parametric analysis, a validation of the proposed numerical model is carried out, using experimental results by Casagrande et al.2021a and Gavric et al.2015b, representing monolithic shearwall configurations with and without openings, respectively. Other full-scale experimental data on monolithic shearwalls with openings are available in the literature and would provide potential for comparisons with the proposed numerical model, however, the lack of information on the non-linear behaviour of the connections and the inclusion of friction parameter at the wall base made it impractical to use these studies in the validation process.

A total of six full-scale shearwalls were investigated by Casagrande et al.2021a to establish the effect of openings on the failure mode and mechanical behaviour of CLT shearwalls, as outlined in Figure 3.7. Two different CLT configurations were used, a three-layer and five-layer CLT panel with 90mm and 100mm thickness, respectively. The CLT panels were constructed of Spruce lumber boards with width of 170 mm. The geometrical properties and layout of the CLT panel are reported in Table 3.5. The height of the shearwall was equal to 2.8 m for all the tested shearwalls. The shearwall specimens were anchored to the steel base using fully nailed WHT-620 hold-downs, which were connected to the panel using 55 4.0x60 mm ring shank nails. Two different hold-down configurations were used to anchor the wall to the foundation, namely by installing hold-down at the ends of shearwall (SH) or at the end of each segment (DH). It should be noted that the sliding behaviour of the tested shearwalls was blocked using steel plates without restraining the rotation of the shearwall. The tests were conducted according to EN594, and no vertical load was applied on the shearwalls.

The comparison in terms of push-over curve, maximum strength, F_{max}, and stiffness, K, between the current numerical model and the experimental test results are reported in

Figure 3.8 and Table 3.6. As shown in Table 3.6, the same failure mechanism can be seen in both numerical modelling and experimental tests, with the exception of Wall 4, where net shear failure was observed in numerical modelling, while bending failure was found in the experimental test. This difference was attributed to the proximity between net shear and bending failure mode for this particular wall. This is also evident when comparing the peak load obtained by the numerical model with that from the experimental test, where a ratio of 1.04 is obtained, as shown in Table 3.6. In general, comparing the results obtained from the model prediction and the reported test results for peak load and stiffness, a maximum error of 20% and 30%, respectively, were found. A corresponding average error of 7.3% (peak load) and 11.6% (stiffness) were obtained. The discrepancy obtained in the comparison with the experimental tests of Wall 02 and 03 can be mainly attribute to the variability of strength and stiffness related to the hold-down. The mechanical behaviour of such shearwalls is largely dependent on the mechanical properties of the hold-down whose variability may cause less accuracy in the prediction of the behaviour of the entire shearwall.

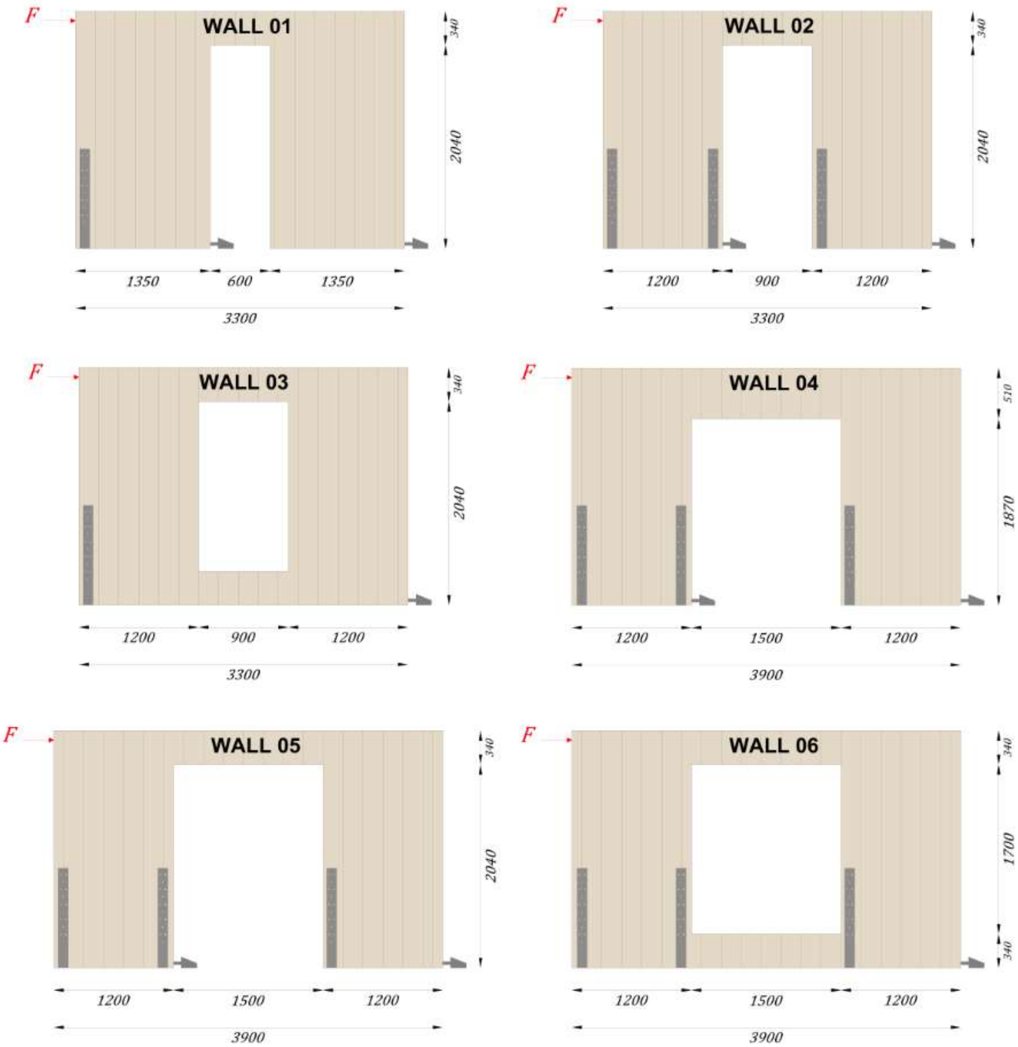

Figure 3.7: *Layout of shearwalls tested by Casagrande et.al2021a*

Table 3.5: *Geometry properties of tested shearwalls by Casagrande et al.2021a*

Test	number of layers	t_{tot} (mm)	l_{wall} (mm)	h_{lintel} (mm)	$h_{parapet}$ (mm)	l_{top} (mm)	Opening type	Hold-down configuration
Wall 01	3	90	3300	340	-	600	Door	SH
Wall 02	5	100	3300	340	-	900	Door	DH
Wall 03	5	100	3300	340	340	900	Window	SH
Wall 04	3	90	3900	510	-	1500	Door	DH
Wall 05	5	100	3900	340	-	1500	Door	DH
Wall 06	5	100	3900	340	340	1500	Window	DH

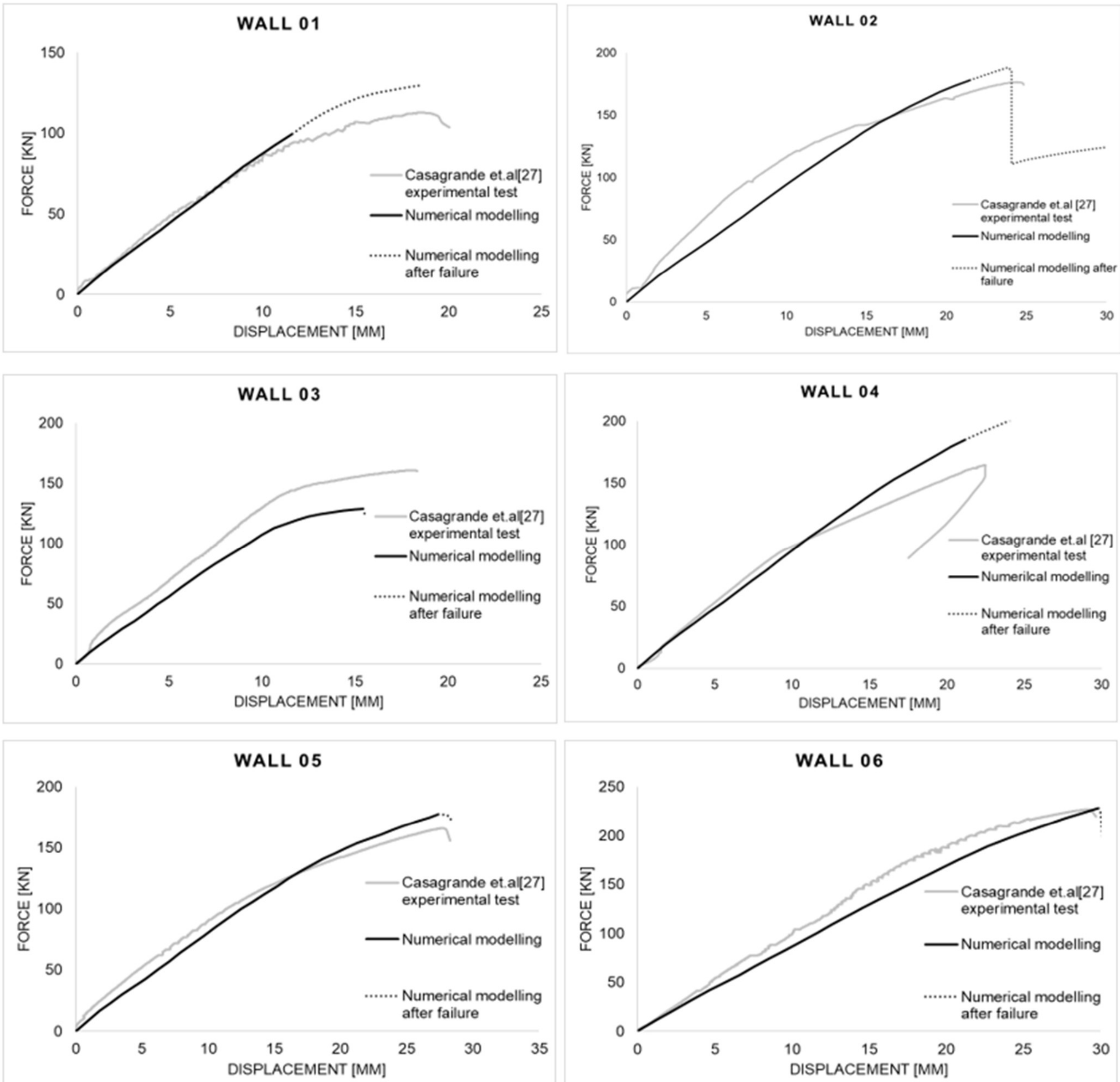

Figure 3.8: *Comparison of equivalent curves presented by Casagrande et al.2021a and the push-over curve from the numerical model*

Table 3.6: *Comparison between the proposed method in this paper with results obtained from experimental test by Casagrande et.al2021a*

Wall	Numerical modelling			Casagrande et.al.,2021a experimental tests			Ratios	
	Failure mode	F_{max} [KN]	K [KN/mm]	Failure mode	F_{max} [KN]	K [KN/mm]	$\frac{F_{max,Num.}}{F_{max,Exp.}}$	$\frac{K_{Num.}}{K_{Exp.}}$
Wall 01	CLT (Net shear)	99.8	8.97	CLT (Net shear)	112.8	9.5	0.88	0.94
Wall 02	HD	178.2	9.53	HD	176.5	13.7	1.01	0.70
Wall 03	HD	129	11.31	HD	161	12.8	0.80	0.88
Wall 04	CLT (Net shear)	185.1	9.6	CLT (Bending)	178.6	10.2	1.04	0.94
Wall 05	HD	177.4	8.12	HD	165.9	8.6	1.07	0.94
Wall 06	HD	227.8	8.7	HD	226.8	9.7	1.00	0.90

The shearwall specimen reported in Gavric et al.2015b had height and length equal to 2950 mm and was constructed of five-ply, 85 mm thick CLT panels. The shearwall was anchored to the steel base using two HTT22 hold-downs connected to the panel with 12 4.0x60 mm annular-ringed shank nails and four BMF90x48x3.0x116 angle brackets connected to the panel with 11 114x60 mm annular-ringed shank nails. A uniformly distributed vertical load equal to 18.5 kN/m was applied at the top of the panel, as illustrated in Figure 3.9.

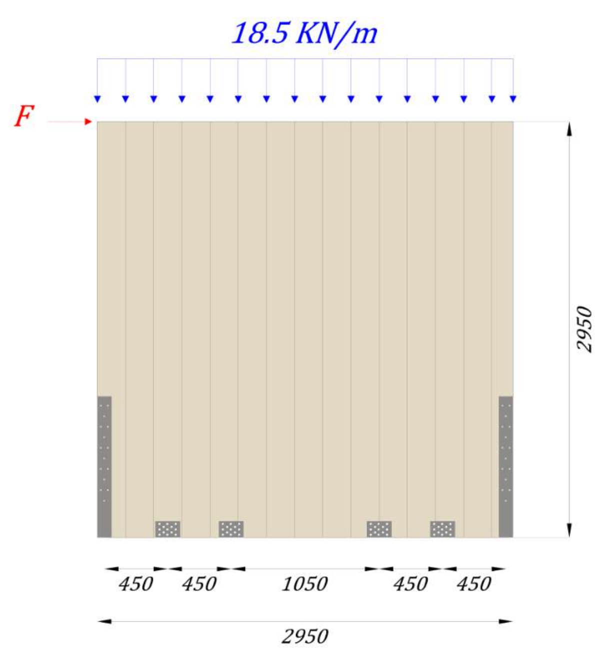

Figure 3.9: *Shearwall tested by Gavric et al2015b and used for the validation of the numerical model*

The EN12512 cyclic loading protocol was adopted for the experimental tests. This loading protocol involves set of three cycles at increasing amplitudes of slip. The yield load was determined based on the intersection of two straight lines: the first line connects the point of the experimental backbone curve corresponding to 10% and 40% of the peak load; the second line is defined as the tangent with slope equal to one-sixth of the slope of the first line.

The same protocol was adopted to determine the yield and peak load and displacement from the push-over curve obtained from the numerical model. Figure 3.10 presents the result of comparison between the equivalent tri-linear backbone curve presented by Gavric et al.,2015b and that obtained through the push-over analysis from the proposed numerical model.

The ratios in terms of yield load, yield displacement, peak load and displacement corresponding to the peak load, obtained from the experimental tests and numerical simulations, are reported in Table 3.7. It can be seen that an error of less than 10% is obtained.

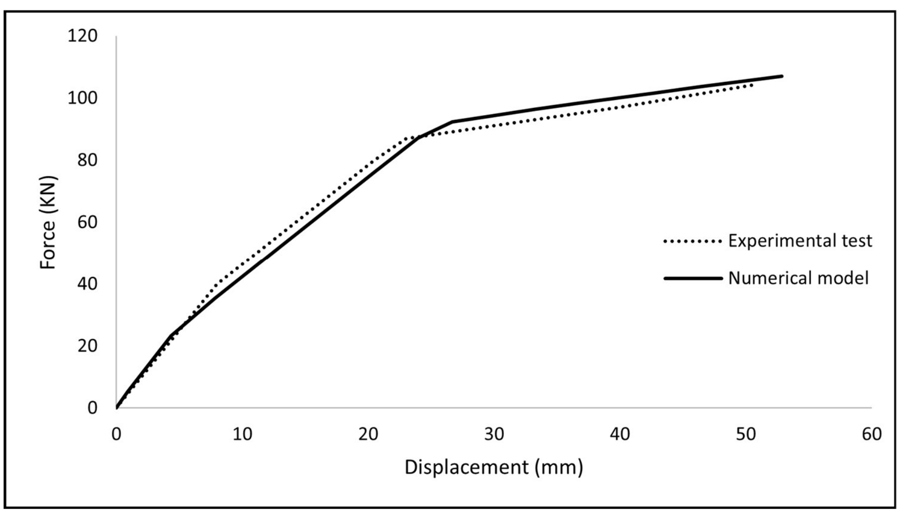

Figure 3.10: *Equivalent trilinear backbone curve presented by Gavric et al.,2015 and the push-over curve from the numerical model*

Table 3.7: *Comparison of numerical and experimental results of yield and maximum point of tested CLT shear wall*

	Experimental test (Gavric et al.,2015)	**Numerical modelling**	**Discrepancy**
Yield Force	87.4	91.5	5%
Yield displacement	23	25.1	9%
Maximum Force	104.2	107.1	3%

Based on the comparisons presented in this chapter, it can be concluded that the proposed model provides an acceptable representation of the failure mode and mechanical behaviour of the CLT shearwalls, with and without openings.

3.5 Results and discussion

The results from the numerical analyses are presented in terms of lateral stiffness, K, peak load, F_{max}, and failure mode, for each analysed shearwall. The lateral stiffness was determined as the slope of the line connecting the origin to the point on the push-over curve related to 40% of the peak load, according to ASTM E2126 procedure.

3.5.1 Monolithic shearwalls

The influence of the geometrical and mechanical parameters related to lintels and parapets, gravity load and hold-down configuration on the lateral stiffness and peak load of monolithic shearwalls was investigated.

Six different analysis cases were implemented by changing the values of the target parameter for each case, while maintaining constant values of the other parameters, as presented in Table 3.8.

Table 3.8: *Values of the studies parameters*

<table>
<tr><th>Case</th><th>Target parameter</th><th>Variable values
(*Reference value)</th><th></th><th colspan="5">Fixed value for non-target parameter</th></tr>
<tr><td></td><td></td><td></td><td>h_L [m]</td><td>w_L
[m]</td><td>w_S
[m]</td><td>h_P
[m]</td><td>q
[kN/m]</td><td>HD
conf.</td></tr>
<tr><td>#1a</td><td>Lintel's height h_L [m]</td><td>0.0; 0.2; 0.4*; 0.6; 0.8</td><td>-</td><td>1.6</td><td rowspan="3">2.4</td><td rowspan="4">1.2</td><td rowspan="5">15.0</td><td rowspan="6">1-HD</td></tr>
<tr><td>#1b</td><td>Lintel's height h_L [m]</td><td>0.0; 0.2; 0.4*; 0.6; 0.8</td><td>-</td><td>2.4</td></tr>
<tr><td>#2</td><td>Lintel's width w_L [m]</td><td>1.6*; 2.4</td><td rowspan="5">0.4</td><td>-</td></tr>
<tr><td>#3</td><td>Width of the wall segments w_S [m]</td><td>0.6; 1.2*; 2.4</td><td rowspan="4">1.6</td><td>-</td></tr>
<tr><td>#4</td><td>Parapet's height h_P [m]</td><td>0.0; 0.2; 0.4;0.6; 0.8; 1.2*</td><td rowspan="3">2.4</td><td>-</td></tr>
<tr><td>#5</td><td>Vertical load q [kN/m]</td><td>0.0; 15.0*; 30.0</td><td rowspan="2">1.2</td><td>-</td></tr>
<tr><td>#6</td><td>HD configuration [-]</td><td>1-HD*; 2-HD: A-HD</td><td>15.0</td><td>-</td></tr>
</table>

3.5.1.1 Shearwalls with window openings

For each value of the target parameter, the failure mode, values of lateral stiffness and peak load, variation in lateral stiffness and peak load compared to the reference parameter, are reported for two-, four- and six-storey shearwalls, as presented in Table 3.9. Figure 3.11 also shows the push-over curves of a four-storey shearwall obtained from case #1a where the height of the lintel was changed from 0.0 to 0.8m, and from case #4, where the height of the parapet was changed from 0.0 to 1.2 m. In Figure 3.12, the distribution of axial and shear internal forces of the four-storey shearwall for case #4 with 0.2 m parapet height is shown at the first storey. A concentration of the internal forces at the corners around the end sections of lintel beams can be observed.

The results of the analysis show that shear failure of angle brackets is the dominant failure mode for the two-storey models. By increasing the number of storeys, it can be observed that the behaviour tends to be more governed by hold-down failure. Only for shearwalls with parapet height equal to or smaller than 0.4 m, was the axial failure mode achieved in the end section of lintel, Changing the height of the lintel beam does not seem to have any significant effect on the failure modes along the storey height. It is interesting to note that the parapet height seems to have a great influence on the failure mechanism, even though no structural function is typically associated with the parapet. It can be observed that shearwalls with parapet heights equal to or smaller than 0.4 m were characterized by failure in the CLT panel, whereas walls with parapet heights greater than 0.4 m tended to fail in the mechanical anchors. As anticipated, increasing the vertical load shifted the failure mechanism from rocking to sliding, due to the countering effect induced by the vertical gravity load to resist the overturning moment caused by the shear force.

Table 3.9: *Failure mode, values and variation (VAR) of lateral stiffness and peak load for shearwall with window openings*

Case	Target parameter	Variable value	Two-Storey			Four-Storey			Six-Storey		
			Failure	F_{max} (VAR)	K (VAR)	Failure	F_{max} (VAR)	K (VAR)	Failure	F_{max} (VAR)	K (VAR)
#W1a	Lintel's height h_L [m] ($w_L = 1.6\ m$)	0.0	AB-S	367 **(0%)**	8.01 **(-9%)**	HD	273 **(-9%)**	4.09 **(-10%)**	HD	222 **(-11%)**	2.63 **(-10%)**
		0.2	AB-S	367 **(0%)**	8.47 **(-4%)**	HD	297 **(-1%)**	4.4 **(-3%)**	HD	248 **(0%)**	2.87 **(-2%)**
		0.4	AB-S	367	8.81	HD	301	4.54	HD	249	2.93
		0.6	AB-S	367 **(0%)**	9.22 **(5%)**	HD	301 **(0%)**	4.73 **(4%)**	HD	244 **(-2%)**	3.07 **(5%)**
		0.8	AB-S	367 **(0%)**	9.58 **(9%)**	HD	294 **(-2%)**	4.96 **(9%)**	HD	245 **(-2%)**	3.18 **(9%)**
#W1b	Lintel's height h_L [m] ($w_L = 2.4\ m$)	0.0	AB-S	367 **(0%)**	7.82 **(-10%)**	HD	306 **(-12%)**	4.05 **(-9%)**	HD	248 **(-17%)**	2.73 **(-10%)**
		0.2	AB-S	367 **(0%)**	8.32 **(-4%)**	AB-S	349 **(0%)**	4.29 **(-4%)**	HD	293 **(-2%)**	2.93 **(-3%)**
		0.4	AB-S	367	8.69	AB-S	349	4.45	HD	299	3.02
		0.6	AB-S	367 **(0%)**	9.18 **(6%)**	AB-S	349 **(0%)**	4.68 **(5%)**	HD	300 **(0%)**	3.17 **(5%)**
		0.8	AB-S	367 **(0%)**	9.73 **(12%)**	AB-S	349 **(0%)**	4.94 **(11%)**	HD	299 **(0%)**	3.34 **(11%)**
#W2	Lintel's width w_L [m]	**1.6**	AB-S	367	8.81	HD	301	4.54	HD	249	2.93
		2.4	AB-S	367 **(0%)**	8.69 **(-1%)**	AB-S	349 **(16%)**	4.45 **(-2%)**	HD	299 **(20%)**	3.02 **(3%)**
#W3	Width of the wall segments w_S [m]	0.6	HD	91 **(-75%)**	1.41 **(-84%)**	HD	65 **(-78%)**	0.85 **(-81%)**	HD	53 **(-79%)**	0.48 **(-84%)**
		1.2	AB-S	157 **(-57%)**	3.4 **(-61%)**	AB-S	139 **(-54%)**	1.63 **(-64%)**	HD	110 **(-56%)**	0.91 **(-69%)**
		2.4	AB-S	367	8.81	HD	301	4.54	HD	249	2.93
#W4	Parapet's height h_P [m]	0.0	L-A	211 **(-43%)**	5.66 **(-36%)**	L-A	183 **(-39%)**	2.58 **(-43%)**	L-A	166 **(-33%)**	1.6 **(-45%)**
		0.2	L-A	237 **(-35%)**	5.89 **(-33%)**	L-A	207 **(-31%)**	2.67 **(-41%)**	L-A	187 **(-25%)**	1.67 **(-43%)**
		0.4	L-A	282 **(-23%)**	6.29 **(-29%)**	L-A/P-A	269 **(-10%)**	2.91 **(-36%)**	HD	245 **(-2%)**	1.86 **(-37%)**
		0.6	L-A	332 **(-10%)**	7.06 **(-20%)**	HD	293 **(-3%)**	3.39 **(-25%)**	HD	249 **(0%)**	2.24 **(-24%)**
		0.8	AB-S	365 **(-1%)**	7.55 **(-14%)**	HD	299 **(-1%)**	3.87 **(-15%)**	HD	250 **(0%)**	2.55 **(-13%)**
		1.2	AB-S	367	8.81	HD	301	4.54	HD	249	2.93
#W5	Vertical load q [kN/m]	0.0	HD	334 **(-9%)**	7.17 **(-19%)**	HD	197 **(-35%)**	2.57 **(-43%)**	HD	140 **(-44%)**	1.13 **(-61%)**
		15.0	AB-S	367	8.81	HD	301	4.54	HD	249	2.93
		30.0	AB-S	369 **(1%)**	9.76 **(11%)**	AB-S	348 **(16%)**	5.1 **(12%)**	AB-S	328 **(32%)**	3.28 **(12%)**
#W6	HD configuration [-]	A-HD	AB-T	367 **(0%)**	9.91 **(12%)**	AB-T	267 **(-11%)**	5.81 **(28%)**	AB-T	227 **(-9%)**	3.55 **(21%)**
		1-HD	AB-S	367	8.81	HD	301	4.54	HD	249	2.93
		2-HD	P-A/P-S	668 **(82%)**	11.2 **(27%)**	HD	442 **(47%)**	5.42 **(19%)**	HD	367 **(47%)**	3.22 **(10%)**

F_{max} : Peak load (KN); K: Lateral stiffness (KN/mm); HD: failure in hold-down; AB-S: Failure in angle brackets due to shear load; AB-T: Failure in angle brackets due to tensile load; L-A: Axial failure in the lintel beam; P-A: Axial failure in the parapet section; P-S: Shear failure in the parapet section

In terms of peak load, the lintel height does not seem to have a significant effect, as demonstrated in Figure 3.13. This could be explained by the fact that the parapet couples the two wall segments and as such the additional effect due to the lintel beam connecting the wall segments together becomes less significant. A different behaviour is expected in the case of door opening, where the lintel beam is the primary connection between the wall segments, as will discussed later.

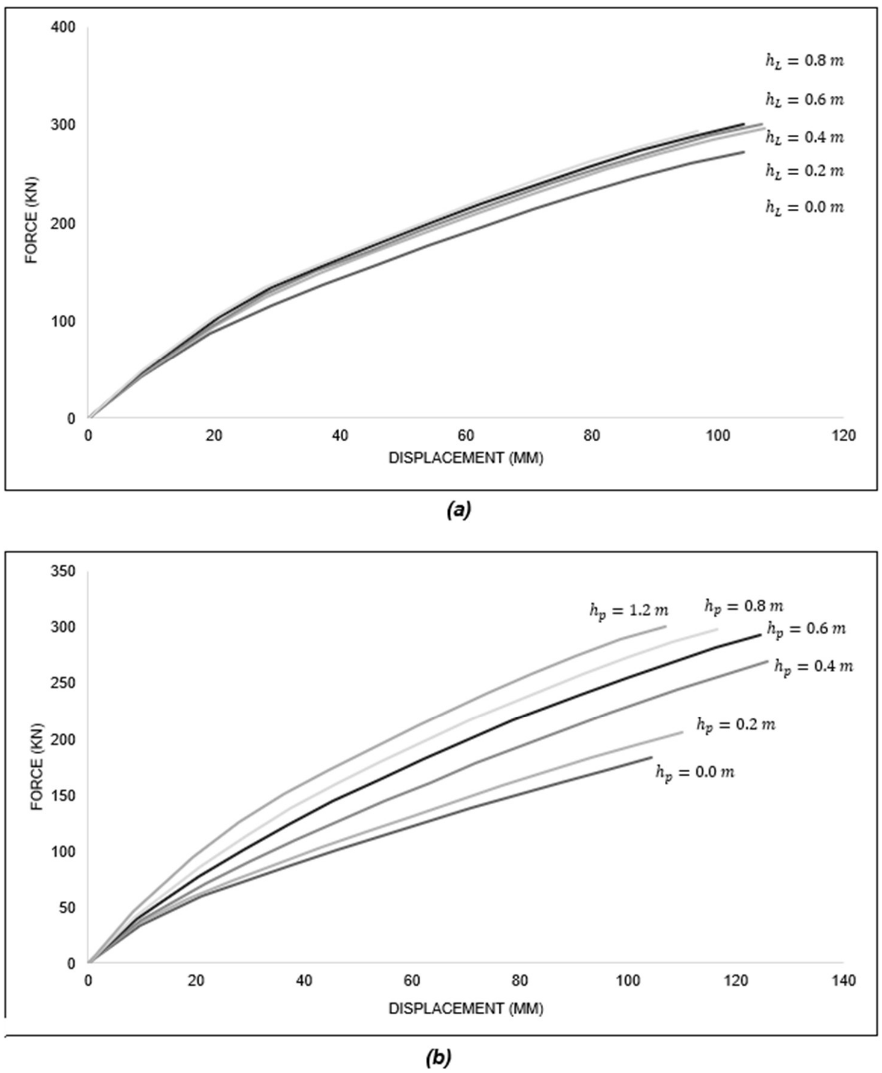

Figure 3.11*: Push-over curves of four-storey shearwalls for case #W1a (a) and case #W4 (b)*

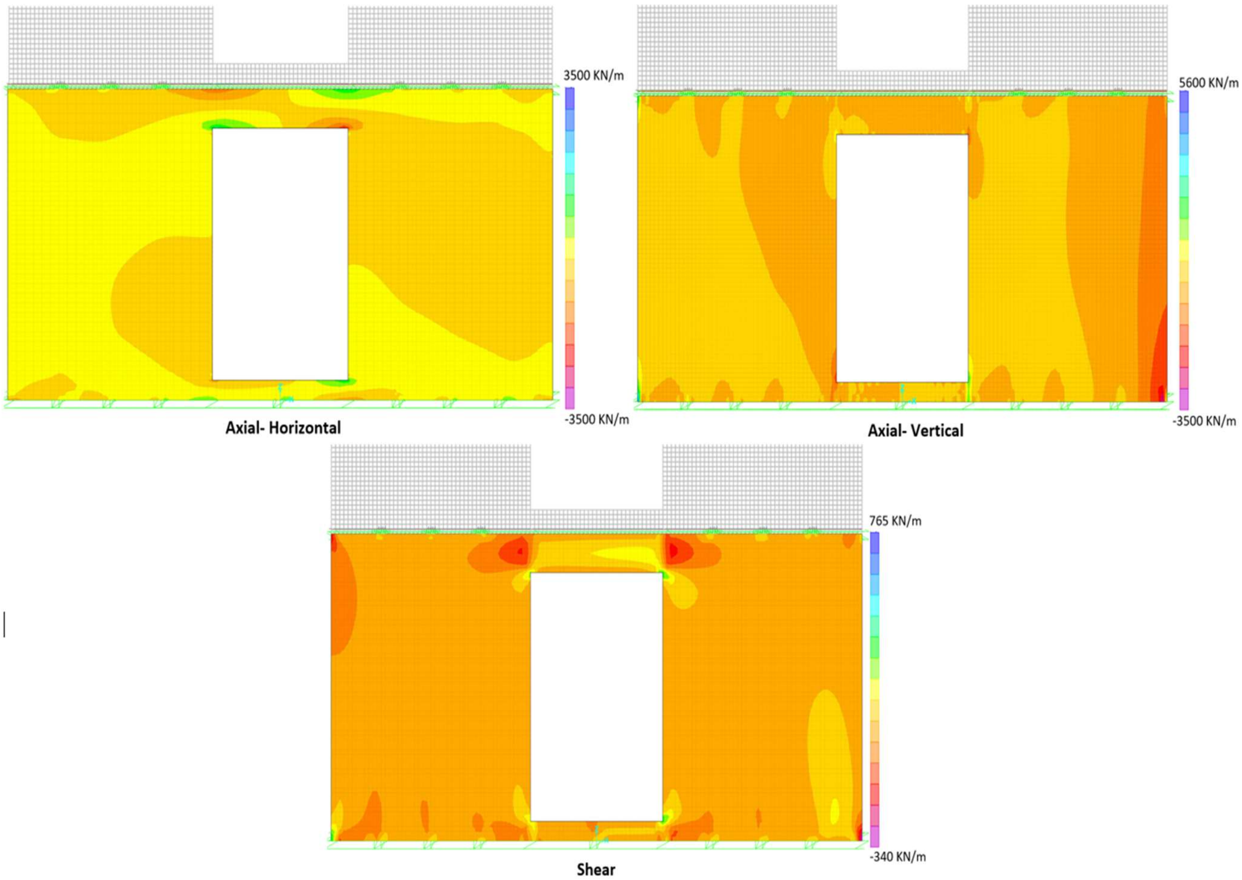

Figure 3.12***: Distribution of internal force of 4-storey shearwall obtained from case#4 with 0.2 m parapet height***
($F_{base\ shear}$=207 KN)

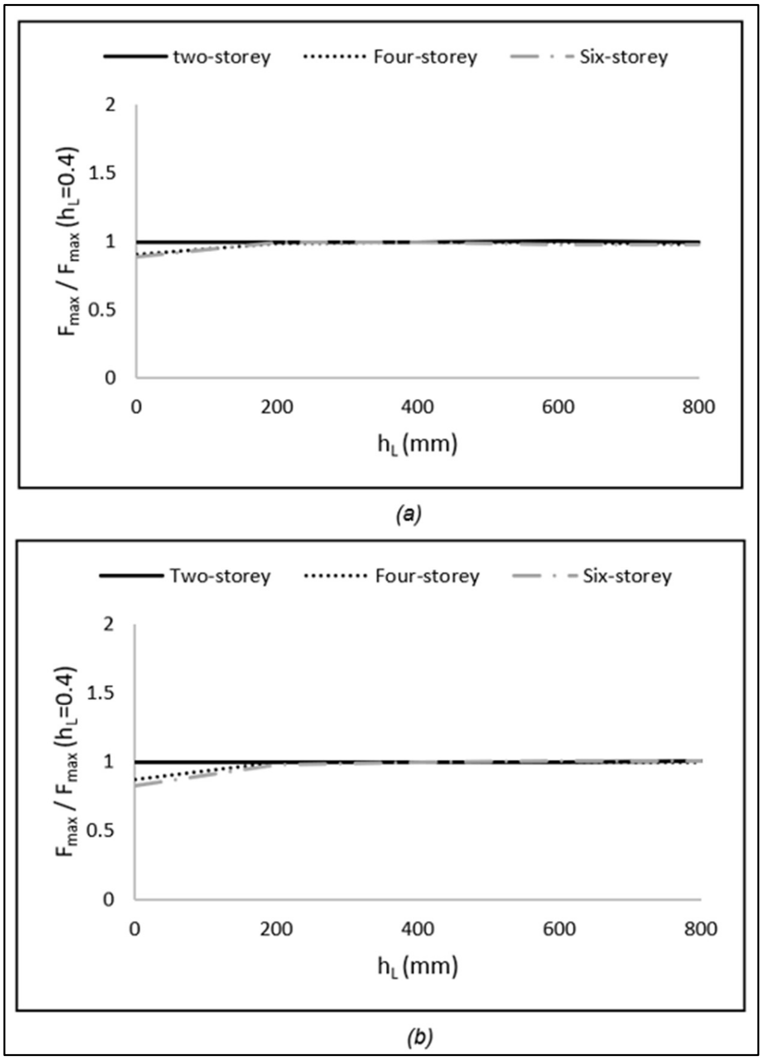

Figure 3.13*: peak load vs lintel's height for case #W1a (a) and case #W1b (b)*

Increasing the lintel width seems to have a much more significant effect on buildings with increased number of storeys. For example, an increase in peak load of up to 20% is observed for the six-storey shearwall by increasing the lintel width from 1.6 m to 2.4 m, while no effect was observed for a two-storey shearwall with similar configurations. The parapet seems to have a very significant influence on the peak load, where it can be observed that the peak load is reduced by the 43% and 33% for two- and six-storey shearwalls, respectively, when the case with parapet height equal to 1.2 m was compared with that with no parapet (door opening). Figure 3.14 shows that the peak load does not increase beyond a parapet height of 0.8 m, which corresponds to the point where failure occurs in connections.

A noteworthy observation concerns the discrepancies between the experimental and numerical results in the case of parapets. In full-scale tests, cracking at parapet corners triggered sudden drops in capacity, whereas the FE simulations predicted continuous stiffness increase up to connection failure. This divergence arises from the linear-elastic material assumption for panels, which does not capture brittle fracture initiation. While the FE model provided accurate predictions for shearwalls with door openings, its performance for parapet-dominated cases highlights the need for nonlinear fracture mechanics formulations. This limitation is acknowledged and further discussed in Chapter 6.

The vertical load has a significant impact on the peak load, especially for shearwalls with increased number of storeys and where rocking behaviour is predominant. Doubling the number of hold-down devices (from 1-HD to 2-HD configuration) resulted in a significant increase in peak load (up to 47% for a six-storey shearwall), although the increase is significantly lesser than that corresponding to a doubling of the peak load.

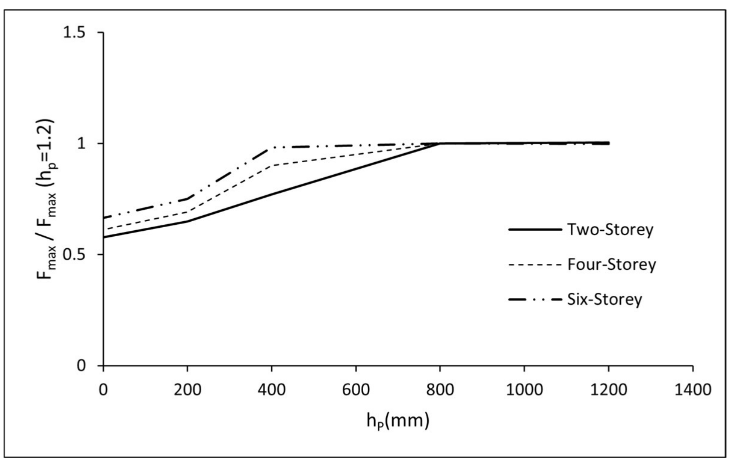

Figure 3.14: *Peak load vs the parapet's height (case #W4)*

The height of the lintel appears to have a small influence on the overall shearwall stiffness, as shown in Figure 3.15 for case #W1A. The relatively small effect (a reduction of about 10% for four- and six-storey shearwalls between 0.4 m lintel eight and no lintel) could be attributed to the contribution of the parapet in coupling the two wall segments. This coupling effect from the parapet seems to have a significant effect on the stiffness of the shearwall. For example, the stiffness is reduced by 36% and 45% for a two- and six-storey shearwall, respectively, when the parapet height was reduced from 1.2 m to the case of no parapet. From Figure 3.15, it can be observed that the trend is almost constant up to a height equal to 0.4 m and then increases linearly. Unexpectedly, only a moderate increase in stiffness is observed when the double hold-down configuration (HD-2) is considered and compared to that with single hold-down device (HD-1), e.g. up to 27% for a two-storey shearwall but only 10% for a six-storey. This behaviour may be attributed to the presence of vertical load.

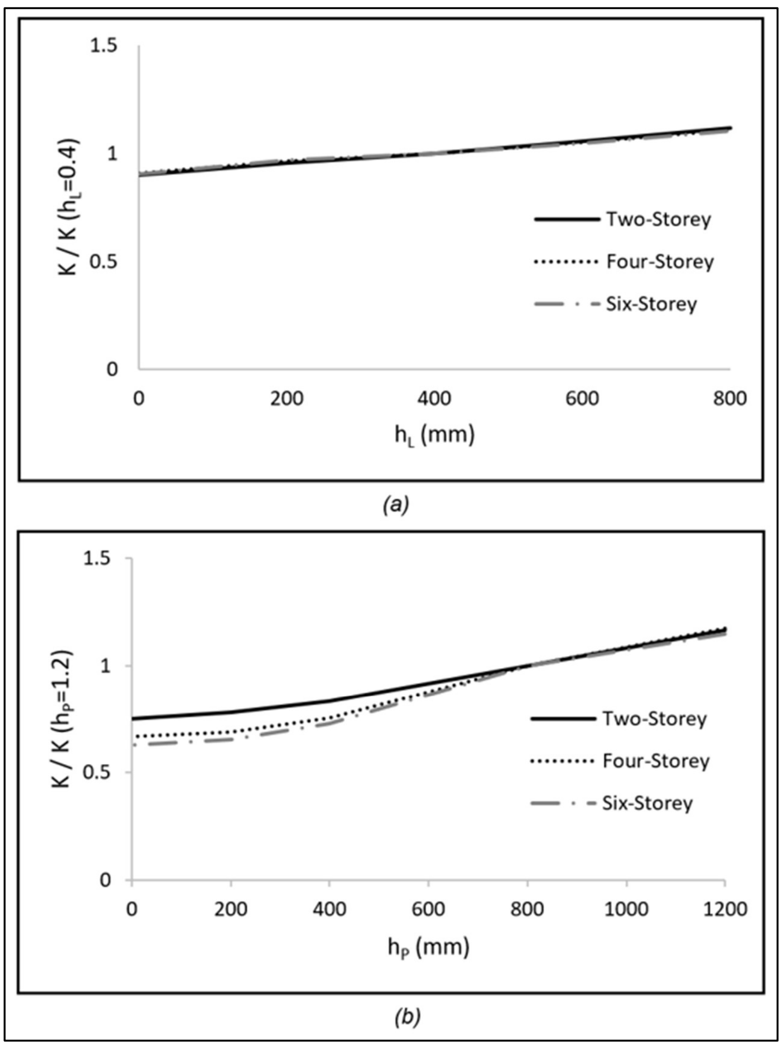

Figure 3.15*: Stiffness vs lintel height (case #W1a) (a); stiffness vs parapet height (case #W4) (b).*

3.5.1.2 Shearwalls with door openings

The results from the sensitivity analysis are reported in Table 3.10. In general, it can be observed that a significant shift in failure mode, due to increase in lintel height, is observed when door openings are investigated. The failure mechanism is mostly related to CLT panel, especially at the lintel beam member, rather than at the mechanical anchors, as was observed when window openings were considered. This further emphasizes the important effect of the parapet section on the failure mode. Contrary to the case with window openings, for walls with door openings, the lintel height significantly affects the failure mechanism of the shearwalls.

In general, it is observed that failure occurs in the lintel when intermediate values of lintel heights are used, while for small values of lintel heights, the wall segments behaved like two cantilevered walls and the failure occurred in hold-downs. For large values of lintel heights, the shearwalls behave mostly like a single-panel shearwall with no opening and the failure occurred in the mechanical anchors. The lintel height was also observed to have a great influence on the peak load, as shown in Figure 3.16. Figure 3.17 presents the distribution of axial and shear internal forces of a four-storey shearwall for case #D1b with 0.4 m lintel height.

Table 3.10: *Failure mode and the variation of lateral stiffness, peak load and ultimate inter-storey drift from the reference for shearwall with door openings*

Case	Target parameter	Variable value	Two-Storey			Four-Storey			Six-Storey		
			Failure	**F_{max} (VAR)**	**K (VAR)**	**Failure**	**F_{max} (VAR)**	**K (VAR)**	**Failure**	**F_{max} (VAR)**	**K (VAR)**
#D1a	Lintel's height h_L [m] ($w_L = 1.6m$)	0.0	HD	162 **(-26%)**	3.97 **(-29%)**	HD	106 **(-39%)**	1.49 **(-44%)**	HD	85 **(-47%)**	0.73 **(-55%)**
		0.2	HD	194 **(-11%)**	4.54 **(-19%)**	L-A	138 **(-20%)**	1.97 **(-26%)**	L-A	117 **(-27%)**	1.1 **(-32%)**
		0.4	L-A	219	5.58	L-A	172	2.65	L-A	160	1.62
		0.6	L-A	284 **(30%)**	6.4 **(15%)**	HD	241 **(40%)**	3.11 **(17%)**	HD	222 **(39%)**	2 **(23%)**
		0.8	AB-S	308 **(40%)**	7.21 **(29%)**	HD	255 **(48%)**	3.67 **(38%)**	HD	224 **(40%)**	2.41 **(49%)**
#D1b	Lintel's height h_L [m] ($w_L = 2.4m$)	0.0	HD	161 **(-18%)**	3.94 **(-28%)**	HD	106 **(-30%)**	1.49 **(-41%)**	HD	85 **(-44%)**	0.72 **(-50%)**
		0.2	HD	190 **(-3%)**	4.59 **(-17%)**	L-A	127 **(-16%)**	2.07 **(-19%)**	L-A	103 **(-32%)**	1.12 **(-22%)**
		0.4	L-A	196	5.51	L-A	152	2.54	L-A	152	1.43
		0.6	L-A	231 **(18%)**	6.27 **(14%)**	L-A	218 **(43%)**	2.95 **(16%)**	L-A	211 **(39%)**	1.85 **(29%)**
		0.8	AB-S	311 **(58%)**	6.81 **(24%)**	L-A	257 **(69%)**	3.49 **(37%)**	HD	256 **(69%)**	2.26 **(58%)**
#D2	Lintel's width w_L [m]	**1.6**	L-A	219	5.58	L-A	172	2.65	L-A	160	1.62
		2.4	L-A	196 **(-10%)**	5.51 **(-1%)**	L-A	152 **(-12%)**	2.54 **(-4%)**	L-A	152 **(-5%)**	1.43 **(-12%)**
#D4	Width of the wall segments w_S [m]	0.6	L-A	62 **(-72%)**	0.67 **(-88%)**	L-A	55 **(-68%)**	0.35 **(-87%)**	HD	50 **(-69%)**	0.23 **(-86%)**
		1.2	L-A	102 **(-53%)**	1.63 **(-71%)**	L-A	82 **(-53%)**	0.78 **(-71%)**	L-A	83 **(-48%)**	0.49 **(-70%)**
		2.4	L-A	219	5.58	L-A	172	2.65	L-A	160	1.62
#D5	Vertical load q [kN/m]	0.0	L-A	185 **(-16%)**	4.07 **(-27%)**	L-A	142 **(-18%)**	1.49 **(-44%)**	HD	120 **(-25%)**	0.77 **(-52%)**
		15.0	L-A	219	5.58	L-A	172	2.65	L-A	160	1.62
		30.0	L-A	247 **(13%)**	6.87 **(23%)**	L-A	201 **(17%)**	3.3 **(25%)**	L-A	205 **(28%)**	1.84 **(14%)**
#D6	HD configuration [-]	A-HD	L-A	189 **(-14%)**	5.86 **(5%)**	L-A	172 **(0%)**	2.79 **(5%)**	L-A	163 **(2%)**	1.74 **(7%)**
		1-HD	L-A	219	5.58	L-A	172	2.65	L-A	160	1.62
		2-HD	L-A	280 **(27%)**	7.27 **(30%)**	PA	207 **(20%)**	3.15 **(19%)**	PA	171 **(7%)**	1.88 **(16%)**

F_{max} : Peak load (KN); K: Lateral stiffness (KN/mm); HD: failure in hold-down; AB-S: Failure in angle brackets due to shear load; AB-T: Failure in angle brackets due to tensile load; L-A: Axial failure in the lintel beam

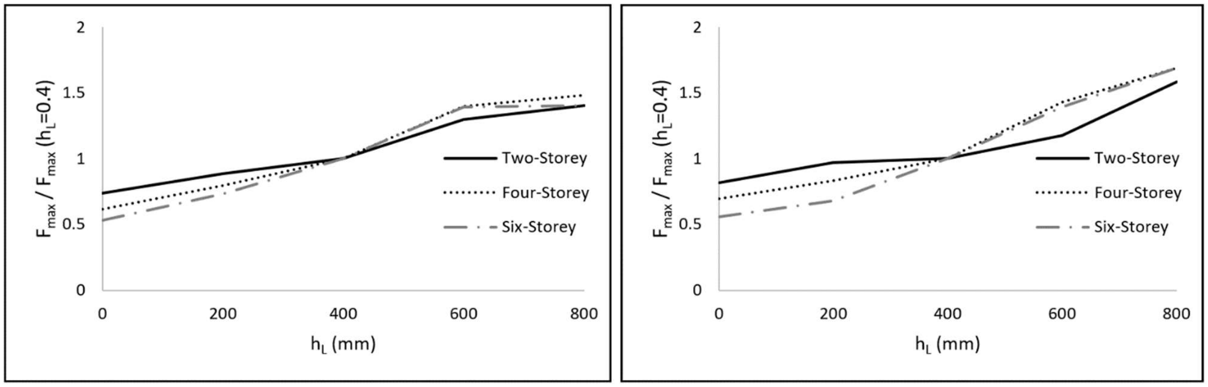

(a) *(b)*

Figure 3.16*: Peak load vs lintel's height for case #D1a and #D1b*

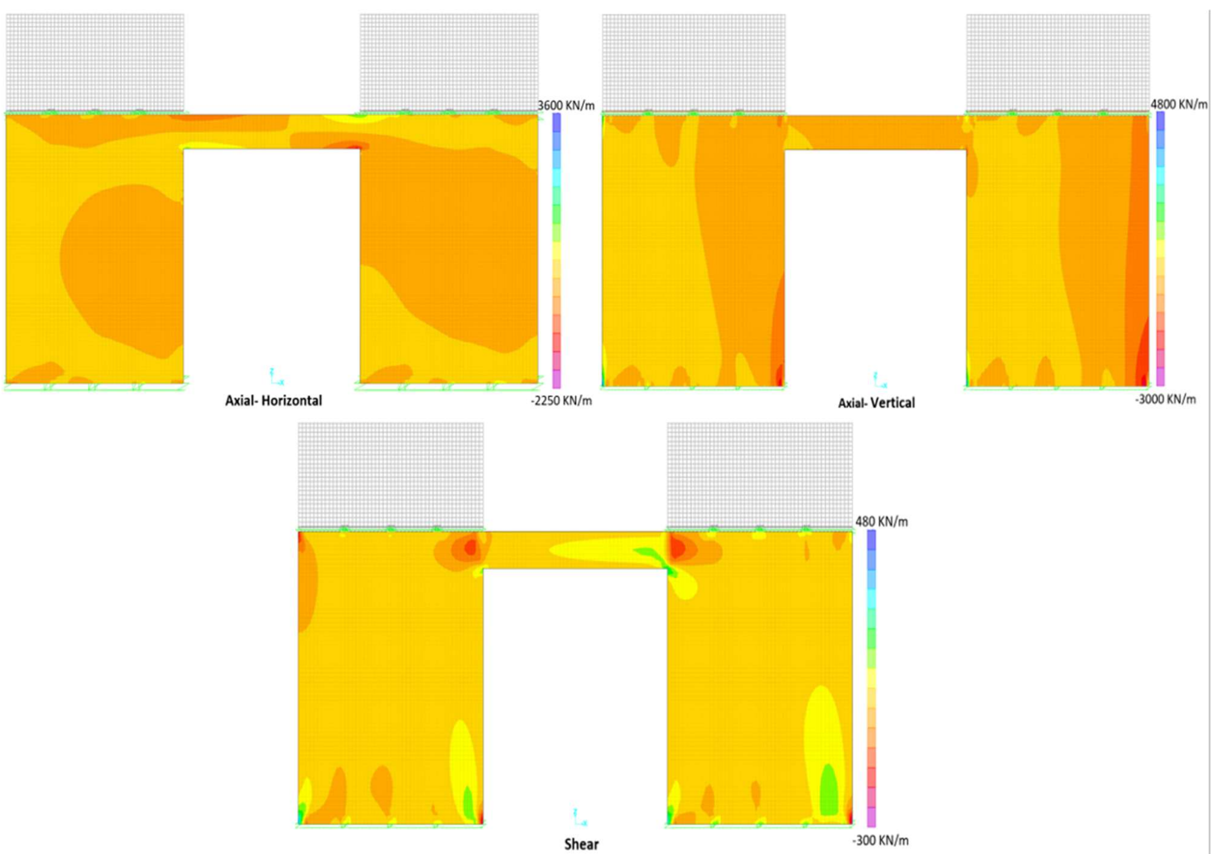

Figure 3.17: *Distribution of internal force of 4-storey shearwall obtained from case# D1b with 0.4 m lintel height ($F_{base\ shear}$=152 KN)*

It was observed that the effect of vertical gravity load on the peak load for four- and six-storey shearwalls with door openings is less significant than that observed for walls with window openings. This can possibly be attributed to the effect of both parapet and lintel beams resulting in the shearwall acting as a monolithic wall for walls with window openings. Similarly, the effect of considering double rather than single hold-down configurations is less significant in the case of walls with door openings compared to that with window openings. The effect of lintel height on the stiffness is very significant and follows an almost linear relationship, as shown in Figure 3.18. The change towards double hold-down configuration moderately increased the stiffness.

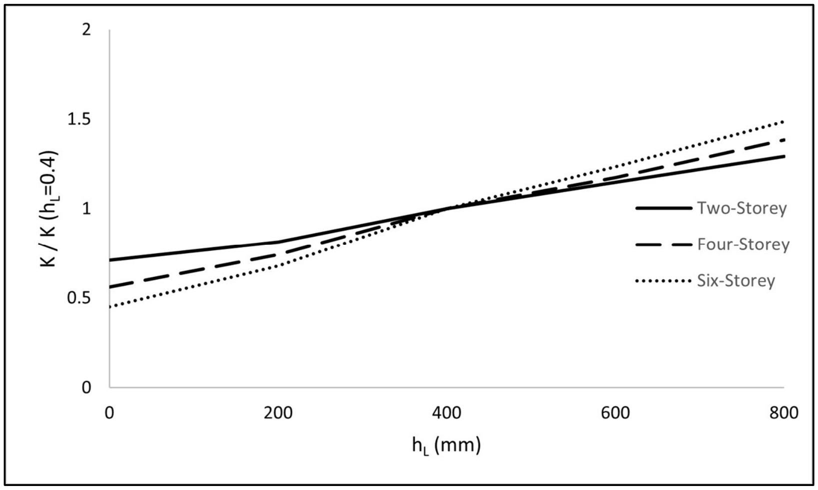

Figure 3.18*: Stiffness vs lintel's height (case #D1a)*

3.5.2 Monolithic versus Segmented shearwalls with openings

In this section, a comparison between the mechanical behaviour of multi-storey shearwalls, where openings are assembled with separated elements or cut out of the panel, is presented.

For all MSW vs SSW comparisons, anchor layouts, spacings, and panel dimensions were held identical; only the construction assumption (continuous cut-out vs assembled segments) was changed, ensuring the reported differences isolate monolithic continuity effects.

For each configuration presented in section 3.5 and summarized in Table 3.8, push-over curves for both SSW and MSW cases were obtained from the numerical analyses. The ratios between the values of stiffness (R_K) and peak load (R_F) obtained from MSW and SSW cases were calculated, as outlined in Equation 7.

$$R_K = \frac{K_{MSW}}{K_{SSW}};\ R_F = \frac{F_{max,MSW}}{F_{max,SSW}} \tag{7}$$

where K_{MSW}, K_{SSW}, $F_{max,MSW}$ and $F_{max,SSW}$ are the values of lateral stiffness and peak load related to MSW and SSW models, respectively. The push-over curves obtained from the four different configurations, as presented in Figure 3.19, are reported in Figure 3.20.

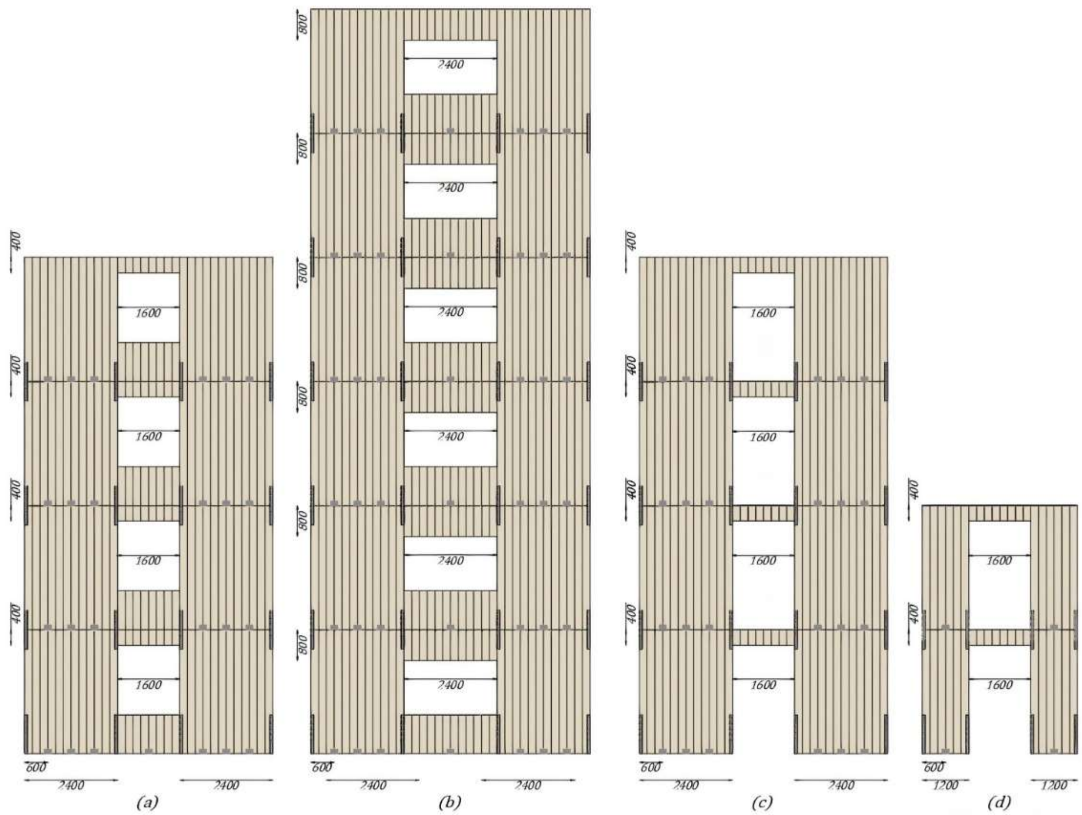

Figure 3.19*: Four cases examples. Case #W1a with h_L=0.4 m, four-storey, (a); Case #W1b with h_P=0.8 m, six-storey, (b); Case #D1a with h_L=0.4 m, four-storey (c); Case #D4 with w_S=1.2 m, two-storey (d)*

Table 3.11 and Table 3.12 present the ratio of stiffness (R_K) and peak load (R_F) between the MSW and SSW cases for shearwalls with window and door openings, respectively. The values of the peak load and lateral stiffness for all MSW cases are reported in Tables 3.9 and 12, whereas the values of peak load $\mathrm{F_{max,SSW}}$ and lateral stiffness $\mathrm{K_{SSW}}$ for the SSW models are shown in Tables 3.11 and 3.12.

In general, it can be observed that the MSW models with window openings resulted in strength and stiffness values that are significantly higher than those obtained in case of segmented shearwall with identical configurations.

In the vast majority of the investigated cases, a ratio above 2.0 (an increase of more than 100%) could be observed. It can be noted that the observed difference between the MSW and SSW models is more pronounced when the number of storeys is increased.

The increase in terms of peak load can reach a value of nearly 7 times (case #W4 w_s=0.6 m, six-storey) that observed when using the segmented shearwall assumption. The minimum increase observed for the range of parameters used is 1.46 and 1.50 times for peak load and stiffness, respectively, which can still be considered very significant on design decisions.

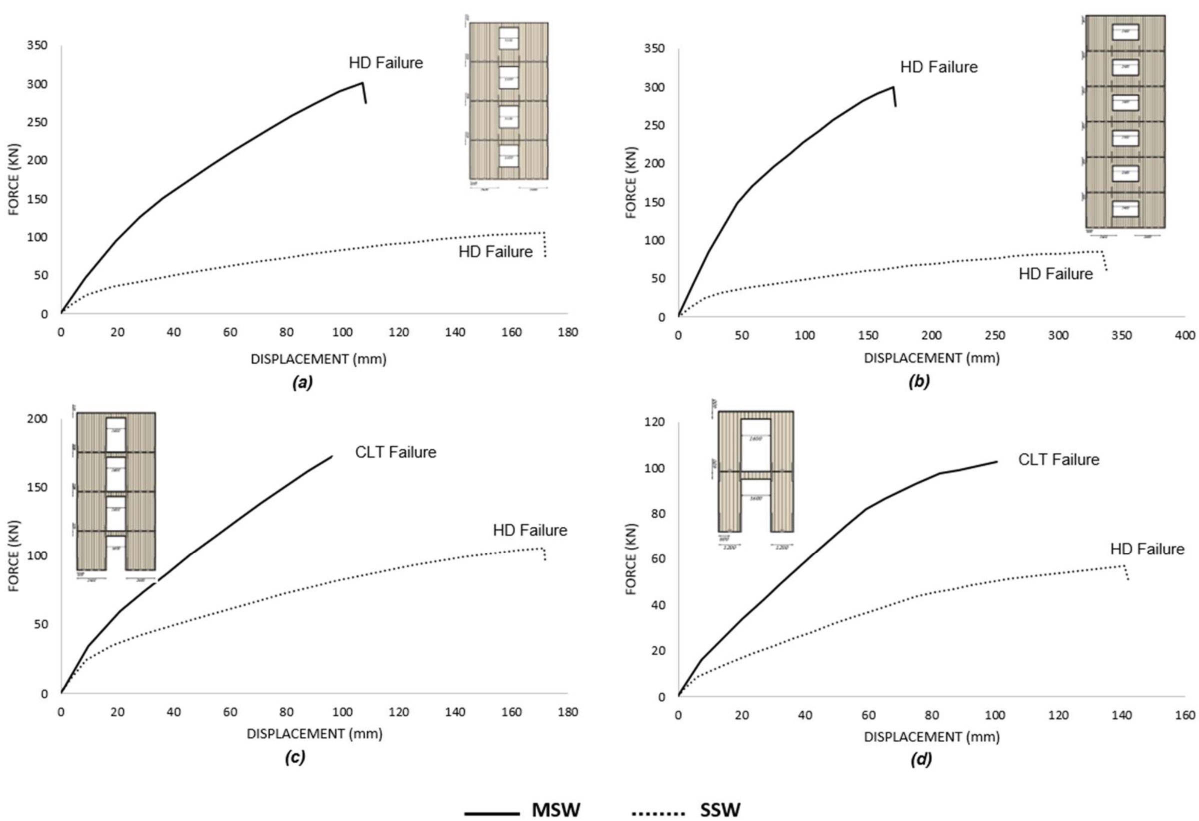

Figure 3.20*: Push-over curves for the four cases examples by considering a MSW and a SSW behaviour*

The increase in the ratios appears to be more pronounced for parapet than lintel height, which confirms that the coupling effect of the parapet is much more significant. This is due to the fact that when the contribution of lintels is investigated (cases #W1a and #W1b) the height of parapet is kept constant and equal to 1.0 m. Conversely, when the contribution of parapet is analysed the height of lintel is equal to 0.4 m in all cases #W3. Since the coupling effect of lintel of parapet is strictly related to their shear and bending stiffness, the greater height of parapets than lintels causes a higher contribution.

As shown in Figure 3.21, the peak load ratio (R_F) increases from 1.30 to 2.25 for two-storey shearwalls and from 1.95 to 2.93 for six-storey shearwalls, when the parapet height increases from zero to 0.8 m. A constant value of the peak ratio is observed for values of parapet height greater than 0.8 m, which corresponds to the shift to failure occurring in the connections.

Table 3.11: *Ratio of peak load $\mathbf{R_F}$ and stiffness $\mathbf{R_K}$ of MSW to SSW for shearwalls with window openings*

Case	Target parameter	Variable value	Two-Storey				Four-Storey				Six-Storey			
			$\mathbf{F_{max,SSW}}$**[KN]**	$\mathbf{R_F}$	K_{SSW}**[KN/m]**	$\mathbf{R_K}$	$\mathbf{F_{max,SSW}}$**[KN]**	$\mathbf{R_F}$	K_{SSW}**[KN/m]**	$\mathbf{R_K}$	$\mathbf{F_{max,SSW}}$**[KN]**	$\mathbf{R_F}$	K_{SSW}**[KN/m]**	$\mathbf{R_K}$
#W1a	Lintel's height h_L [m] ($w_L = 1.6\ m$)	0.0	162	2.26	3.97	2.02	106	2.58	1.49	2.74	85	2.62	0.73	3.60
		0.2	162	2.26	3.97	2.13	106	2.80	1.49	2.95	85	2.93	0.73	3.93
		0.4	162	2.26	3.97	2.22	106	2.84	1.49	3.05	85	2.94	0.73	4.01
		0.6	162	2.26	3.97	2.32	106	2.84	1.49	3.17	85	2.88	0.73	4.21
		0.8	162	2.26	3.97	2.41	106	2.77	1.49	3.33	85	2.88	0.73	4.36
#W1b	Lintel's height h_L [m] ($w_L = 2.4\ m$)	0.0	161	2.26	3.94	1.99	106	2.88	1.49	2.72	85	2.92	0.72	3.79
		0.2	161	2.26	3.94	2.12	106	3.3	1.49	2.88	85	3.44	0.72	4.07
		0.4	161	2.26	3.94	2.22	106	3.3	1.49	2.99	85	3.51	0.72	4.19
		0.6	161	2.26	3.94	2.34	106	3.29	1.49	3.14	85	3.53	0.72	4.4
		0.8	161	2.26	3.94	2.48	106	3.29	1.49	3.32	85	3.52	0.72	4.64
#W2	Lintel's width w_L [m]	**1.6**	162	2.26	3.97	2.22	106	2.84	1.49	3.05	85	2.94	0.73	4.01
		2.4	161	2.26	3.94	2.21	106	3.30	1.49	2.99	85	3.51	0.73	4.19
#W3	Parapet's height h_P [m]	0.0	162	1.30	3.97	1.44	106	1.73	1.49	1.73	85	1.95	0.73	2.22
		0.2	162	1.46	3.97	1.50	106	1.95	1.49	1.79	85	2.20	0.73	2.32
		0.4	162	1.73	3.97	1.60	106	2.54	1.49	1.95	85	2.88	0.73	2.58
		0.8	162	2.25	3.97	1.93	106	2.82	1.49	2.60	85	2.94	0.73	3.54
		1.2	162	2.26	3.97	2.25	106	2.84	1.49	3.05	85	2.93	0.73	4.07
#W4	Width of the wall segments w_S [m]	0.6	17	5.38	0.12	11.75	10.3	6.30	0.03	28.33	7.8	6.79	0.013	36
		1.2	57	2.78	0.75	4.53	35.7	3.91	0.23	7.09	27.4	4.03	0.1	9.10
		2.4	162	2.26	3.97	2.22	106	2.84	1.49	3.05	85	2.94	0.73	4.01
#W5	Vertical load q [kN/m]	0.0	132	2.54	2.64	2.72	74	2.66	0.62	4.15	51	2.74	0.22	5.14
		15.0	162	2.26	3.97	2.22	106	2.84	1.49	3.05	85	2.94	0.73	4.01
		30.0	190	1.94	5.19	1.88	137	2.53	2.18	2.34	117	2.81	1.04	3.15
#W6	HD configuration [-]	A-HD	128	2.86	3.35	2.96	88	3.02	1.28	4.54	73	3.12	0.66	5.38
		1-HD	162	2.26	3.97	2.22	106	2.84	1.49	3.05	85	2.94	0.73	4.01
		2-HD	290	2.31	4.87	2.30	176	2.25	1.49	3.64	133	2.76	0.66	4.88

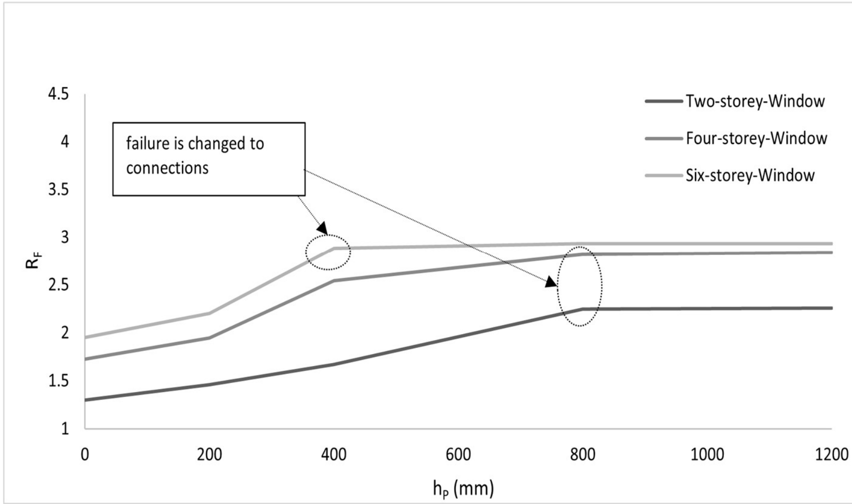

Figure 3.21: *Values of R_F as a function of parapet's height (case #W3) in shearwalls with window openings*

From Table 3.12, it can be observed that the increases in stiffness and peak load values are relatively smaller for shearwalls with door openings than those obtained from walls with window openings (Table 3.11), thereby confirming the important contribution of the parapet.

When considering peak load ratios, Figure 3.22 corroborates previously established observation that the effect of lintel height is much more pronounced in shearwalls with door openings than window openings. Although the absolute value of peak ratio is higher for walls with window opening, a much lower level of increase is observed as a function of lintel height increase. This is attributed to the contribution of the parapet which, as shown earlier, has a much more dominant effect on coupling the two wall segments.

Table 3.12: Ratio of peak load R_F and stiffness R_K of MSW related to SSW with door openings

Case	Target parameter	Variable value	Two-Storey				Four-Storey				Six-Storey			
			$F_{max,SSW}$[KN]	R_F	K_{SSW}[KN/m]	R_K	$F_{max,SSW}$[KN]	R_F	K_{SSW}[KN/m]	R_K	$F_{max,SSW}$[KN]	R_F	K_{SSW}[KN/m]	R_K
#D1 a	Lintel's height h_L [m] ($w_L = 1.6\ m$)	0.0	162	-	3.97	-	106	-	1.49	-	85	-	0.73	-
		0.2	162	1.20	3.97	1.14	106	1.30	1.49	1.32	85	1.38	0.73	1.51
		0.4	162	1.35	3.97	1.41	106	1.63	1.49	1.78	85	1.88	0.73	2.22
		0.6	162	1.75	3.97	1.61	106	2.27	1.49	2.09	85	2.62	0.73	2.74
		0.8	162	1.90	3.97	1.82	106	2.41	1.49	2.46	85	2.64	0.73	3.30
#D1 b	Lintel's height h_L [m] ($w_L = 2.4\ m$)	0.0	161	-	3.94	-	106	-	1.49	-	85	-	0.72	-
		0.2	161	1.17	3.94	1.17	106	1.20	1.49	1.39	85	1.21	0.72	1.56
		0.4	161	1.21	3.94	1.41	106	1.44	1.49	1.70	85	1.78	0.72	1.99
		0.6	161	1.42	3.94	1.60	106	2.05	1.49	1.98	85	2.49	0.72	2.57
		0.8	161	1.91	3.94	1.74	106	2.43	1.49	2.34	85	3.01	0.72	3.14
#D2	Lintel's width w_L [m]	**1.6**	162	1.35	3.97	1.41	106	1.63	1.49	1.78	85	1.88	0.73	2.22
		2.4	161	1.22	3.94	1.40	106	1.44	1.49	1.7	85	1.78	0.73	1.99
#D4	Width of the wall segments w_S [m]	0.6	17	3.64	0.12	5.58	10.3	5.31	0.03	11.67	7.8	6.44	0.013	2300
		1.2	57	1.81	0.75	2.17	35.7	2.29	0.23	3.39	27.4	3.04	0.1	4.90
		2.4	162	1.35	3.97	1.41	106	1.63	1.49	1.78	85	1.88	0.73	2.22
#D5	Vertical load q [kN/m]	0.0	132	1.41	2.64	1.54	74	1.92	0.62	2.40	51	2.35	0.22	3.50
		15.0	162	1.35	3.97	1.41	106	1.63	1.49	1.78	85	1.88	0.73	2.22
		30.0	190	1.30	5.19	1.32	137	1.46	2.18	1.51	117	1.75	1.04	1.77
#D6	HD configuration [-]	A-HD	128	1.47	3.35	1.75	88	1.94	1.28	2.18	73	2.25	0.66	2.64
		1-HD	162	1.35	3.97	1.41	106	1.63	1.49	1.80	85	1.88	0.73	2.22
		2-HD	290	1.04	4.87	1.49	176	1.18	1.49	2.11	133	1.29	0.66	2.85

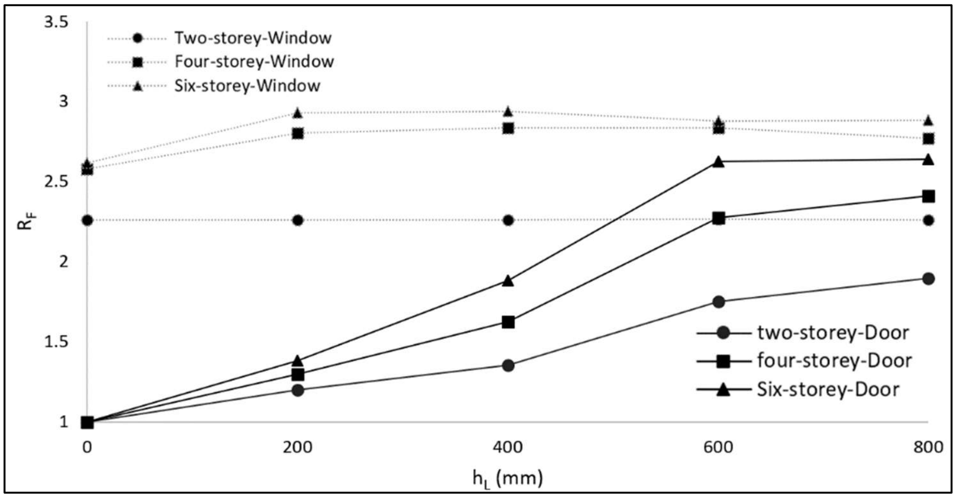

Figure 3.22: *Values of R_F as a function of lintel's height (case #D1a) in shearwalls for both window and door openings*

The results for shearwalls with door openings also show that a significant increase in stiffness and peak load is obtained when openings are cut out of the panels rather than obtained by assembling separate elements.

Despite the fact that the interaction between the wall segments and lintels beams or parapets is typically ignored by designers, an alternative analysis method which takes into account the contributions of these elements is shown here to lead to increased design efficiency and reduction of tensile loads on hold-downs. This increased efficiency is particularly evident in the case of shearwalls with window openings.

CHAPTER 4- EXPERIMENTAL CAMPAIGN (PART I) – CLT BEAMS WITH VERTICAL OUTER LAMINATION

4.1 Introduction

Research on CLT shearwalls has traditionally focused on the performance of mechanical connections that transfer shear and overturning loads, leveraging the panel's high in-plane stiffness and the energy-absorbing capacity of ductile connectors, especially in seismic regions. However, when openings are introduced, the behaviour of the shearwall becomes more complex because the panels themselves contribute significantly to deformation, and high stress concentrations, particularly at the corners, can lead to premature, brittle failures.

In monolithic CLT shearwalls with cut-out openings, the structural continuity between the wall segments and the lintel beams or parapets produces behaviour more akin to a framed system rather than a set of independent cantilevers. Experimental observations have shown that cracks can initiate and propagate around the opening corners, especially in the lintel region. The unique mechanical response of lintel beams with vertical outer layers is typically less favorable for bending compared to conventional horizontal configurations and impacts shear stress distribution and failure modes.

This section presents the results of the experimental study conducted on a total of 42 CLT beams (i.e. 36 with vertical and 6 with horizontal outer laminations) aimed at investigating their failure modes and mechanical behaviour, particularly those with vertical outer laminations. The inclusion of beams with horizontal outer laminations, selected from the same batch as those with vertical outer laminations, was aimed at highlighting potential differences in the behaviour and failure mechanism between the two layouts.

Although the beam tests reproduce the lamination layups of lintel elements in monolithic walls, the boundary conditions differ. In the experimental program, beams were tested under simple supports with four-point bending, whereas lintels within shearwalls experience partial fixity at wall-parapet interfaces. These differences imply that absolute stress states in lintels cannot be directly replicated through beam tests. Nevertheless, the beams provide essential material parameters and confirm governing failure modes, making them valuable for calibrating the FE model and interpreting lintel behaviour within the wall system.

4.2 Materials

All beam specimens consisted of E1 stress grade CLT, manufactured by Nordic Structures, and using boards of width, b, equal to 89 mm, in accordance with the PRG 320 standard (ANSI/APA 2019). Two different beam thicknesses, t_{CLT}, corresponding to two different layups, were selected, including 105 mm for 3-ply beams with 35-35-35 lamination layup and 143 mm for 5-ply beams with 35-19-35-19-35 lamination layup.

The effect of the number of horizontal laminations along the beam depth, h, was also investigated by selecting three different depths comprised of a set multiple of the board width. This resulted in beams of 178 mm, 267 mm and 356 mm, corresponding to the number of laminations, m, equal to 2, 3 and 4, respectively. Additionally, a constant depth, equal to 356 mm, was used for the CLT beams with horizontal outer laminations. The cross sections of the tested beams are illustrated in Figure 4.1.

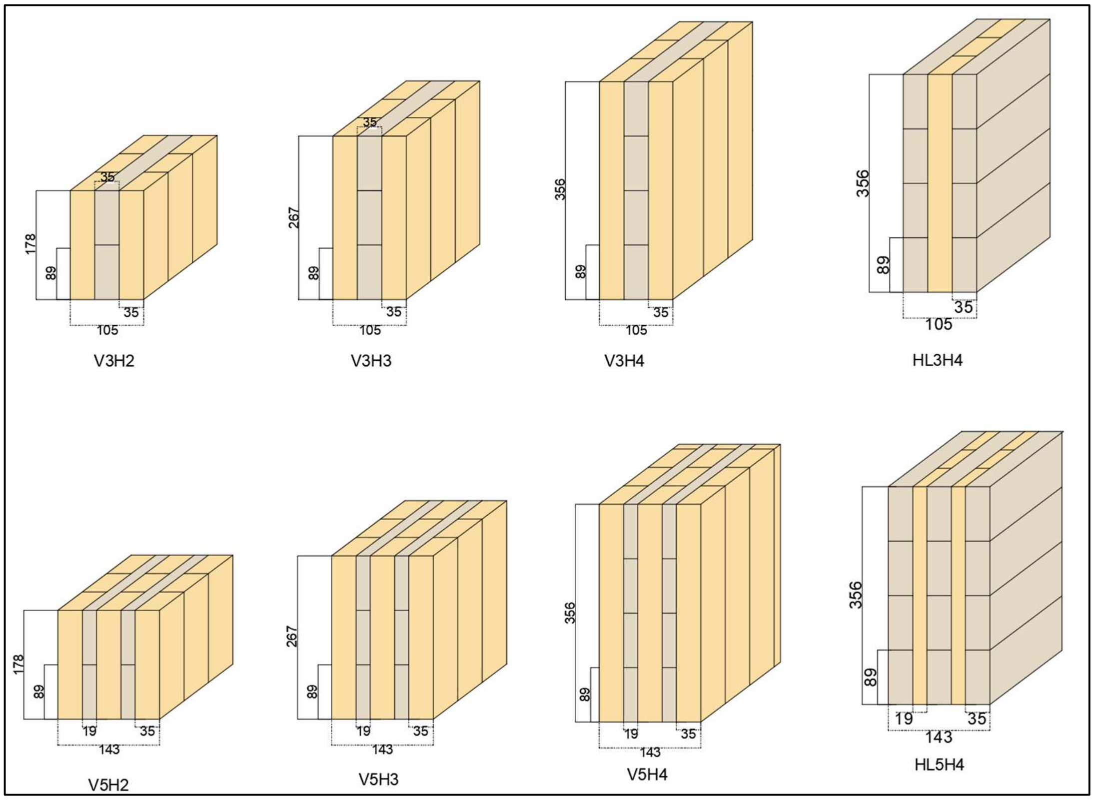

Figure 4.1: *Cross section of beam specimens*

The geometrical dimensions, lamination layup and number of specimens for each configuration are reported in Tables 4.1 and 4.2, for configurations with vertical and horizontal outer laminations, respectively, where the notation ‘‘v” and ‘‘h” refer to the orientation of the lamination being vertical or horizontal, respectively. Also included in Tables 4.1 and 4.2 are the expected failure mode for each configuration based on preliminary analysis and considerations for setup, specimen geometry as well as material properties obtained from the manufacturer’s literature. The variables in the tables include the length of the beam, l, and the total thickness of laminations along the horizontal, t_H, and vertical, t_V, directions. Three repeats were tested of each configuration.

4.3 Test Setup

A symmetrical four-point bending test set-up was adopted for this investigation, with simply-supported boundary conditions simulated by steel rollers at the beam ends, as shown in Figure 4.2. Three different test set-up geometrical configurations were utilized in order to promote either bending or shear failure mode. This was done by varying the span, l_s, and the distance between the loading point from the support, a, as a function of the beam depth, h (Figure 4.3). Test configurations *I* and *II* were selected to promote bending failure in beams with depth smaller than and equal to 356 mm, while test configuration *III* was used to promote shear failure.

Table 4.1: *Configurations of CLT beams with vertical outer laminations*

Beam ID	**Depth**	**Length**	**n.of layers**	**n. of horizontal layers**	**Lay-up**	**Number of horizontal laminations along the depth**	**Total thickness**	**Total Thickness of horizontal layers**	**Test set-up/ l_{led}**	**Expected failure mode**
$[-]$	$h\ [mm]$	$l\ [mm]$	$n\ [-]$	$n_H\ [mm]$	$[-]$	$m\ [-]$	$t_{CLT}\ [mm]$	$t_H\ [mm]$	**[-]-[mm]**	***/-/***
Vb_3P_m2	178	1602	3	1	35v-35h-35v	2	105	35	*I*-420	bending
Vb_5P_m2	178	1602	5	2	35v-19h-35v-19h-35v	2	143	38	*I*-420	bending
Vb_3P_m3	267	2403	3	1	35v-35h-35v	3	105	35	*I* -680	bending
Vb_5P_m3	267	2403	5	2	35v-19h-35v-19h-35v	3	143	38	*I* -680	bending
Vb_3P_m4	356	2670	3	1	35v-35h-35v	4	105	35	*II* -712	bending
Vb_5P_m4	356	2670	5	2	35v-19h-35v-19h-35v	4	143	38	*II* -712	bending
Vs_3P_m2	178	1335	3	1	35v-35h-35v	2	105	35	*III*	shear
Vs_5P_m2	178	1335	5	2	35v-19h-35v-19h-35v	2	143	38	*III*	shear
Vs_3P_m3	267	2003	3	1	35v-35h-35v	3	105	35	*III*	shear
Vs_5P_m3	267	2003	5	2	35v-19h-35v-19h-35v	3	143	38	*III*	shear
Vs_3P_m4	356	2670	3	1	35v-35h-35v	4	105	35	*III*	shear
Vs_5P_m4	356	2670	5	2	35v-19h-35v-19h-35v	4	143	38	*III*	shear

Table 4.2: *Configurations of CLT beams with horizontal outer laminations*

Beam ID	**Depth**	**Length**	**n.of layers**	**n. of horizontal layers**	**Lay-up**	**Number of horizontal laminations along the depth**	**Total thickness**	**Total Thickness of horizontal layers**	**Test set-up/ l_{led}**	**Expected failure mode**
$[-]$	$\boldsymbol{h}\,[\boldsymbol{mm}]$	$\boldsymbol{l}\,[\boldsymbol{mm}]$	$\boldsymbol{n}\,[-]$	$\boldsymbol{n_H}\,[\boldsymbol{mm}]$	$[-]$	$\boldsymbol{m}\,[-]$	$\boldsymbol{t_{CLT}}\,[\boldsymbol{mm}]$	$\boldsymbol{t_H}\,[\boldsymbol{mm}]$	**[-]/[mm]**	***[-]***
Hb_3P_m4	356	2670	3	2	35h-35v-35h	4	105	70	*II*-680	bending
Hb_5P_m4	356	2670	5	3	35h-19v-35h-19v-35h	4	143	105	*II*-680	bending

The load was applied monotonically using a 250 kN hydraulic jack, and the loading procedure followed the EN 408 standard. Two LVDTs were placed at each side of the beam, as shown in Figure 4.3, to measure the relative displacement, w_L, between the centre of the beam and two fixed point located within the null-shear zone, represented by the ledger of length, l_{led}. Load cells were positioned at each support to measure the reactions.

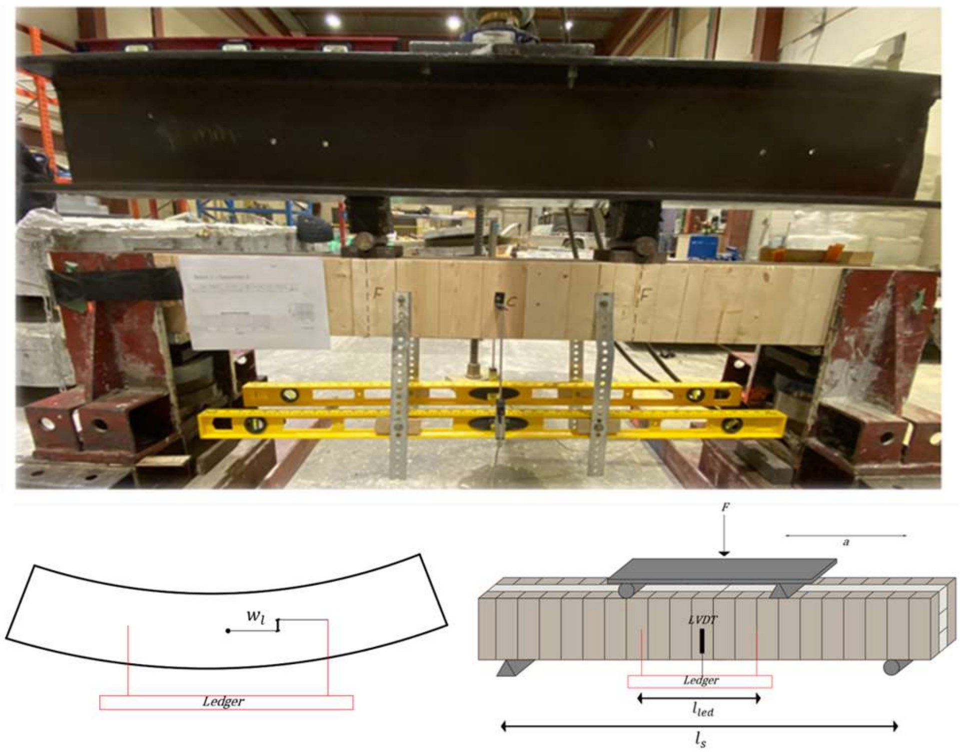

Figure 4.2: *Four-point bending test*

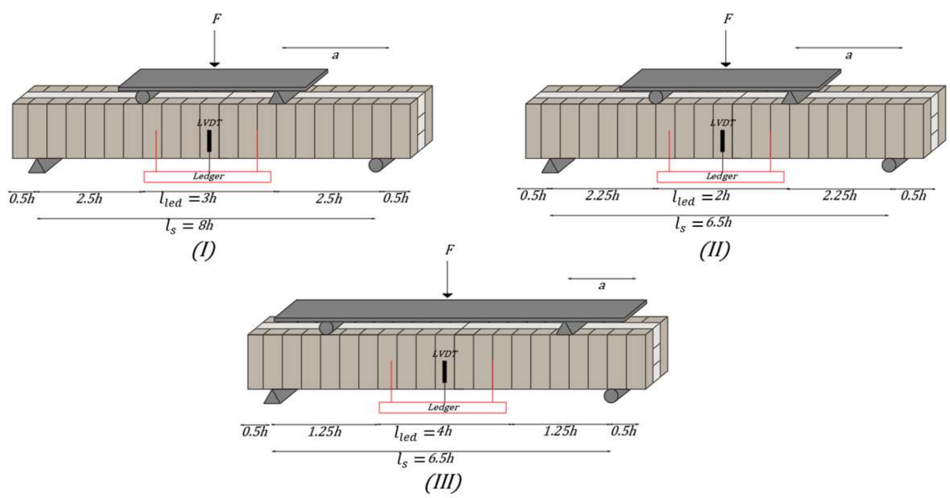

Figure 4.3: *Test set-up configurations I, II and III*

4.4 Results

In this section, the results are reported and discussed in terms of the failure modes observed as well as the general behaviour of the beam specimens. Due to the large number of specimens tested in this study, the results are presented in three groups, namely those with horizontal outer laminations expected to fail in bending as reported in Table 4.3, and beams with vertical outer laminations tested to promote bending or shear failure as reported in Table 4.4 and 4.5, respectively. The former consists of a relatively small number of tests mainly due to the fact that several other studies have already investigated this configuration, while for the latter groups more specimens and test configurations are considered.

Overall, the observed failure modes in beams with horizontal outer laminations aligned closely with findings from previous studies discussed in Chapter 2. For the 3-ply beams, although the anticipated failure mode was bending for all three specimens, two specimens failed in torsional shear (Figure 4.4a), while one failed in bending (Figure 4.4b). Despite that some discrepancy was observed relative to the predicted failure mode, it should be noted that the predicted failure mode is based on preliminary estimates, while more details will be provided in the subsequent sections to evaluate and compare the experimentally observed failure modes. As anticipated, all 5-ply specimens failed in bending within the null-shear region. Table 4.3 reports the results in terms of maximum load, F_{max}, local displacements corresponding to the 10% and the 40% of the maximum load, $W_{L,10}$ and $W_{L,40}$, respectively, as well as the distance X_F from the support, where the failure occurred. Labels *M* and *S* in Table 4.3 refer to whether the actual failure occurred in the moment or shear dominant regions, respectively.

With few exceptions, specimens with vertical outer laminations designed to predominantly fail in bending achieved that failure mechanism. The failure was characterized by crack initiation and development in the inner horizontal laminations at the beam tension face (Figure 4.4), which occurred either in the constant moment zone (14 specimens) or near the load application points (4 specimens), as shown in Figure 4.5a and 4.5b, respectively. As anticipated, no visual cracks or damage were observed in outer vertical layers. Table 4.4 reports the results for this group.

From the results, it can be noted that despite having approximately the same total thickness of horizontal layers between the 3- and 5-ply beams (i.e. 35 mm and 38 mm, respectively), the two 19 mm thick horizontal laminations in the 5-ply beams exhibited significantly higher strength than those obtained from the single 35 mm thick laminations in 3-ply beams. This can potentially be associated with the probability of critical defects in the larger dimension lumber (i.e., volume effects) and system effect due to the fact that two laminations rather than one are present in 5-ply beams.

Promoting shear failure in CLT beams is notoriously difficult, and this is reflected in the range of failure modes obtained for this test series. Both bending and shear failure was observed even though this group was designed to primarily fail in shear. Both torsional and net shear failures were achieved. Figure 4.6a shows an example of a typical bending failure, while representative torsional shear failure is illustrated in Figure 4.6b, where rotation of the outer vertical laminations and separation from the inner layers was observed. A net shear failure was identified in specimens where parallel sliding between the outer laminations was observed, similar to what is depicted in Figure 4.6c. For some of the specimens, distinguishing between bending and net shear failure modes was not obvious (e.g., specimen Vs_5P_m2, shown in Figure 4.7a), while for others it was not clear whether the shear failure mode was related primarily to net shear or torsional shear (e.g., specimen 01 of series Vs_5P_m4, shown in Figure 4.7b). Table 4.5 presents the results from this test series.

Table 4.3: *Result for beams with horizontal outer laminations*

Beam ID	**Specimen**	**Depth**	***n.of layers***	***Total Thickness of horizontal layers***	***Failure mode***	***Maximum load***	***Local displacement at 10% F_{max}***	***Local displacement at 40% F_{max}***	***X_F - Zone***
$[-]$	$[-]$	$h\ [mm]$	$n\ [-]$	$t_H\ [mm]$		F_{max} *[kN]*	$W_{L,10}$ *[mm]*	$W_{L,40}$ *[mm]*	*[mm]/[-]*
Hb_3P_m4	01	356	3	70	Bending	127.5	0.08	0.42	1223/M
	02				Torsional shear	103.1	0.00	0.35	435/S
	03				Torsional shear	122.5	0.00	0.21	10/S
					Average (CoV)	117.7 (11%)			
Hb_5P_m4	01	356	5	105	Bending	186.5	0.05	0.22	1157/M
	02				Bending	175.4	0.00	0.21	1415/M
	03				bending	190.5	0.01	0.23	1205/M
					Average (CoV)	184.1 (4%)			

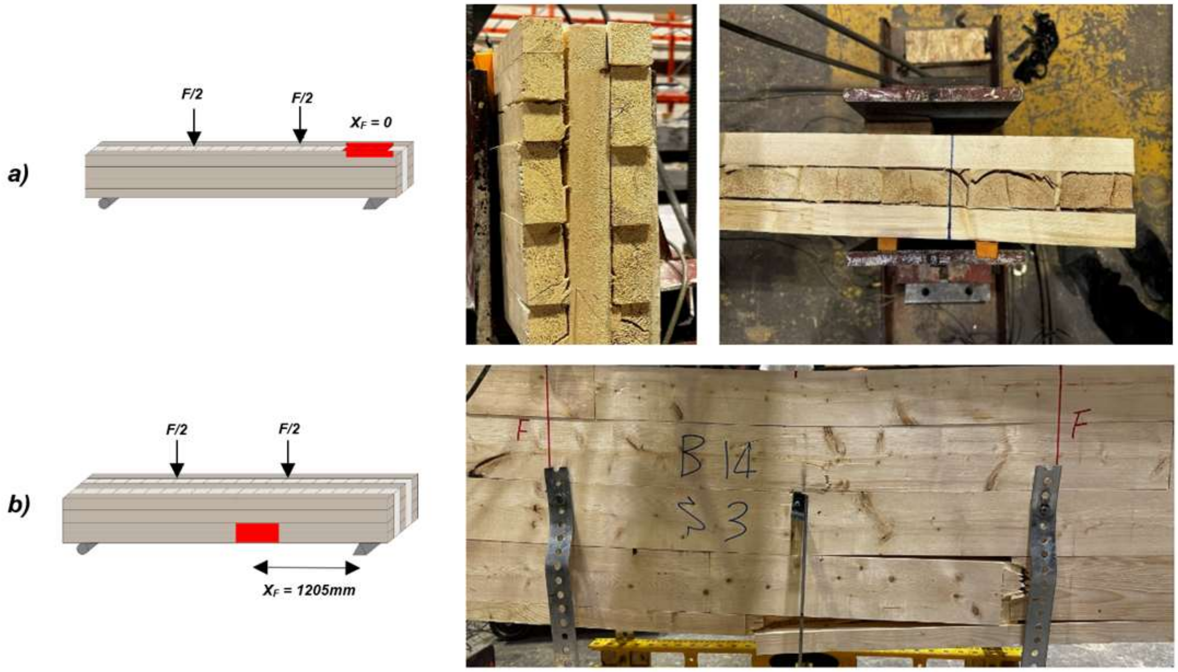

Figure 4.4: *Torsional shear failure for specimen 03 of series Hb_3P_m4 (a) and bending failure for specimen 03 of series Hb_5P_m4 (b)*

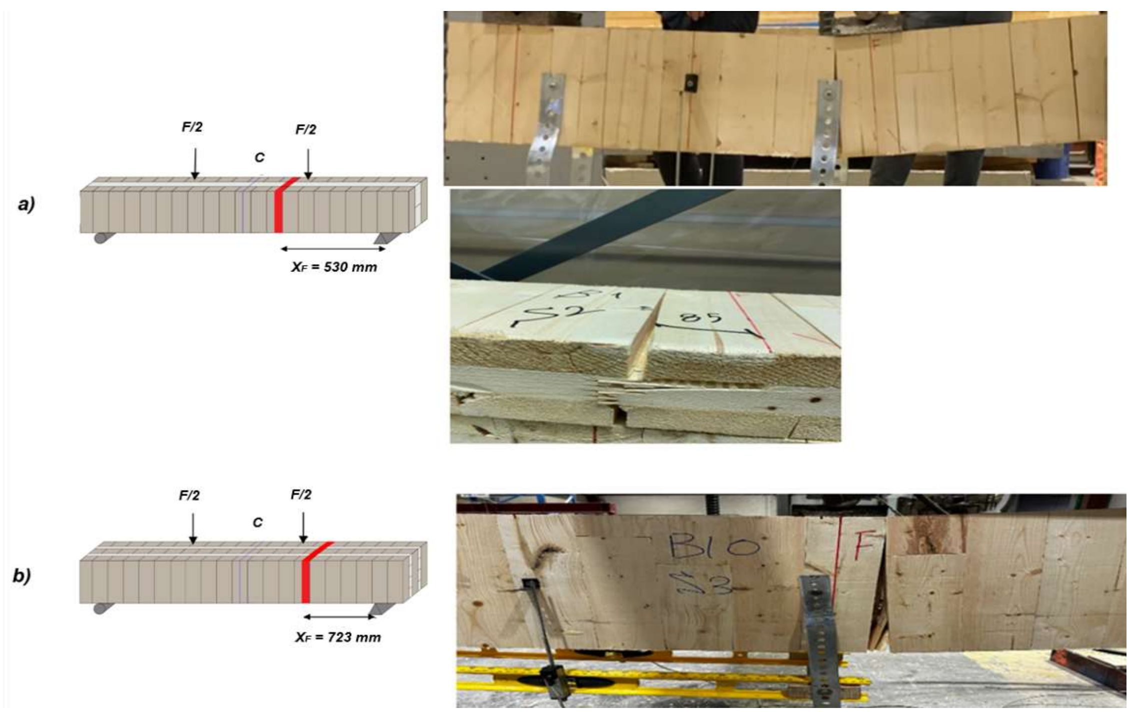

Figure 4.5: *Bending failure for specimen 02 of series Vb_3P_m2 (a) and specimen 03 of series Vb_5P_m4 (b)*

Table 4.4: *Results for beams with vertical outer laminations designed to fail in bending*

Beam ID	**specimen**	**Depth**	***n.of layers***	***Total Thickness of horizontal layers***	***Failure mode***	***Maximum load***	***Local displacement at 10% F_{max}***	***Local displacement at 40% F_{max}***	***X_F - Zone***
$[-]$	$[-]$	h $[mm]$	n $[-]$	t_H $[mm]$		F_{max} *[kN]*	$W_{L,10}$ *[mm]*	$W_{L,40}$ *[mm]*	*[mm]/[-]*
	01				Bending	36.4	0.09	0.28	667/M
Vb_3P_m2	02	178	3	35	Bending	30.9	0.00	0.16	530/M
	03				Bending	32.1	0.01	0.18	1054/S
					Average (CoV)	33.1 (9%)			
	01				Bending	57.6	0.06	0.29	667/M
Vb_5P_m2	02	178	5	38	Bending	70.0	-	-	582/M
	03				bending	53.5	0.05	0.35	580/M
					Average (CoV)	60.4 (14%)			
	01				Bending	63.1	0.00	0.40	1860/S
Vb_3P_m3	02	267	3	35	Bending	57.5	0.00	0.44	712/M
	03				bending	58.9	0.00	0.68	1248/M
					Average (CoV)	52.9 (18%)			
	01				Bending	86.6	0.06	0.60	998/M
Vb_5P_m3	02	267	5	38	Bending	76.4	0.09	0.60	1128/M
	03				bending	67.5	0.04	0.50	1081/M
					Average (CoV)	76.8 (12%)			
	01				Bending	73.1	0.00	0.35	989/M
Vb_3P_m4	02	356	3	35	Bending	69.7	0.00	0.32	801/M
	03				bending	55.7	0.00	0.21	1583/S
					Average (CoV)	66.2 (14%)			
	01				Bending	111.7	-	-	890/M
Vb_5P_m4	02	356	5	38	Bending	115.6	-	-	1185/M
	03				Bending	134.4	0.00	0.42	723/S
					Average (CoV)	120.6 (10%)			

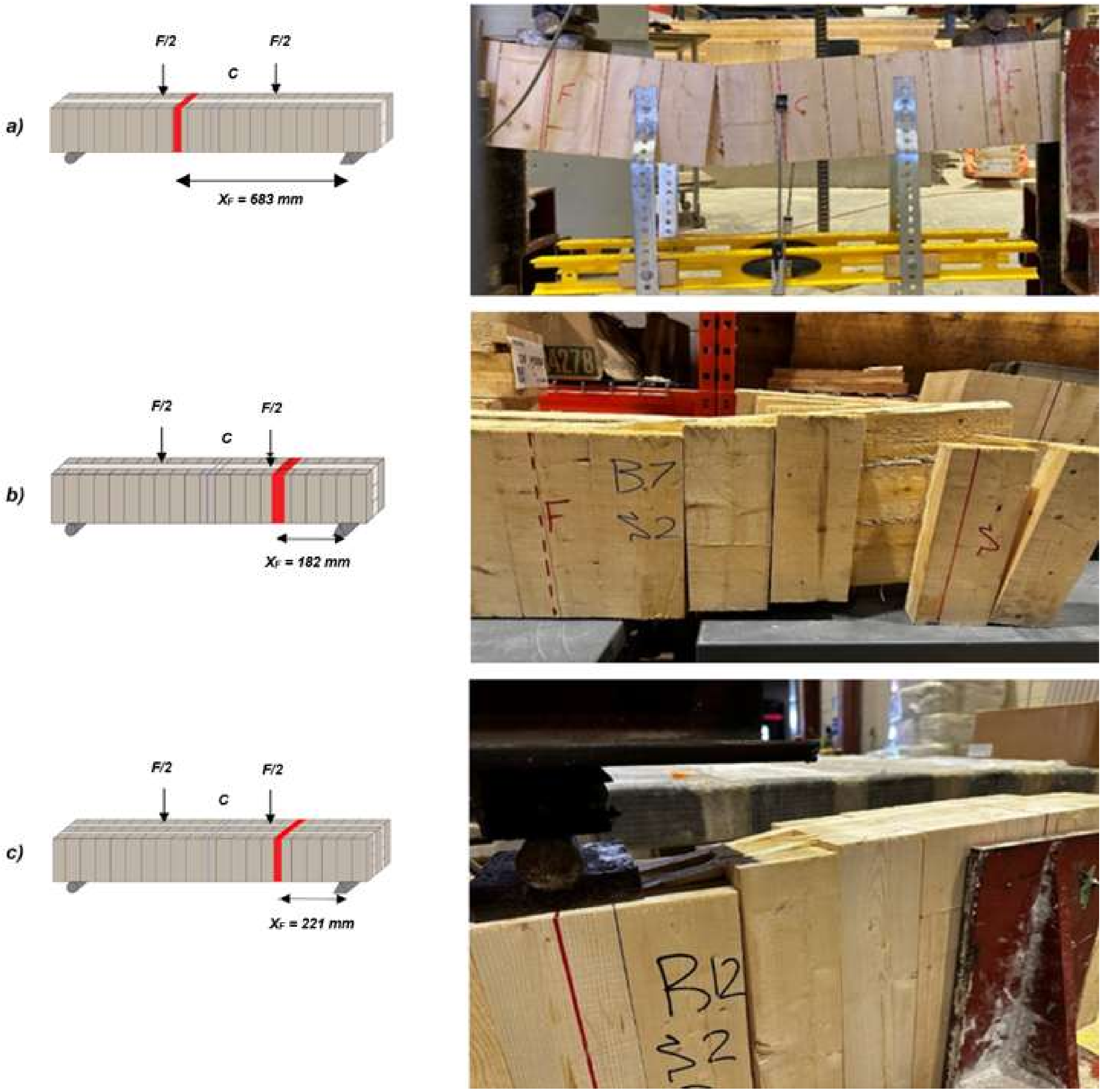

Figure 4.6: *Bending failure for specimen 03 of series Vs_3P_m2 (a), torsional shear failure for specimen 02 of series Vs_3P_m3 (b), and net shear failure mode for specimen 02 of series Vs_5P_m4 (c).*

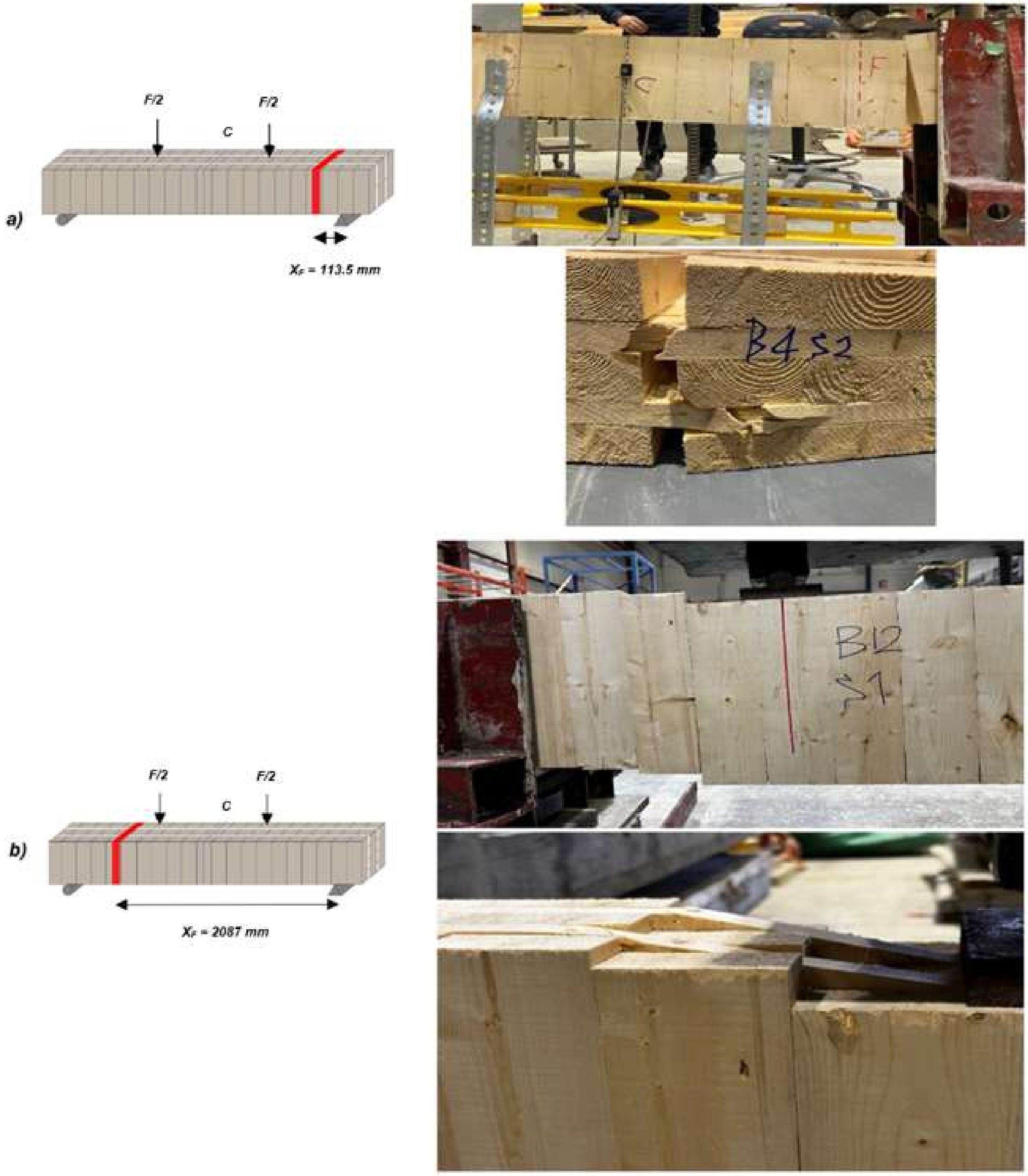

Figure 4.7: *Specimen 02 of series Vs_5P_m2 (a), specimen 01 of series Vs_5P_m4 (b).*

Table 4.5: *Results for beams with vertical outer laminations designed to fail in shear*

Beam ID	**specimen**	**Depth**	***n.of layers***	***Total Thickness of horizontal layers***	***Failure mode***	***Maximum load***	***X_F - Zone***
$[-]$	$[-]$	$h\ [mm]$	$n\ [-]$	$t_H\ [mm]$		F_{max} ***[kN]***	***[mm]/[-]***
Vs_3P_m2	01	178	3	35	Bending	75.3	963/M
	02				Bending	66.1	749/M
	03				Bending	66.3	684/M
					Average (CoV)	69.2 (8%)	
Vs_5P_m2	01	178	5	38	Bending/Net shear	110.8	995/S
	02				Bending/Net shear	99.5	114/S
	03				Net shear	86.1	132/S
					Average (CoV)	98.8 (13%)	
Vs_3P_m3	01	267	3	35	Torsional shear	94.3	1598/S
	02				Torsional shear	93.1	182/S
	03				Torsional shear	98.2	103/S
					Average (CoV)	95.2 (3%)	
Vs_5P_m3	01	267	5	38	Net shear	147.9	1602/S
	02				Net shear	131.8	179/S
	03				Net shear	150	1592/S
					Average (CoV)	143.2 (7%)	
Vs_3P_m4	01	356	3	35	Bending	89.7	1833/M
	02				Torsional shear	108.8	223/S
	03				Bending	101.7	1950/S
					Average (CoV)	95.7 (9%)	
Vs_5P_m4	01	356	5	38	Net shear/Torsional shear	183.9	2087/S
	02				Net shear	189.4	221/S
	03				Bending	174.5	1554/M
					Average (CoV)	186.6 (2%)	

4.5 Determination of strength and stiffness parameters

The analytical models developed for CLT beams with horizontal outer laminations available in literature are adapted in this section to CLT beams with vertical outer laminations in order to propose a methodology to determine the strength and stiffness parameters of CLT beams. The applicability of such methodology is discussed, and the determined parameters are compared with those obtained from CLT beams available in literature and from this study.

4.5.1 Adaptation of existing calculation models to CLT beams with vertical outer laminations

4.5.1.1 Bending strength, gross shear strength and net shear strength

The existing calculation models developed for the determination of bending strength f_m, gross shear strength $f_{v,gross}$ and net shear strength $f_{v,net}$ of CLT beams with horizontal outer laminations can be adopted without any adjustment for CLT beams with vertical outer laminations. The values of resistance are dependant on either the total thickness of the horizontal layers t_H or the total thickness of the beam t_{CLT} without considering the orientation of laminations in the beam lay-up.

The bending strength f_m can be calculated as expressed in Equation 8, while only considering the horizontal layers to be effective and assuming full composite action between longitudinal laminations (Karacabeyli E etal.,2019; Gagnon S et al.,2014).

$$f_m = \frac{6 \cdot M_R}{t_H \cdot h^2} \quad (8)$$

where M_R is the bending moment resistance and h is the depth of the beam.

The shear strength related to the gross-section $f_{v,gross}$ and the shear strength related to the net cross section $f_{v,net}$ can be calculated as proposed by Flaig and Blaß 2013 and expressed in Equations 9 and 10, respectively. According to the beam theory, a parabolic distribution of shear stresses along both the gross and net section of the beam is assumed

(Figure 4.8). The total shear force is uniformly distributed over the longitudinal (i.e. horizontal) laminations, as proposed by Danielsson and Serrano 2018.

$f_{v,gross} = \frac{3}{2}\frac{V_R}{h \cdot t_{CLT}}$ (9)

$f_{v,net} = \frac{3}{2}\frac{V_R}{h \cdot t_{net}}$ (10)

where V_R is the shear load resistance and t_{net} is the effective beam thickness calculated as:

$t_{net} = \min\,(t_H; t_{CLT} - t_H)$ (11)

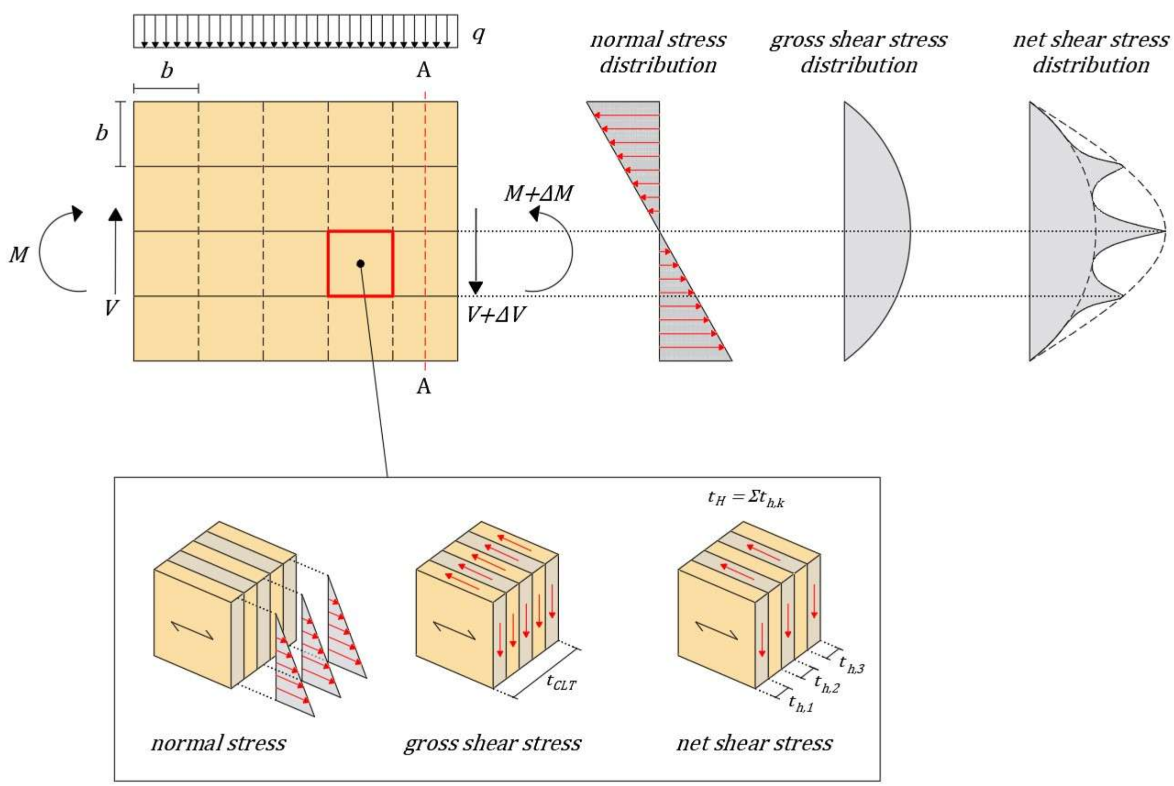

Figure 4.8: *Normal, gross shear and net shear stress distributions in CLT beams with horizontal outer laminations*

4.5.1.2 Torsional shear strength

The calculation model for the prediction of the torsional shear failure in CLT beams subjected to uniformly distributed vertical load q, which was presented by Flaig and Blaß 2013 and further developed by Danielsson et al.,2024, cannot be used for all CLT beam lay-ups in its original form when outer laminations are oriented along the vertical direction. The determination of the shear stress components acting in the crossing areas between the *i-th* horizontal lamination in the *k-th* horizontal layer and the adjacent vertical laminations, namely longitudinal $\tau_{xz,i,k}$, transversal $\tau_{yx,i,k}$ and torsional $\tau_{tor,i,k}$ shear stresses, strongly depends on the position of horizontal layers in the beam lay-up.

The analytical framework adopted in this study was first developed for a separate research project; its key findings are summarised below, and the complete methodology is presented in Khajehpour et al. (2023).

The original form of the analytical method proposed by Danielsson and Serrano 2018 can be adopted for 3-ply CLT beams with vertical outer laminations without any other adjustment (the index *k* in this case refers only to the inner horizontal layer, namely *k=1*). The same analytical model can also be used without any other modification for 5-ply CLT beams with outer vertical laminations (*k=1* and *2*) provided that the ratio between the thickness of the *p-th* vertical layer $t_{v,p}$ and the number of crossing areas $n_{CA,p}$ (equal to either 1 or 2) for the vertical layer under consideration is the same for all the three vertical layers (*p =1 to 3*), as shown in Figure 4.8.

For the two cases presented above, the shear stress components $\tau_{tor,i,k}$, $\tau_{yx,i,k}$ and $\tau_{xz,i,k}$, acting on the crossing areas between the *i-th* horizontal lamination of the *k-th* horizontal layer and the adjacent vertical laminations, are the same for all crossing areas.

It is common however that the ratio $t_{v,p}/n_{CA,p}$ is not constant for 5-ply CLT beams, resulting in the transversal $\tau_{yx,i,k}$ and torsional $\tau_{tor,i,k}$ shear stress components not being the same in the two crossing areas. As a results, Equations (Khajehpour et al.,2025) cannot be used directly for the determination of the shear stress components and an adaptation of the methodology is needed. In order to take into account the real distributions of shear stress components on the crossing areas between the *i-th* lamination of the *k-th* horizontal layer and the adjacent vertical laminations, factors $\beta_{CA,inn}$ and $\beta_{CA,out}$ are introduced and presented in Equations 12 to 15.

Due to the layup symmetry, the calculation needs only to be performed for the two crossing areas of the first horizontal layer. The shear stress components for the two adjacent crossing areas (inner and outer) of the *i-th* lamination in the first (k=1) horizontal layer can hence be calculated as expressed by Equations 12 to 15 (see also Figure 4.9).

For the inner crossing area, one obtains:

$$\tau_{yz,i,k,inn} = \frac{q}{h} \cdot \frac{1}{\beta_{CA,inn}} \cdot \frac{t_{h,k}}{t_H} \quad (12)$$

$$\tau_{tor,i,k,inn} = \frac{3 \cdot V}{b^2} \cdot \frac{1}{\beta_{CA,inn}} \cdot \frac{t_{h,k}}{t_H} \cdot \left(\alpha_i - \frac{1}{m^3}\right) \quad (13)$$

with i = *1 to m* and *k=1*.

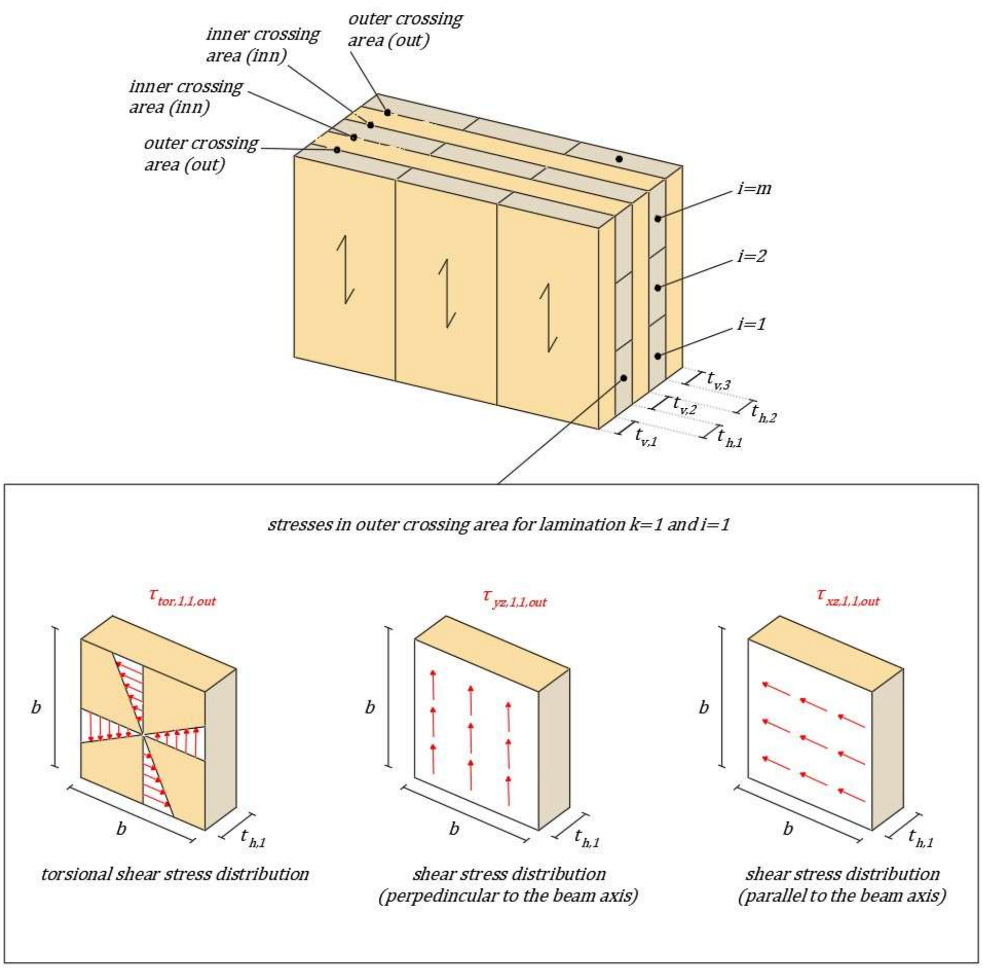

Figure 4.9: *Torsional shear stress distributions in a 5-ply CLT beam with vertical outer laminations*

For the outer crossing area, one obtains:

$$\tau_{yz,i,k,out} = \frac{q}{h} \cdot \frac{1}{\beta_{CA,out}} \cdot \frac{t_{h,k}}{t_H} \quad (14)$$

$$\tau_{tor,i,k,out} = \frac{3 \cdot V}{b^2} \cdot \frac{1}{\beta_{CA,out}} \cdot \frac{t_{h,k}}{t_H} \cdot \left(\alpha_i - \frac{1}{m^3}\right) \quad (15)$$

with i = *1 to m* and *k=1*.

The factors $\beta_{CA,inn}$ and $\beta_{CA,out}$ are calculated according to Equations 16 and 17, respectively.

$\beta_{CA,inn} = \frac{t_{v,2}+2\cdot t_{v,1}}{t_{v,2}}$ (16)

$\beta_{CA,out} = \frac{2\cdot t_{v,1}+t_{v,2}}{2\cdot t_{v,1}}$ (17)

where $t_{v,1}$ and $t_{v,2}$ are the thickness of the first (i.e. outer) and second (i.e. inner) vertical layer, respectively. The mathematical derivations of Equations are reported in the Khajehpour et al.,2025.

The failure criteria reported in Equations 18 and 19 can be adapted for both the inner and outer crossing area between to the *i-th* lamination of the first (*k*=1) horizontal layer and the adjacent vertical laminations, as expressed in Equations 20 and 23.

$max\left(\frac{\tau_{tor,i,k,R}}{f_{v,tor}} + \frac{\tau_{xz,i,k,R}}{f_{v,rol}}\right) \leq 1$ for *i = 1... m* and for *k = 1,3,...n$_h$* (18)

$max\left(\frac{\tau_{tor,i,k,R}}{f_{v,tor}} + \frac{\tau_{yz,i,k,R}}{f_{v,rol}}\right) \leq 1$ *for i = 1...m and for k = 1,3,..n$_h$* (19)

For the inner crossing area, one obtains:

$max\left(\frac{\tau_{tor,i,k,inn,R}}{f_{v,tor}} + \frac{\tau_{xz,i,k,inn,R}}{f_{v,rol}}\right) \leq 1$ for *i = 1... m* and for *k = 1* (20)

$max\left(\frac{\tau_{tor,i,k,out,R}}{f_{v,tor}} + \frac{\tau_{yz,i,k,out,R}}{f_{v,rol}}\right) \leq 1$ for *i = 1... m* and for *k = 1* (21)

For the outer crossing area, one obtains:

$max\left(\frac{\tau_{tor,i,k,out,R}}{f_{v,tor}} + \frac{\tau_{xz,i,k,out,R}}{f_{v,rol}}\right) \leq 1$ for *i = 1... m* and for k = 1 (22)

$max\left(\frac{\tau_{tor,i,k,out,R}}{f_{v,tor}} + \frac{\tau_{yz,i,k,out,R}}{f_{v,rol}}\right) \leq 1$ for *i = 1... m* and for k = 1 (23) where $\tau_{xz,i,k,inn,R}$, $\tau_{yx,i,k,inn,R}$, $\tau_{tor,i,k,inn,R}$ and $\tau_{xz,i,k,out,R}$, $\tau_{yx,i,k,out,R}$, $\tau_{tor,i,k,out,R}$ represent the shear stress components on the inner and outer crossing areas related to the shear resistance V_R, respectively.

4.5.1.3 Bending stiffness

The analytical models for the calculation of bending stiffness developed for CLT beams with horizontal outer laminations can also be adopted for beams with vertical outer laminations without any modifications to the principles in the procedure.

The effective local modulus of elasticity $E_{m,loc,eff}$ from four-point bending tests on CLT beams is typically calculated according to the procedure reported in EN 408 as expressed by Equation 24, referring to the effective cross-section (EAD130005; Flaig M and Blass H 2013).

$$E_{m,loc,eff} = \frac{a \cdot l_1^2}{16 \cdot J_{eff}} \cdot \frac{\Delta F}{\Delta w} \quad (24)$$

where a is the distance between the loading point and the nearest support, l_1 is the ledger length for the local deflection measuring, ΔF and Δw are the increase in load and deflection in the linear elastic range between 10% and 40% of maximum load applied to the specimen measured during the test and J_{eff} is the effective modulus of inertia equal to $\left[t_H + \left(\frac{t_{CLT} - t_H}{30}\right)\right] \cdot \frac{h^3}{12}$.

The experimental observations revealed mid-span torsional shear failures in several vertical-lamination beams. These failure modes highlight the importance of including torsional shear resistance in analytical and numerical frameworks. In the current FE model, torsional shear was not directly incorporated, and therefore torsional-dominated failures could not be fully reproduced. Despite this limitation, the beam test results confirmed the sensitivity of lintel performance to lamination orientation and thickness, and established baseline parameters for the validation of wall-level models.

4.5.2 Calculated strength and stiffness parameters

4.5.2.1 Summary of calculated values

The analytical models described in Section 4.5.1 were used to determine the strength and stiffness parameters of the tested CLT beams reported in Table 4.6. In this table only the value corresponding to the observed failure mode can be considered to be reflective of the strength of the beam while other values reported for the same test represent the maximum stress reached when the failure occurs. For example, for test #1 of series Vb_3P_m2, the failure mode occurred in bending, and hence the corresponding strength f_m is equal to 43.82 MPa, while the reported values for $f_{v,gross}$, $f_{v,net}$, $f_{v,rol}$, $f_{v,tor}$ represent shear stresses at the point where bending failure occurs. The values for the modulus of elasticity were calculated according to Equation 25. It should be noted that the values of, $f_{v,rol}$, $f_{v,tor}$ are obtained based on the adopted analytical models described in Khajehpour et al.2025.

$$E_{m,loc,eff} = \frac{a \cdot l_1^2}{16 \cdot J_{eff}} \cdot \frac{\Delta F}{\Delta w} \quad (25)$$

The analytical models were also adopted to predict the strength parameters obtained from tests available in literature for CLT beams with either horizontal or vertical outer lamination as summarized in Table 4.7. Given the scarcity of data for CLT beams with vertical outer laminations, the first step was to compare the values obtained in this study with those in the literature for beams with horizontal outer laminations in order to verify that the mechanical behaviour is consistent.

Table 4.6: *Strength and stiffness parameters for tested beams.*

ID	n	Fmax [kN]	f_m [MPa]	$f_{v,gross}$ [MPa]	$f_{v,net}$ [MPa]	$f_{v,rol}$ * [MPa]	$f_{v,tor}$ * [MPa]	$E_{m,loc}$ [MPa]	failure mode
Hb_3P_m4	1	127.5	**34.54**	2.56	7.67	2.07	4.84	9632	Bending
	2	103.1	27.93	2.07	6.21	**1.68**	**3.91**	7638	Torsional shear
	3	122.5	33.18	2.46	7.37	**1.99**	**4.65**	15160	Torsional shear
Hb_5P_m4	1	186.5	**33.68**	2.75	10.34	2.02	4.72	19086	Bending
	2	175.4	**31.67**	2.58	9.72	1.90	4.44	14680	Bending
	3	190.5	**34.40**	2.81	10.56	2.07	4.82	15064	Bending

ID	n	Fmax [kN]	f_m [MPa]	$f_{v.gross}$ [MPa]	$f_{v.net}$ [MPa]	$f_{v.rol}$ * [MPa]	$f_{v.tor}$ * [MPa]	$E_{m.loc}$ [MPa]	failure mode
Vb_3P_m2	1	36.4	**43.82**	1.46	4.38	1.42	3.30	16189	Bending
	2	30.9	**37.20**	1.24	3.72	1.20	2.80	16165	Bending
	3	32.1	**32.13**	1.29	3.86	1.25	2.91	15790	Bending
Vb_5P_m2	1	57.6	**63.87**	1.70	6.39	1.27	2.95	19222	Bending
	2	70.0	**77.62**	2.06	7.76	1.54	3.59	-	Bending
	3	53.5	**59.32**	1.58	5.93	1.18	2.74	13449	Bending
Vb_3P_m3	1	63.1	**20.94**	1.69	5.06	1.45	3.39	15635	Bending
	2	57.5	**46.15**	1.54	4.61	1.33	3.09	12911	Bending
	3	58.9	**47.27**	1.58	4.73	1.36	3.17	8499	Bending
Vb_5P_m3	1	86.6	**64.02**	1.70	6.40	1.13	2.63	14110	Bending
	2	76.4	**56.48**	1.50	5.65	1.00	2.32	13216	Bending
	3	67.5	**49.90**	1.33	4.99	0.88	2.05	12933	Bending
Vb_3P_m4	1	73.1	**39.60**	1.47	4.40	1.19	2.78	10363	Bending
	2	69.7	**37.76**	1.40	4.20	1.13	2.65	10460	Bending
	3	55.7	**26.82**	1.12	3.35	0.91	2.12	13209	Bending
Vb_5P_m4	1	111.7	**55.73**	1.65	6.19	1.16	2.70	-	Bending
	2	115.6	**57.68**	1.70	6.41	1.20	2.79	-	Bending
	3	134.4	**60.53**	1.98	7.45	1.39	3.25	14150	Bending

ID	n	Fmax [kN]	f_m [MPa]	$f_{v.gross}$ [MPa]	$f_{v.net}$ [MPa]	$f_{v.rol}$ * [MPa]	$f_{v.tor}$ * [MPa]	$E_{m.loc}$ [MPa]	failure mode
Vs_3P_m2	1	75.3	**45.94**	3.02	9.07	2.93	6.83	-	Bending
	2	66.1	**40.32**	2.65	7.96	2.57	6.00	-	Bending
	3	66.3	**40.45**	2.66	7.98	2.58	6.02	-	Bending
Vs_5P_m2	1	110.8	**44.73**	3.26	**12.29**	2.44	5.68	-	Bending/Net shear
	2	99.5	**28.26**	2.93	**11.03**	2.19	5.10	-	Bending/Net shear
	3	86.1	47.73	2.54	**9.55**	1.89	4.42	-	Net Shear
Vs_3P_m3	1	94.3	37.84	2.52	7.57	**2.17**	**5.07**	-	Torsional shear
	2	93.1	37.36	2.49	7.47	**2.15**	**5.01**	-	Torsional shear
	3	98.2	39.41	2.63	7.88	**2.26**	**5.28**	-	Torsional shear
	1	147.9	54.66	2.91	**10.93**	1.93	4.50	-	Net shear

Vs_5P_m3	2	131.8	48.71	2.59	**9.74**	1.72	4.01	-	Net shear
	3	150.0	55.44	2.95	**11.09**	1.95	4.56	-	Net shear
Vs_3P_m4	1	89.7	**27.00**	1.80	5.40	1.46	3.41	-	Bending
	2	108.8	32.74	2.18	6.55	**1.77**	**4.13**	-	Torsional shear
	3	101.7	**25.04**	2.04	6.12	1.66	3.86	-	Bending
Vs_5P_m4	1	183.9	50.98	2.71	**10.20**	**1.90**	**4.44**	-	Net/Torsional shear
	2	189.4	52.50	2.79	**10.50**	1.96	4.58	-	Net Shear
	3	174.5	**48.37**	2.57	9.67	1.81	4.22	-	Bending

$f_{v.tor}$ * and $f_{v.rol}$ *: The values are derived using the model presented in Khajehpour et al.2025.

Table 4.7: *Strength and stiffness parameters for some selected tests available in literature*

Authors	Series	f_m [MPa]	$f_{v.gross}$ [MPa]	$f_{v.net}$ [MPa]	$f_{v.rol}$ * [MPa]	$f_{v.tor}$ * [MPa]	$E_{m.loc}$ [MPa]	C.o.V [-]	failure mode
Jöbstl et al. (2008)	1	**59.20**	3.55	8.88	1.87	4.36	-	13.0%	Bending
	2	**34.90**	2.33	11.63	1.59	3.72	-	3.6%	
	3	**37.30**	2.22	7.77	1.12	2.60	-	14.3%	
	4	**34.30**	2.17	8.93	1.28	2.99	-	11.4%	
	5	**31.00**	2.08	10.76	1.16	2.70	-	11.7%	
	6	**35.50**	1.92	5.47	0.90	2.10	-	15.0%	
	7	**39.90**	2.20	6.49	0.88	2.06	-	15.7%	
Andreolli et al. (2012)	A-3	35.42	4.58	13.74	**2.73**	**6.38**	11211	8.7%	Torsional shear
	A-5	34.26	4.95	15.21	**2.82**	**6.58**	15060	-	Torsional shear
	B-5	29.60	3.81	9.51	**2.99**	**6.97**	15215	-	Torsional shear
	C-5	**30.31**	4.60	15.77	2.02	4.72	11476	-	Bending
Flaig & Blaß (2013)	27-27-27	32.83	1.82	5.47	**1.62**	**3.78**	-	8.7%	Torsional shear
	30-20-30	43.60	2.73	10.90	**2.39**	**5.57**	-	20.7%	
Flaig & Blaß (2014)	2-2_1	**45.00**	1.50	7.50	0.82	1.92	14947	21.4%	Bending
	3-2_1	**37.50**	1.17	4.69	0.68	1.60	12715	7.7%	
	2-2_2	**26.40**	0.88	4.40	0.48	1.12	9894	22.9%	
	3-2_2	**27.80**	0.87	3.48	0.51	1.18	9548	14.1%	
Gagnon et al. (2014)	A	35.10	3.90	11.70	**3.10**	**7.24**	-	-	Torsional shear
	B	40.50	4.50	13.50	**3.58**	**8.35**	-	-	
Sikora et al. (2014)	I-5-20	**16.30**	0.41	1.02	0.24	0.54	8883	9.8%	Bending
Jaleč et al. (2019)	1	**39.71**	2.98	11.91	1.46	3.40	15743	10.1%	Bending
	2	**36.46**	3.91	15.63	1.91	4.46	-	4.0%	Bending
	3	25.92	2.96	14.81	**1.36**	**3.17**	-	3.4%	Torsional shear
Daneshvar et al. (2021)	CL-C	**20.64**	3.02	11.29	1.39	3.25	-	-	Bending
	B 01	**50.21**	1.26	3.14	0.34	0.80	13576	7.8%	Bending

Casagrande et al. (2021)	B 02	**48.55**	1.01	3.03	0.44	1.03	13191	49.5%	Bending
	B 03	52.70	4.39	**10.98**	1.20	2.80	-	-	Net shear
	B 04	43.59	3.03	**9.08**	1.32	3.07	-	-	Net shear
Li et al. (2022)	CEB	**42.34**	1.18	3.53	1.35	3.16	12793	2.7%	Bending
	CES	36.14	2.41	7.23	**2.77**	**6.47**	-	6.9%	Torsional shear

$f_{v.tor}$ * and $f_{v.rol}$ *: The values are derived using the model presented in Khajehpour et al. [Forthcoming].

4.5.2.2 Bending strength

For beams with vertical outer laminations that were designed to fail in bending in this study, a significant difference was observed between 3-ply and 5-ply specimens. An average value of 36.9 MPa (CoV 24%) and 60.6 MPa (CoV 13%) was obtained for the 3-ply and 5-ply beams, respectively. This observation in terms of bending strength confirms the argument made in Section 4.4 in terms of maximum load, where the difference was attributed to the probability of critical defects in the larger-dimension lumber.

Figure 4.10 presents the results from 14 test series based on 116 CLT beams available in the literature. All beams in Figure 4.10 consisted of spruce laminations and failed in bending. It seems reasonable to assume that an inverse correlation exists between the bending strength and lamination thickness. It can also be noted that the values of bending strength obtained from the experimental campaign described in this study seem to fit reasonably well within the general trends.

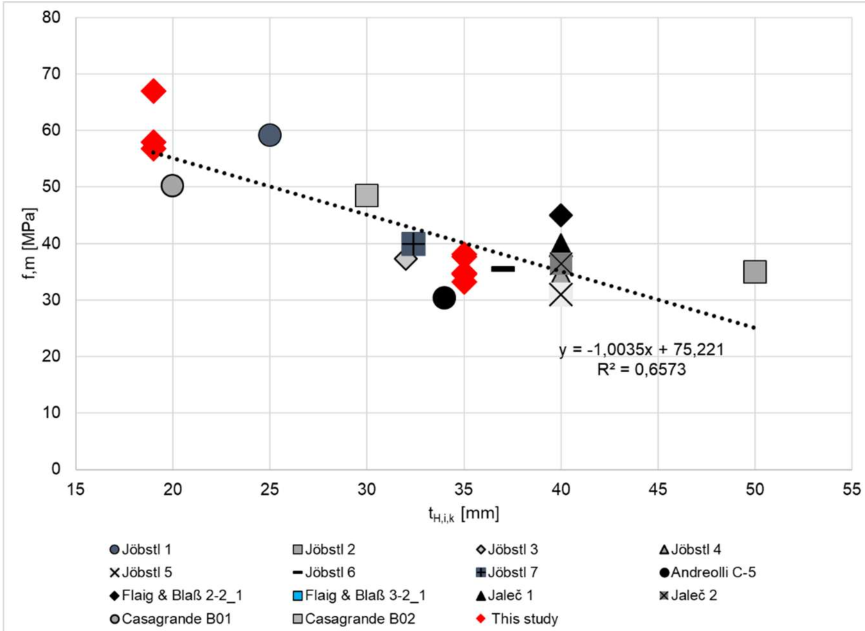

Figure 4.10. *Results of the tested CLT beams made by spruce in literature and failed in bending*

4.5.2.3 Shear strength

The average values for rolling $f_{v,rol}$ and torsional $f_{v,tor}$ shear strengths in this study were calculated based only on the five specimens with vertical outer laminations which actually exhibited torsional shear failure mode. These values are equal to 2.05 MPa (CoV 10%) and 4.79 MPa (CoV 10%), respectively.

For test series Vs_3P_m2 and Vs_5P_m2, all specimens failed in either bending or net shear but the calculated rolling and torsional shear stresses corresponding to the point at which failure occurred are greater than the ones obtained from the five specimens where a torsional shear failure was observed. The latter implies that the overall average of rolling and torsional shear strength is expected to be greater than those reported here.

The rolling and torsional shear strength values obtained from the current study were consistent with those obtained from the literature. For example, the average values obtained from the two series reported by Flaig and Blass 2013 were equal 1.62 MPa and

3.78 MPa (COV 8.78%) and 2.39 MPa and 5.57 MPa (CoV 20.7%), respectively. A slight difference is observed with the values of rolling and torsional shear strength obtained from Jelec et al.2019, equal to 1.36 MPa and 3.17 (CoV 3.4%) MPa, and Andreolli et al. 2012, equal to 2.73 MPa and 6.38 MPa (CoV) for test series A-3, respectively.

The average value of net shear strength $f_{v,net}$ was calculated based only on the six specimens with vertical outer laminations which exhibited net shear failure mode. The value is equal to 9.34 MPa (CoV 6%), which is similar to that obtained by Casagrande et al.2021. It is noteworthy to mention that to the authors knowledge, no other experimental study in the literature has reported net shear failure mode in CLT beams.

4.5.2.4 Modulus of elasticity

The results revealed that the thickness of lamination had insignificant influence on the elastic modulus $E_{m,loc}$. The average value for beams with vertical outer lamination was 13,753 MPa (CoV 19.8%), while for beams with horizontal outer laminations the value was 13,543 MPa (CoV 31%). The average value obtained for beams with vertical outer lamination in this study seems slightly greater than that obtained from literature, which had an average value of 12,635 MPa (Cov 14%).

5- Failure Mechanisms in FULL-SCALE CLT Shearwalls with Cut-Out Openings

5.1. Introduction

The mechanical behaviour of cross-laminated timber shearwalls, where openings are cut-out of the panel, is strongly influenced by the interaction between lintel elements and wall segments as well as by the layout of the hold-down, i.e. single or double hold-down configuration. Differently from CLT shearwalls with no openings, shear and bending deformation of the wooden panels in monolithic walls with openings may significantly contribute to the overall lateral displacement of the shearwall. The rocking behaviour of monolithic CLT shearwalls with a single opening typically involves two distinct kinematic modes characterised by either one centre of rotation for the entire wall or one centre of rotation for each wall segment (Pei S et al.,2016). Moreover, stress concentrations in the corners around the opening may lead premature and unwanted brittle failure modes.

Although it is not desired to design for brittle failure mode in the CLT panel, knowledge about such failure mechanism helps limit or prevent it. The prediction of such failure, however, may be difficult due to multiple reasons, including the variability in strength properties of wood, the possible different failure modes observed in the lintels (e.g. net shear, bending, etc.), and the stress concentrations observed at the corners of structural elements around openings. Moreover, the stresses around openings may not always reflect the actual conditions in the real element due to the reinforcing effects of transverse laminations in the CLT panels.

The main motivation for undertaking the current experimental tests is to examine the failure modes in monolithic CLT shearwalls with cut-out openings by investigating twelve full-scale shearwalls designed to reach failure in the CLT panel. Given that such failure modes are inherently brittle and should be avoided, a deeper understanding through experimental observations is necessary to protect failure modes in the timber panels and promote ductile failure mechanism in connections. The test results were predicted by means of numerical models (Section 5.2.1.2) where mechanical properties of the CLT panels were in-part derived from experimental tests conducted by the authors on CLT beams with vertical outer layers, as described in Chapter 4 of this thesis.

5.2. Experimental campaign

5.2.1 Shearwall tests

Twelve full-scale shearwalls, with either door or window opening, were tested under a monotonic load procedure. The panels were manufactured by Nordic Structures and comprised of E1 stress grade boards with width, *b*, equal to 89 mm, in accordance with the PRG 320 standard. A panel thickness, t_{CLT}, equal to 105 mm with 35-35-35 lamination layup was adopted for all the shearwall specimens. The outer layers were oriented along the vertical direction. The wall height h_{wall} was equal to 2800 mm while the wall length l_{wall} was varied between 2200 and 2700 mm. Details about the dimensions and opening configurations of the shearwall specimens are provided in Table 5.1 and Figure 5.1, where l_{op} is the length of the opening (equal to the length of the lintel and the parapet), h_{lintel} represents the depth of the lintel and h_{par} is the depth of the parapet. Each shearwall configuration is labelled to indicate the opening type (either “D” door or “W” window), wall length, as well as lintel depth and length. For example, a shearwall specimen with a door opening, having a total length of 2200 mm and a lintel depth and length equal to 400 and 600 mm, respectively, is represented with the nomenclature "D-2200-400/600". Nine different configurations of shearwalls were selected. Figure 5.2a shows the test setup using wall specimen W05 as example. In order to assess how the variability in the strength properties of the wood material (e.g. axial and bending strength of laminations) may affect the panel failure modes, two replicates of configurations D-2200_200/600, D-2700_400/1100 and D-2700-400/600 were investigated.

Although parapets were identified as an important variable in the analytical study, the experimental campaign was limited to two window-type shearwalls. This decision was made to maintain a balance between breadth of configurations and the practical constraints of specimen fabrication and testing. Since window openings require both lintel and parapet elements, their inclusion substantially increases the number of parameters that must be controlled in testing. In order to isolate key behaviours while keeping the campaign manageable, two representative window configurations were selected to capture the influence of parapet continuity and to provide validation data for the numerical model. The broader influence of parapet geometry and additional window variations was subsequently explored in the parametric finite element studies, which allowed for systematic variation of parapet depth and opening dimensions beyond what could be achieved experimentally.

Table 5.1: *Shearwall test matrix*

Test ID	Label	l_{wall} [mm]	h_{lintel} [mm]	h_{par} [mm]	l_{op} [mm]	Opening type
W01	D-2200-400/600	2200	400	-	600	Door
W02	D-2200-200/600	2200	200	-	600	Door

W03						
W04	D-2400-400/800	2400	400	-	800	Door
W05	D-2400-200/800	2400	200	-	800	Door
W06 W07	D-2700-400/1100	2700	400	-	1100	Door
W08 W09	D-2700-400/600	2700	400	-	600	Door
W10	D-2700-200/600	2700	200	-	600	Door
W11	W-2700-200/1100	2500	200	800	1100	Window
W12	W-2700-200/1300	2700	400	800	1300	Window

The horizontal lamination layout along the lintel or parapet is shown in Figure 5.3 for the different values of h_{lintel} and h_{par} adopted in the experimental campaign, namely equal to 200, 400 and 800 mm. It is noteworthy to mention that the number of "full-width" laminations, *m*, was equal to 1, 4 and 8, respectively.

Proprietary hold-down WHT620 and angle brackets TCN 200 were used to anchor the shearwalls to a steel base beam as shown in Figure 5.2b. The hold-downs and the angle brackets were connected to the wall panel with 4x60 mm ring nails, and to the steel base beam using an M20 bolt and two M16 bolts, respectively. In all specimens, one angle bracket was located at the bottom centre of each of the two wall segments, while an additional angle bracket was located at the bottom centre of the parapet in specimens with window opening, as shown in Figure 5.2c. In shearwalls with door openings, a hold-down was placed at both ends of each wall segment, while hold-downs were only located at the wall ends of shearwalls with window openings.

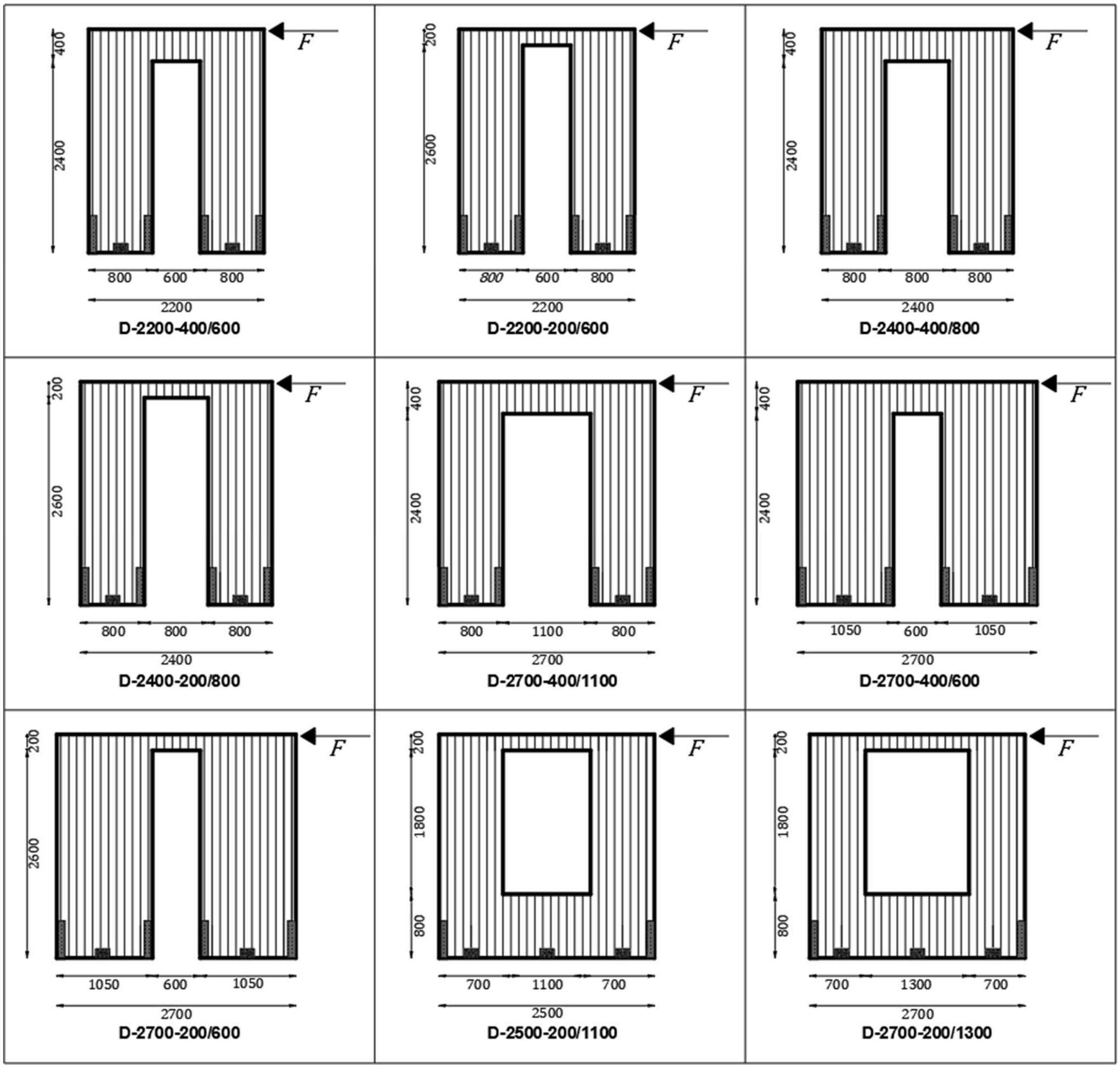

Figure 5.1: *Geometrical dimensions and the opening layout of tested shearwalls*

A horizontal hydraulic jack, connected to a rigid steel frame, was used to apply the lateral load. A 25 mm thick steel plate transferred the load from the jack to the shearwall in order to avoid crushing in the wood at the load application point, as illustrated in Figure 5.4a. Additional lateral restraints were used on both sides of the shearwall to limit out-of-plane displacement and prevent buckling of the lintel beam (Figure 5.4b and c). The testing followed a displacement-controlled procedure with a loading rate equal to 6 mm/min.

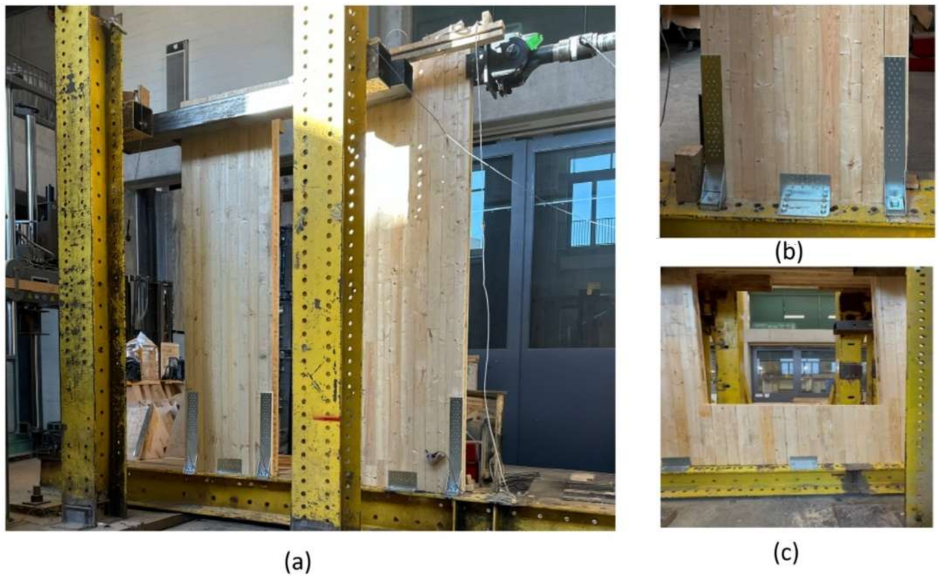

Figure 5.2: *Wall D-2200-200/600(a) hold-down and angle brackets layout in Wall D-2200-200/600 (b), angle bracket layout in Wall W-2700-200/1300 (c)*

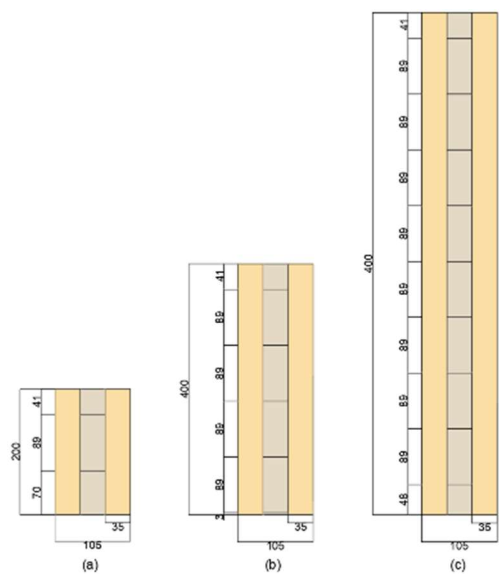

Figure 5.3: *Horizontal lamination layout in lintels (a, b) and parapets (c)*

Three Wire Displacement Sensors (WDS), labelled WDS 01, WDS 02, and WDS 03, measured the horizontal displacements at the top right, top centre, and top left positions of the shear wall (Figure 5.5). These sensors were positioned 30 mm from the top edge of the wall. An inclined WDS 04 measured the CLT panel deformation along a top-left bottom-right direction. Three WDSs (WDS 05, 06 and 07) were adopted to measure the uplift displacement at the bottom corner of the wall segments while WDSs 08 and 09 measured the horizontal sliding displacement at the bottom of the wall. The relative top horizontal displacement δ of the wall was calculated by subtracting the average bottom sliding displacement δ_{slid} (WDSs 08 and 09) from the average top horizontal displacement δ_{top} (WDS 01, WDS 02, and WDS 03). It should be noted that the difference between the measurements obtained from those sensors was insignificant. A load cell was used to measure the applied load.

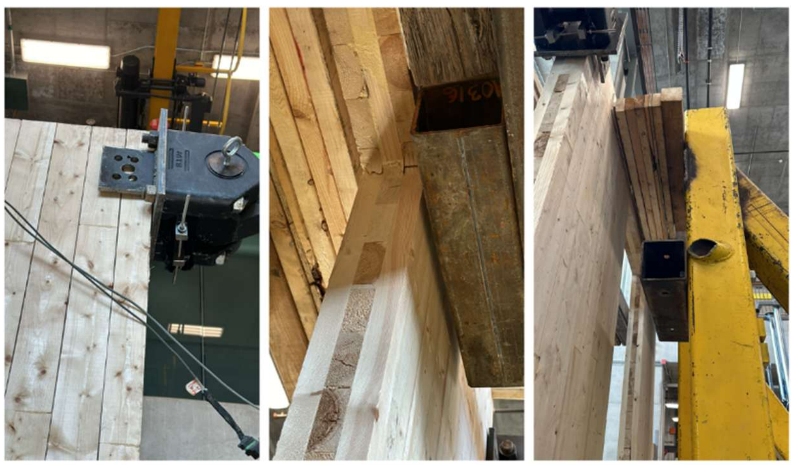

(a) (b) (c)

***Figure 5.4**: Application of lateral load (a) and lateral support system of the wall (b and c)*

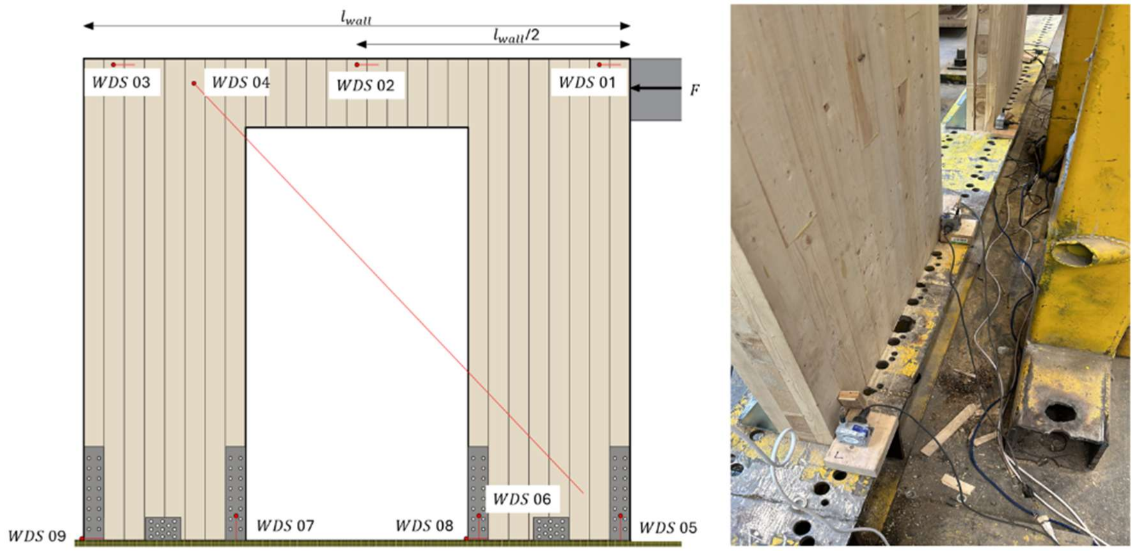

Figure 5.5: *Instruments test set-up*

The primary goal of this chapter is to demonstrate that the numerical approach outlined in Chapter 3 can reliably predict the behaviour of cross-laminated-timber shearwalls. To that end, detailed finite-element models were created for each of the twelve wall specimens later tested in the laboratory. Every model reproduces the exact geometry, lay-up, boundary conditions and fastener layout of its corresponding test wall, ensuring that any differences between the computer results and the lab tests come from the model itself, not from mismatched wall samples.

For every wall, the FE analysis produced three essential outputs: the global failure mode (that is, whether failure occurred in the panel itself or the connections); the ultimate panel capacity, defined as in the chapter 3; and the ultimate connection capacity, namely the force resisted by fasteners or hold-downs at the onset of failure.

These predicted values are summarised in Table 5.2.

Section 5.4 then compares the numerical and laboratory results in detail, highlighting areas of close agreement as well as any discrepancies, thereby clarifying both the strengths and the current limitations of the proposed finite-element method and pointing to aspects that may benefit from further refinement.

Table 5.2: *Failure mode and failure force of panel and hold-downs obtained from FE method*

Test ID	l_{wall} [mm]	h_{lintel} [mm]	h_{par} [mm]	l_{op} [mm]	Opening type	Failure mode	Panel failure force [KN]	Hold-down failure force [KN]
W01	2200	400	-	600	Door	Torsional shear	70.3	100.7
W02 W03	2200	200	-	600	Door	Torsional shear	50.4	104.6
W04	2400	400	-	800	Door	Torsional shear	75.1	117
W05	2400	200	-	800	Door	Bending	63.9	102.1
W06 W07	2700	400	-	1100	Door	Torsional shear	79.9	119
W08 W09	2700	400	-	600	Door	Torsional shear	84	114.2
W10	2700	200	-	600	Door	Torsional shear	75.3	114
W11	2500	200	800	1100	Window	Hold-down	-	113.2
W12	2700	400	800	1300	Window	Torsional shear	112.1	120.8

5.2.2 Experimental tests on Beam Samples from the Full-Scale Shearwall Specimens

The main purpose of conducting the beam tests was to establish the strength characteristics of the lintel beam in flexure. Although the results from the beam tests described in Chapter 4 could, in principle, be used as input into the developed models, testing beams from the same batch as the shear wall tested ensures consistency, as the flexural strength has been known to vary significantly in the transverse lamination. The quality and grade of the cross laminations are as much dependent on material availability as it is on meeting the minimum requirements in the PRG 320 standard. Shear is much less affected by the grade of the laminations and for that reason material properties obtained from the manufacturer were deemed sufficient. Four-point bending tests were conducted on seven CLT beams with vertical outer layers that were cut from the CLT wall panels used in the shearwall tests. The aim was to ensure consistency between beam and wall tests in terms of number and arrangement of layers, orientation of lamination and wood species and grade. It is important to highlight that the portions of panels selected to obtain the beam specimens were carefully identified to ensure that no damage or cracks occurred in such zones during the shearwall tests. These include either lintel beams of the wall that exhibited rigid body rotation and where failure occurred in the hold-downs or specimens taken from wall segments where lintel failure occurred with no damage observed in the walls.

The specimen configurations consisted of three different depths, h_{beam}, namely equal to 89, 178, 205 mm for B01, B02 and B03, respectively. The total beam length l_{beam} was selected to promote bending failure in each configuration. The layout of horizontal lamination consisted of one and two "full width" laminations for configurations B01 and B02 while for configuration B03 the horizontal layout was composed of two full-width laminations and one lamination with reduced width equal to 27 mm. The total lamination thickness in the horizontal t_h and vertical t_v directions was equal to 35 and 70 mm, respectively. Table 5.3 And Figure 5.6 summarize geometrical dimensions and number of specimens for each configuration where l is the length between the supports and a is the distance between the load application point load and the nearest support. Some details of the experimental setup and boundary conditions are depicted in Figure 5.7. One WDS was used to determine the total vertical deflection, w_{glob}, at the mid-span, while another WDS measured the local relative displacement, w_{loc}, between the centre of the beam and two fixed point located within the null-shear zone, represented by the ledger of length, l_{led} according to EN408.

Table 5.3: *Configurations of CLT beams with vertical outer laminations*

Specimen number	n. of specimen	h_{beam} [mm]	l_{beam} [mm]	l [mm]	a [mm]	l_{led} [mm]
B 01	3	89	1050	1020	300	400
B 02	3	178	1050	1020	300	400
B 03	1	205	2700	2522	850	400

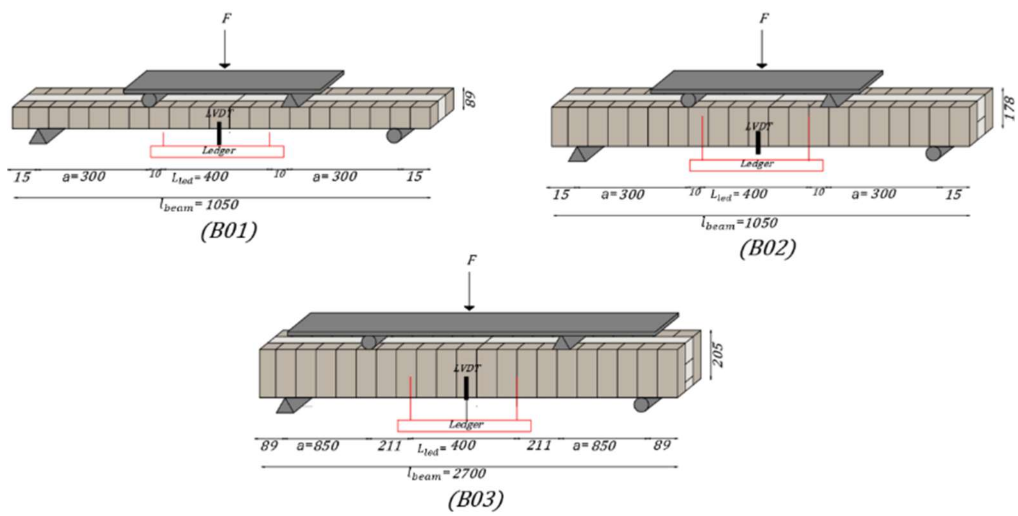

Figure 5.6: *Test set-up configurations*

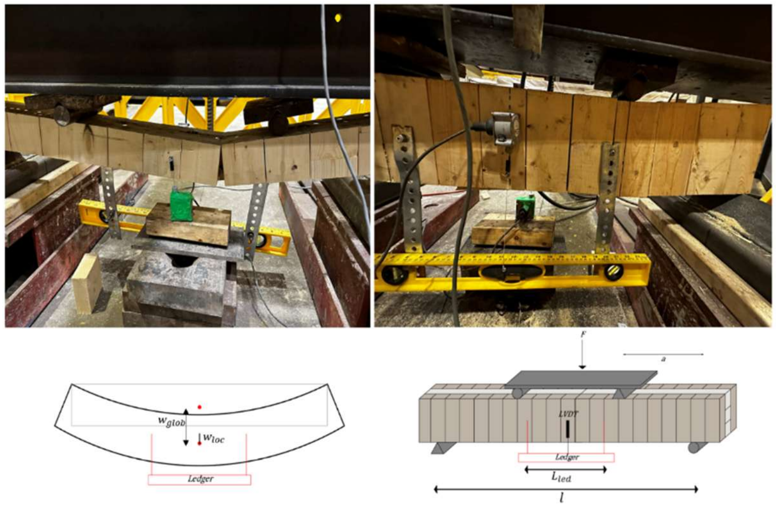

Figure 5.7: *Four-point bending test*

The results from the beam tests (Figure 5.8) are summarized in Table 5.4, including maximum load F_{max}, calculated bending strength, f_m, using Equation 1 and the effective modulus of elasticity along the longitudinal direction E_l.

$$f_m = \frac{M_{max}}{W_{net,h}} \tag{1}$$

where the maximum bending moment, M_{max}, and the elastic section modulus, W_{net}, are obtained from Equation (2) and (3), respectively:

$$M_{max} = \frac{F_{max} \cdot a}{2} \tag{2}$$

$$W_{net} = \frac{t_h \cdot h^2}{6} \tag{3}$$

where a is the distance between the support and the load application point and t_h is the total thickness of horizontal layers of the beams equal to 35 mm. The effective local modulus of elasticity along the longitudinal direction, E_l is calculated using a linear regression between 10% and 40% of the maximum load, following EN408.

In determining the area moment of inertia, I_{net} only the contribution of horizontal layers was considered.

Figure 5.8: *Mid-span failure observed in the beam during Specimen B01, Test 3*

Table 5.4: *Maximum load and bending strength of CLT beam tests*

Specimen number	Test	F_{max} $[kN]$	f_m [kN]	E_l [kN]
B 01	#I	4.6	14.0	7.2
	#II	9.0	27.0	7.5
	#III	7.8	24.0	7.4
B 02	#I	19.0	14.5	5.1
	#II	19.6	14.9	5.0
	#III	7.6	-	-
B 03	#I	6.5	10.6	4.4

5.3. Behaviour of full-scale shearwalls

All shearwall specimens were loaded until complete failure. The displacement-controlled loading process continued even after the initiation and full development of cracks in either the lintel or parapet in order to observe the progression of failure beyond the initial panel failure and until hold-down failure. All shearwalls exhibited crack initiation in the lintel or parapet, however, two different scenarios related to the propagations of cracks were observed. Scenario 1 (Figure 5.9) can be described by a rapid propagation of cracks in the lintel, which caused a significant drop in the load of more than 15%. The loading increased after the drop until the ultimate failure occurred in the hold-down. Scenario 2 represents a relatively slow propagation of cracks in either lintel or parapets that resulted in a small drop of less than 10% in the load, and/or contributed to a decrease in the lateral stiffness of the wall in conjunction with yielding of the mechanical anchors (Figure 5.10). Similar to Scenario 1, the ultimate failure was related to the failure of either one or two hold-downs.

Typical examples of walls that behaved in a manner consistent with what is described in Scenario 1 are Wall 01, Wall 08 and 09. To illustrate this, Wall 01 is used as an example, where the drop in capacity occurred immediately after the crack initiation, which occurred at the opening corner (Point 1 in Figure 5.9). The observed failure mode was identified as net shear and the ultimate failure occurred in the hold-down (Point 2 in Figure 5.9). While Wall 08 exhibited very similar overall performance to that described for Wall 01, including the initial failure being in net shear, Wall 09 had a more complex failure mechanism involving crack propagation due to both net shear and torsional shear. This observation was substantiated in the force-displacement curve, as shown in Figure 5.11, where failure initiated in net shear at the center of the lintel (Point 1) followed by torsional shear failure (Point 2). Plastic behaviour was then observed until the ultimate failure in the outer hold-down (Point 3).

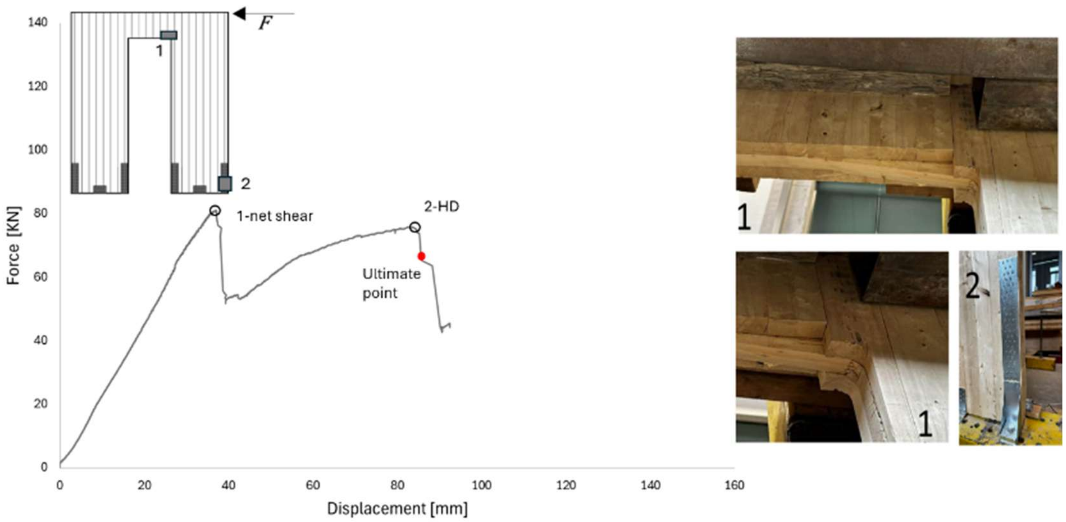

Figure* 5.9*: Force-displacement curve and crack propagation of Wall 01

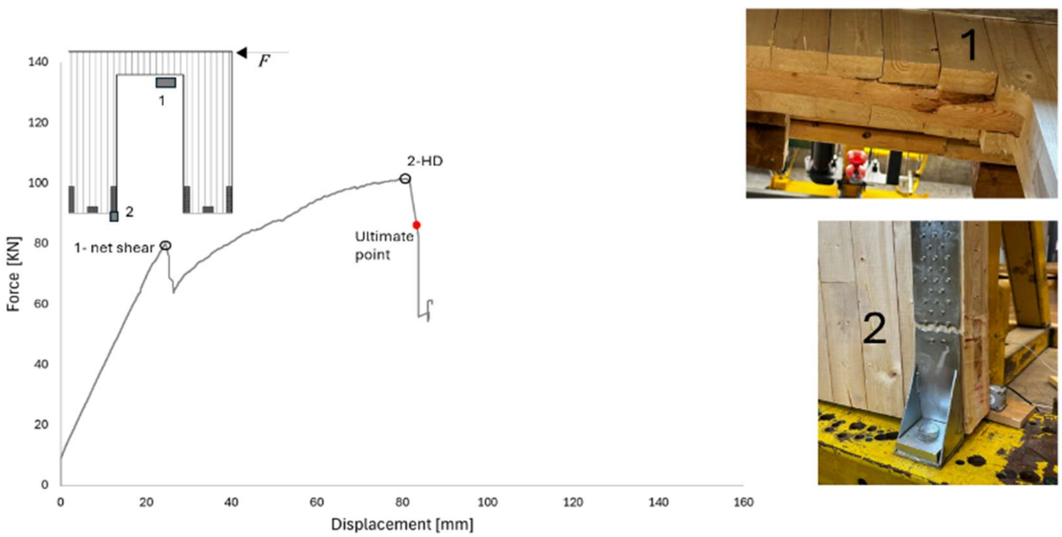

Figure* 5.10*: Force-displacement curve and crack propagation of Wall 08

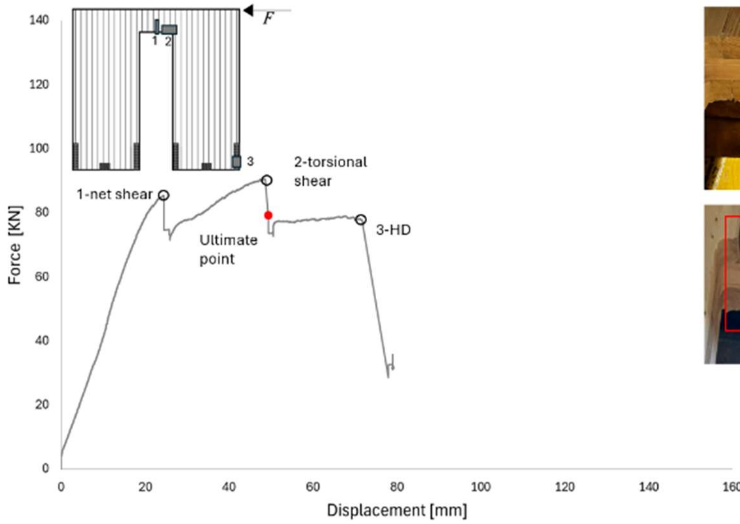

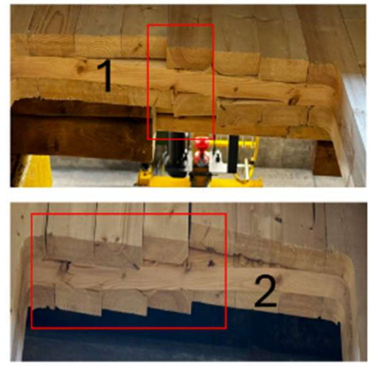

***Figure* 5.11**: *Force-displacement curve and crack propagation of Wall 09*

Scenario 2 can be illustrated using Walls 02 and 03 (Figures 5.12 and 5.13). These walls had similar configurations and exhibited similar behaviour despite different initial failure modes were observed in the lintels, namely net shear for Wall 02 and bending for Wall 03. Although the initial crack propagation occurred at the corner of the lintel (Figure 5.12) the initial drop in this scenario was insignificant and the walls experienced gradual increased in capacity. The failure of the inner hold-down anchor resulting in a sudden drop in load capacity (Point 2). Failure in the outer hold-down caused the ultimate failure of the walls (Point 3).

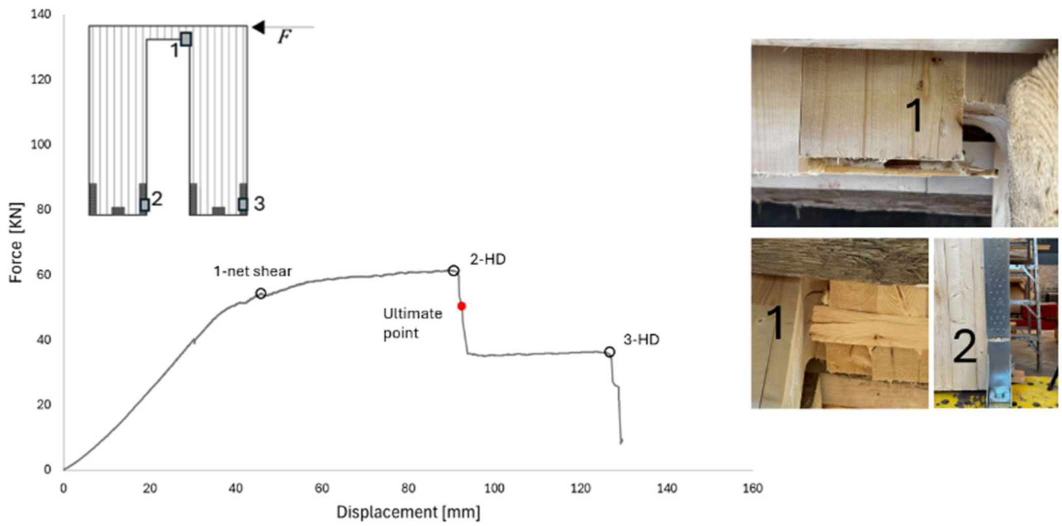

Figure* 5.12: Force-displacement curve and crack propagation of Wall 02*

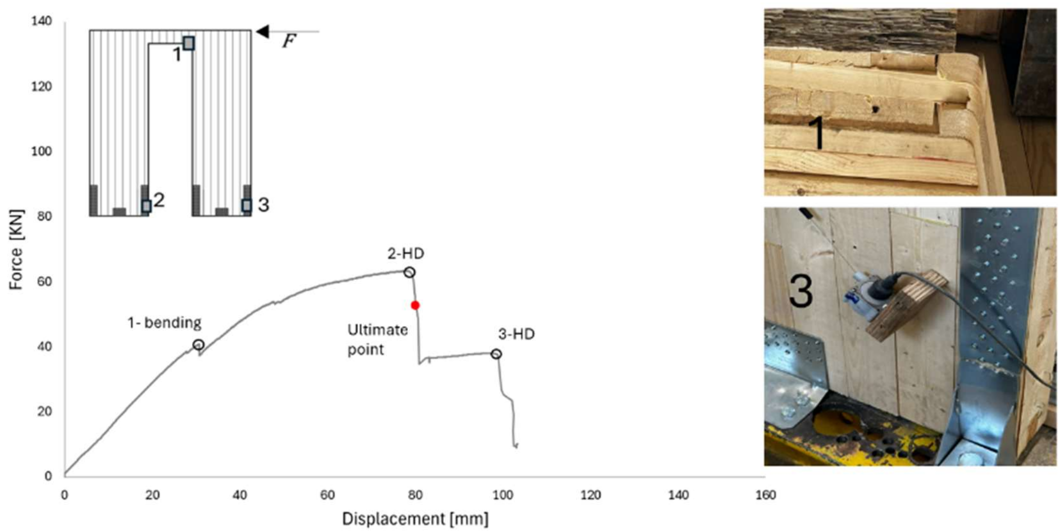

Figure* 5.13: Force-displacement curve and crack propagation of Wall 03*

A slight variation from Scenario 2 described above for Wall 02 is demonstrated by Wall 04 and Wall 06, which exhibited a small drop in the capacity (Point 1 in Figures 5.14 and 5.15) due to torsional shear failure. The wall capacity was maintained even after the separation in the outer laminations caused by the torsional failure, while the stiffness was reduced significantly, since only the horizontal layers contribute to the shear stress propagation.

The general behaviour of Walls 05 to 08 was very similar to those observed in Wall 04.

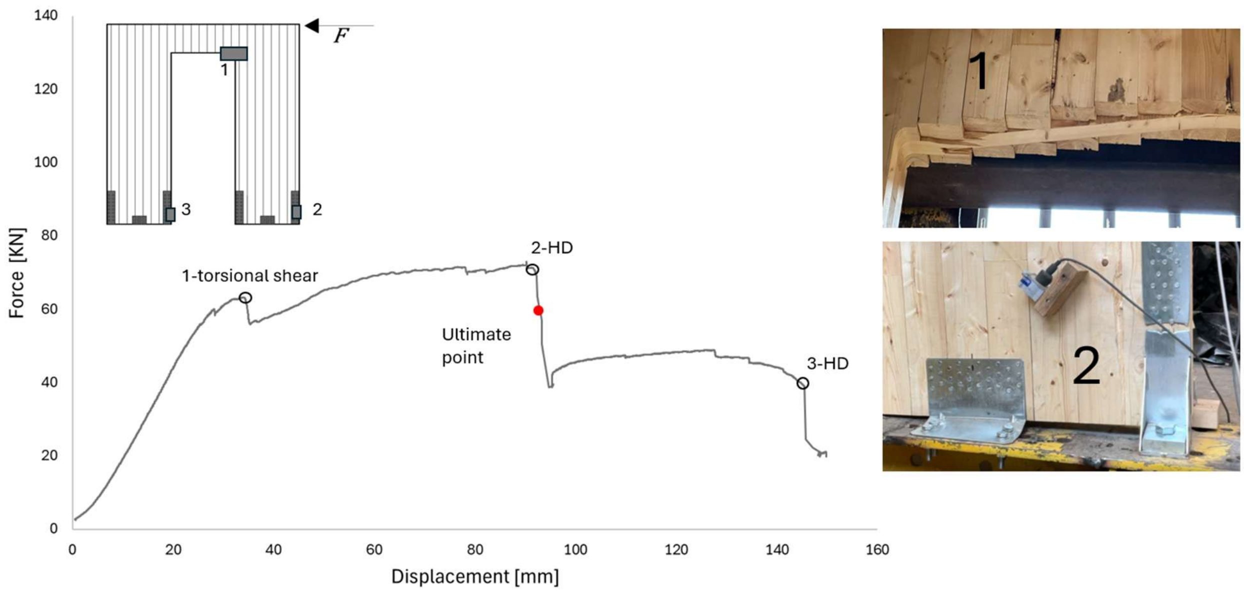

***Figure* 5.14**: *Force-displacement curve and crack propagation of Wall 04*

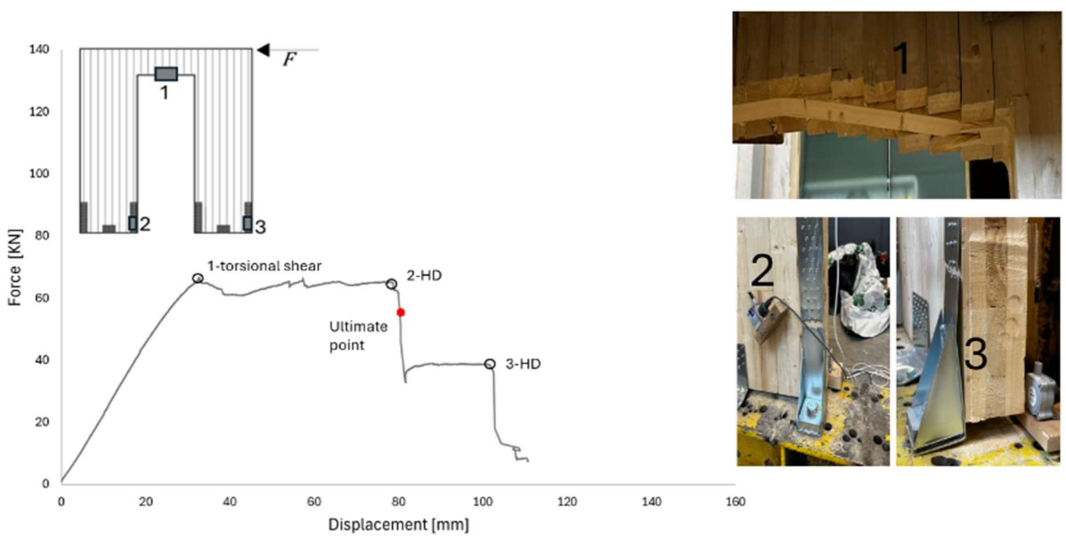

***Figure* 5.15**: *Force-displacement curve and crack propagation of Wall 06*

A particular case was observed in Wall 10, where the failure of the inner hold-down (Point 2 in Figure 5.16) occurred immediately after the crack opening due to net shear failure in the lintel, which caused the ultimate failure in the wall. If the hold-down had higher displacement capacity it would be anticipated that the behaviour of Wall 10 would also be similar to that of Wall 04.

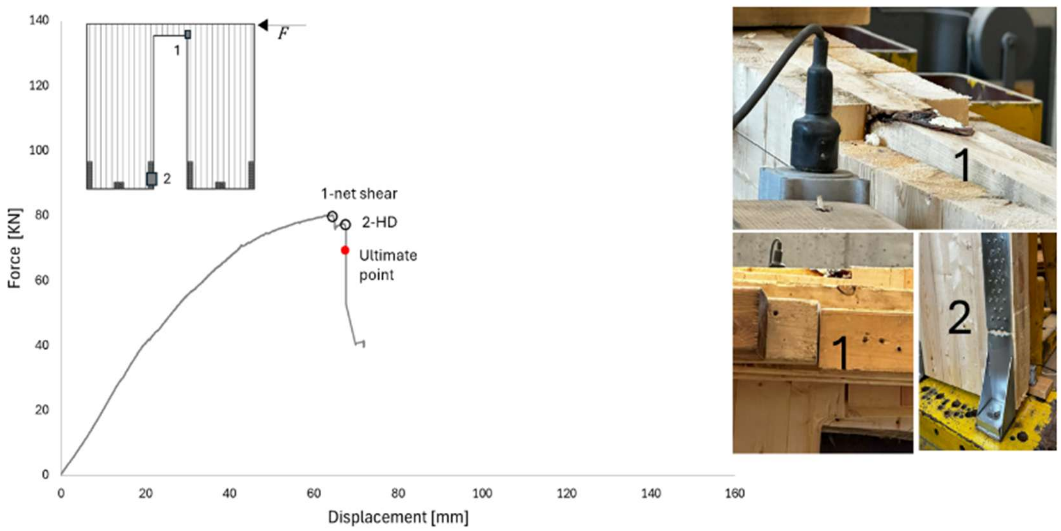

Figure* 5.16*:* *Force-displacement curve of Wall 10

Crack development in the parapet was only observed in Walls 11 and 12, however this did not alter the fact that these walls had consistent behaviour to that observed in Walls 02 to 07. The failure mechanism is illustrated in Figure 5.17 and 5.18 for Walls 11 and 12 respectively.

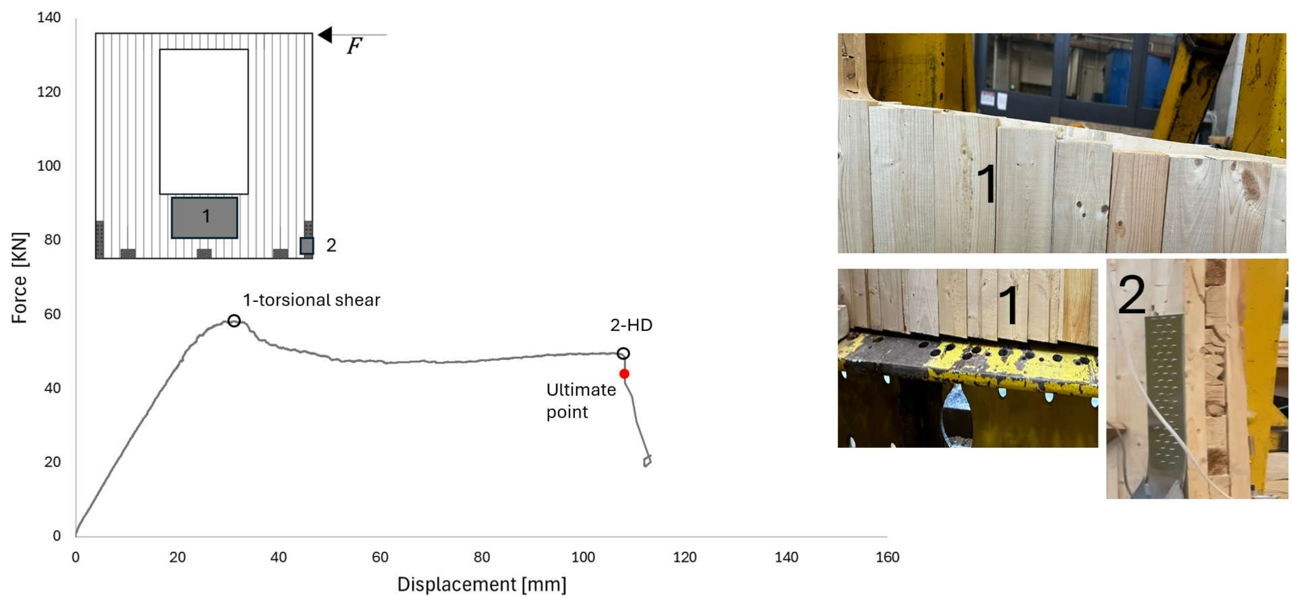

Figure* 5.17*: Force-displacement curve of Wall 11

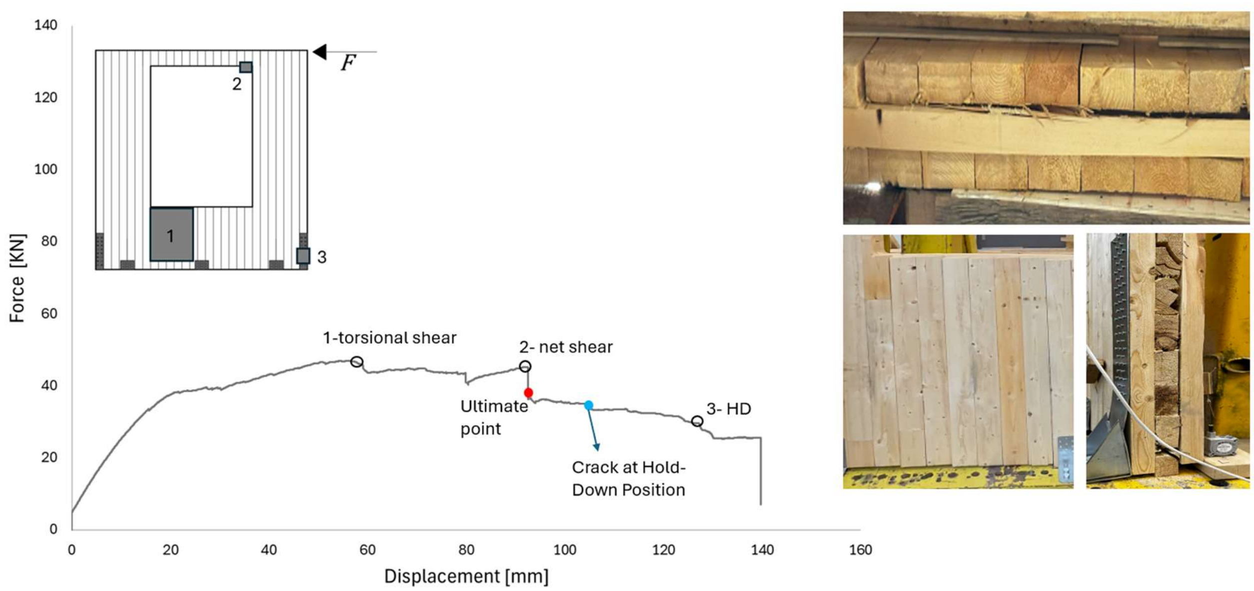

Figure* 5.18*: Force-displacement curve and crack propagation of Wall 12

The observation regarding the failure modes in the walls showed multiple and complex failure mechanisms; however, initial failure mode was always in the CLT panels for all the configurations investigated. In general, walls which had identical configurations behaved in a similar and consistent way. Relatively minor differences can be attributed to variability in wood especially when dealing with cut openings and potential difference in the transverse laminations. The fact that net shear failure caused a sudden and significant drop in capacity in some walls (Walls 01, 08 and 09), could not be generalized since other walls exhibited net shear failure but the drop was not significant (Wall 02 and 10). This could be partially attributed to the difficulty the authors encountered in identifying net shear failure in some cases.

For example, in Wall 05 (Figure 5.19), a clear distinction between net shear and bending failure was not possible. It was also observed that when the crack initiation was due to torsional shear failure, the drop in capacity was insignificant and the capacity was maintained, the stiffness was significantly reduced and the shearwall exhibited a long plateau (Walls 06, 07 and 12). As mentioned earlier this could be due to the loss of outer vertical laminations and the reliance on the horizontal laminations to contribute to the shear stress propagation. It is noteworthy to mention that in shearwalls with door opening, the failure of hold-down occurred in either the outer or inner hold-down, since the wall segments were characterized by one centre of rotation each, resulting in a similar tensile load in hold-downs.

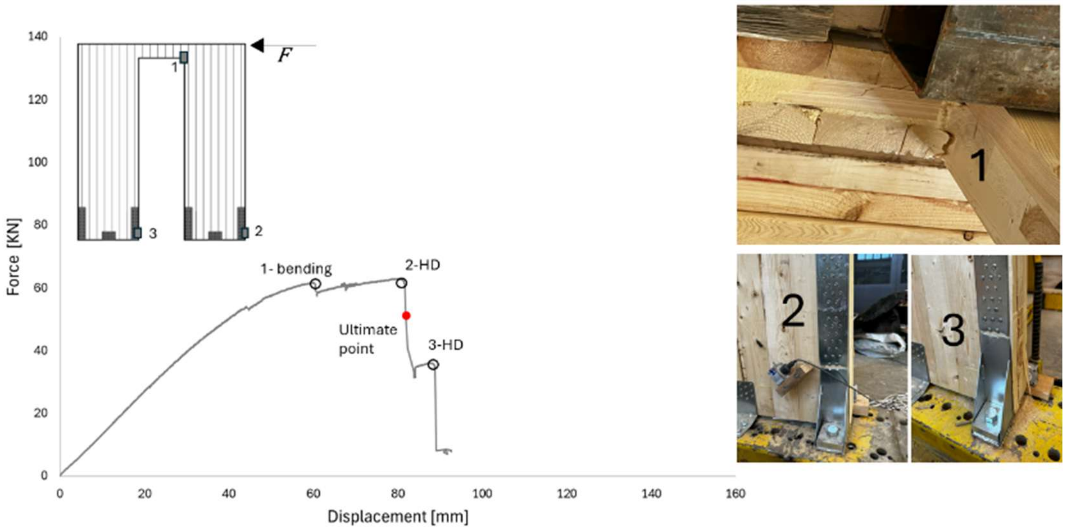

***Figure* 5.19**: *Force-displacement curve and crack propagation of Wall 05*

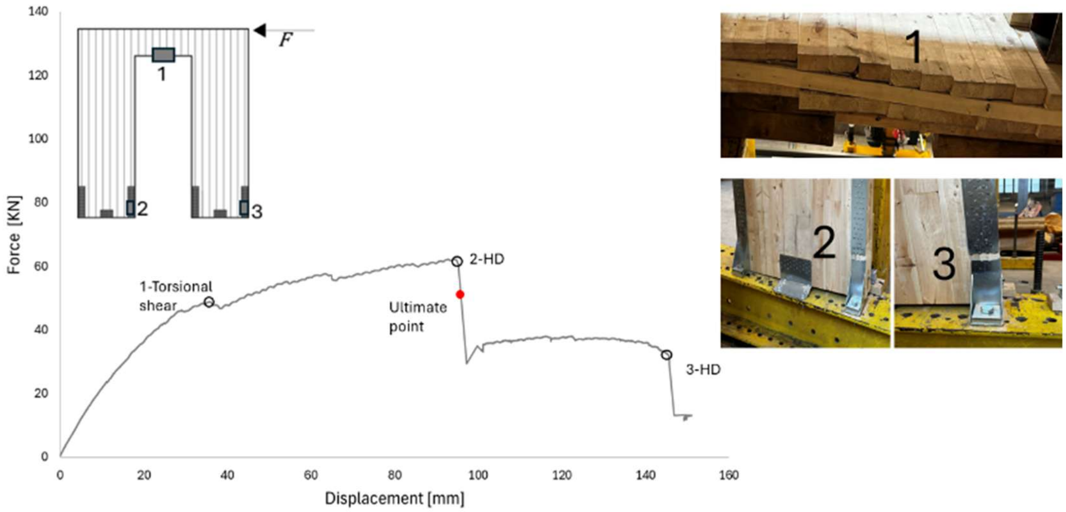

Figure* 5.20**:*** *Force-displacement curve and crack propagation of Wall 07*

A summary of failure modes and magnitude of load drops for CLT shearwall specimens is reported in Table 5.5. The experimental results, including the maximum load F_{max} and its corresponding displacement $\delta_{F_{max}}$, lateral stiffness of the shear wall k (calculated as the slope between 10% and 40% of the maximum load), ultimate load F_u and displacement δ_u are reported in Table 5.6.

Standard procedures typically define the ultimate conditions in timber connections and assemblages as the condition corresponding to a value of load equal to 80% of the maximum load. After the maximum load, either a decrease of the load associated with a ductile behaviour of the assemblage or a significant drop caused by a brittle failure is observed, and the ultimate condition conventional corresponds to a drop in the load equal to 20%. Such procedure is certainly appropriate for CLT shearwalls with cut-out openings where Scenario 2, as described in the current study, is observed. The load drop related to crack opening is relatively small, and the maximum load corresponds to the ultimate condition related to the failure of first hold-down. Conversely, when Scenario 1 occurred, after a significant load drop due to the CLT panel failure, the shearwalls were capable of increasing the load up to failure in the hold-down. The procedure reported in the testing standards does not seem appropriate for, for example, Wall 01, where the initial drop after the maximum load was greater than 20%, but where a significant amount of the strength was recovered and the load increased to over 90% of the maximum load. As a result, the second drop can be considered for the definition of the ultimate condition. It is noteworthy to mention that, for Wall 09, the drop of the maximum load (equal to 20%) was not followed by any increase of the load. For this reason, differently from Wall 01, it was assumed that the ultimate condition corresponded to the first drop.

***Table 5.5**: Summary of Failure Modes and Load Drops for CLT Shearwall Across Multiple Scenarios*

		Failure Step 1				Failure Step 2				Failure Step 3			
Wall ID	Scenario	Failure Mode	F [kN]	δ $[mm]$	Load drop [%]	Failure mode	F [kN]	δ $[mm]$	Load drop [%]	Failure mode	F [kN]	δ $[mm]$	Load drop [%]
Wall 01	1	P. **Net Shear**	76.1	37.7	28.1	HD-out	75.2	84.6	41	-	-	-	-
Wall 02	2	P.**Net Shear**	54.5	45.9	1.7	HD-inn	61.1	91	41.4		35.2	127	76.7
Wall 03	2	P. **Bending**	41	31.7	9	HD-inn	63.4	78.9	44.3		37.4	98.9	75.9

Wall 04	2	P. **Torsional Shear**	63.3	34.9	11.5	HD-out	71.4	93	45.7		39	145.5	48.2
Wall 05	2	P. **Bending***	61.7	60.5	6.8	HD-out	62	81.7	49.2	-	35.1	88.8	79.8
Wall 06	2	P. **Torsional Shear**	66.7	33	3	HD-out	60.1	81	44.6	-	36	106	77.8
Wall 07	2	P. **Torsional Shear**	47.9	37.8	2.7	HD-inn	60.2	95.3	51	-	31.2	145.8	57.7
Wall 08	1	P. **Net Shear**	80	24.6	20.2	HD-out	98.9	81.9	44.6	-	-	-	-
Wall 09	1	P.**Net Shear**	85.4	24.5	16.2	P.**Torsional Shear**	90.5	48.6	19.3	HD-out	76.1	72	62.3
Wall 10	2	P. **Net Shear**	80.2	64.5	5.6	HD-inn	76.2	67.6	47.6	-	-	-	-
Wall 11	2	P. **Torsional Shear**	58	32.9	2.2	HD-inn	48.5	108.2	61	-	-	-	-
Wall 12	2	P. **Torsional Shear**	46.2	58.4	5.7	P. **Net Shear**	45.3	92.6	22.3	-	29.7	127	6.4

P.: Panel; HD-out: outer hold-down; HD-inn: inner hold-down

* a clear distinction between bending and net-shear failure was not possible

***Table 5.6**: Mechanical parameter obtained from the force-displacement curve*

Test	Label	F_{max} [kN]	$\delta_{F_{max}}$ [mm]	k [kN/mm]	F_u [kN]	δ_u [mm]
Wall 01	D2200-400/600	81.0	37.1	2.30	60.2	85.7
Wall 02	D2200-200/600	61.5	89.6	1.34	49.2	92.6
Wall 03		63.5	78.1	1.40	50.8	80.4
Wall 04	D2400-400/800	73.1	90.1	2.16	58.5	93.3
Wall 05	D2400-200/800	62.9	80.5	1.36	50.3	82.0
Wall 06	D2700-400/1100	66.8	32.9	2.17	53.4	80.3
Wall 07		62.2	94.9	1.98	49.8	96.1
Wall 08	D2700-400/600	101.5	81.7	3.34	81.2	83.8
Wall 09		90.5	48.5	3.87	72.4	74.2
Wall 10	D2700-200/600	80.2	64.4	2.17	64.2	67.6

Wall 11	D2500-200/1100	58.3	31.4	2.33	46.6	108.2
Wall 12	D2700-200/1300	47.0	56.2	2.14	37.6	92.6

5.4. Comparison of results obtained from FEM with experimental test

A detailed comparison between the finite-element predictions presented in Chapter 3 and the laboratory data summarised in Table 5-7 shows that the numerical model reproduces the global response of the walls with mixed success (Figures 5.21 till 5.32). In terms of failure *type*, the FE analysis consistently distinguishes bending-dominated from shear-dominated behaviour; however, it occasionally misclassifies net-shear failures as torsional-shear failures (and vice-versa). This discrepancy is chiefly attributed to the shear- and torsional-strength parameters adopted for the model, which were derived as mean values from independent beam tests and therefore do not capture specimen-to-specimen variability.

When peak panel capacity is examined, performance depends on the opening configuration. For the ten shearwalls containing door openings, the mean ratio of experimental test strength to FE strength is 0.93, indicating very good agreement.

By contrast, the two shearwalls incorporating window openings and a parapet section are markedly over-predicted, with a mean ratio of 0.41. The load–displacement curves for Walls 11 and 12 (Figures 5.31 and 5.32) reveal that the numerical stiffness matches the experimental curve up to the onset of cracking, after which the real wall exhibits an abrupt strength drop that the present linear model cannot simulate.

Agreement is poorer for the hold-down failure force comparison. The average strength obtained from experimental test to FE ratio is 0.38. Because the analysis is linear elastic, the computed anchor load continues to rise until ultimate capacity is reached, whereas the physical anchors experience a sudden post yield drop that the model omits.

In summary, the current FE framework provides reliable stiffness, and strength estimates for walls with door openings and accurately differentiates bending from shear failures. Nevertheless, it requires improved material characterisation or, more realistically, a nonlinear constitutive upgrade before it can predict torsional-shear mechanisms, parapet effects, and the rapid strength accurately capture how the hold-down anchors start to weaken so engineers can use the results in design.

An important source of discrepancy is observed in shearwalls with window openings and parapets. Experimental results consistently showed crack initiation and rapid stiffness reduction in the parapet, whereas the FE model predicted a more ductile progression governed by connections. This observation indicates that while the FE framework is reliable for walls where door lintels dominate the behaviour, its predictive capability for parapet-sensitive configurations remains limited. Addressing this shortcoming requires nonlinear panel formulations or fracture mechanics approaches to model crack initiation and propagation in parapet regions.

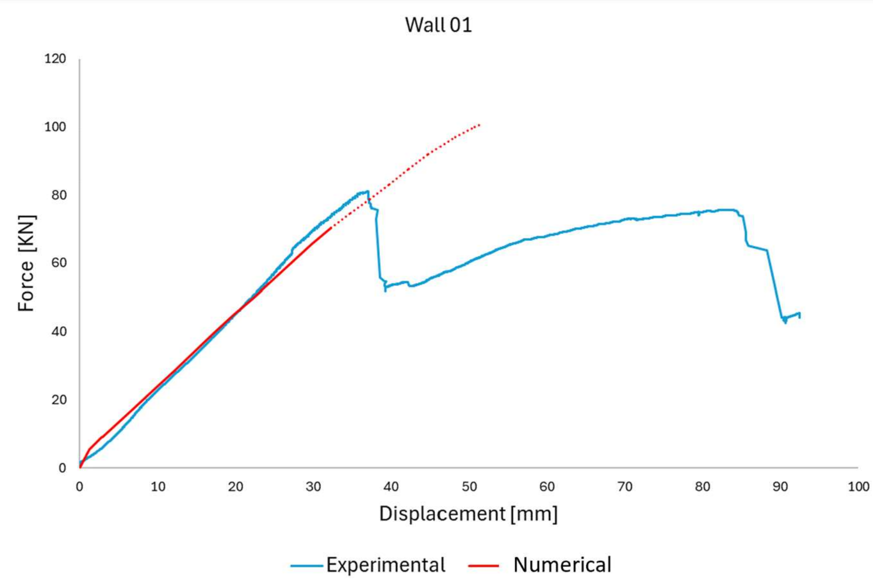

***Figure 5.21**: Push-over curves obtained from experimental test compared with FE model for wall 1*

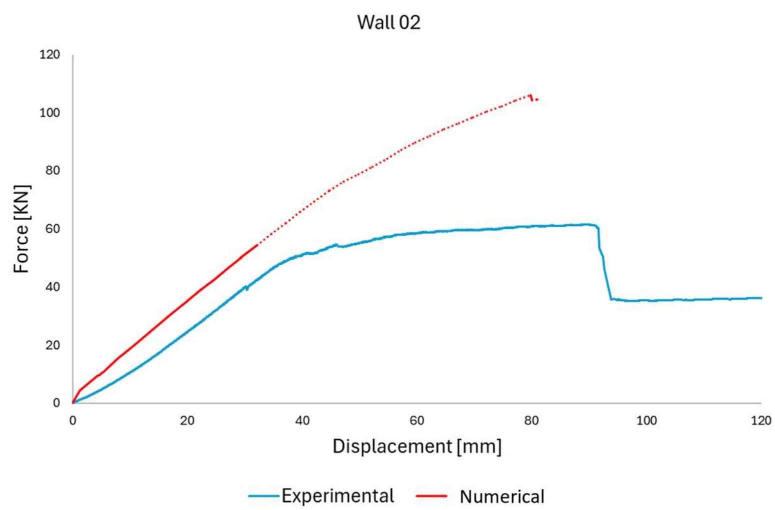

***Figure 5.22**: Push-over curves obtained from experimental test compared with FE model for wall 2*

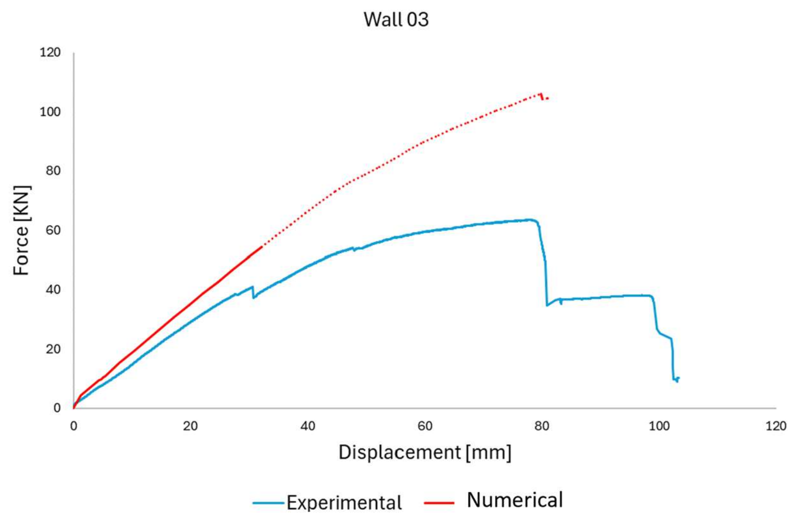

Figure 5.23: *Push-over curves obtained from experimental test compared with FE model for wall 3*

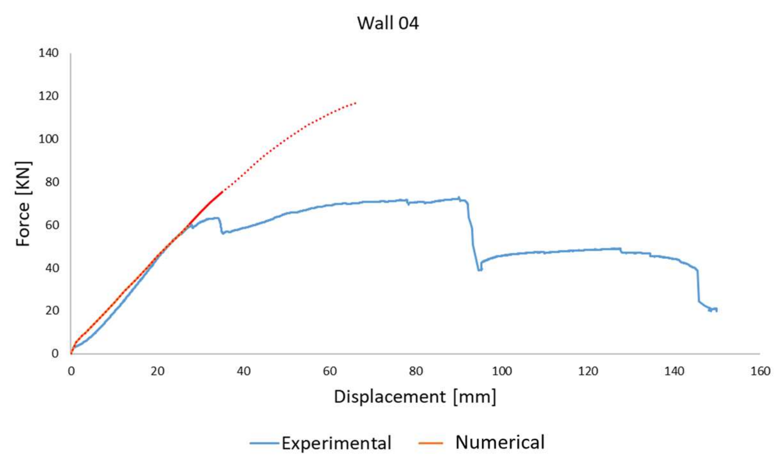

Figure 5.24: *Push-over curves obtained from experimental test compared with FE model for wall 4*

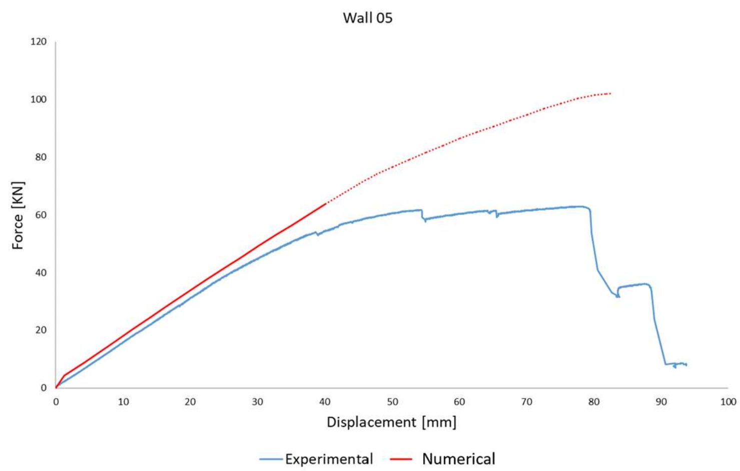

Figure 5.25: *Push-over curves obtained from experimental test compared with FE model for wall 5*

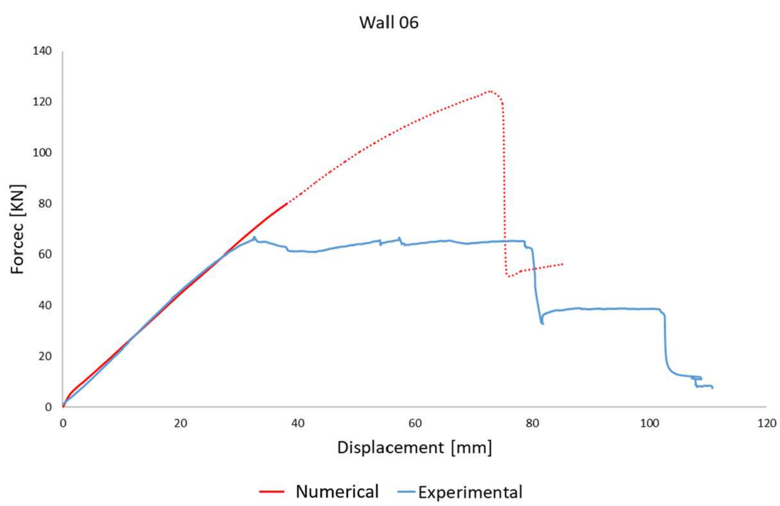

Figure 5.26: *Push-over curves obtained from experimental test compared with FE model for wall 6*

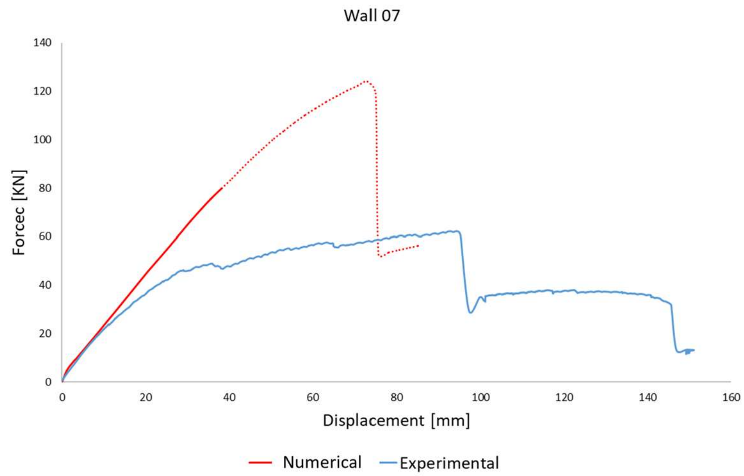

Figure 5.27: *Push-over curves obtained from experimental test compared with FE model for wall 7*

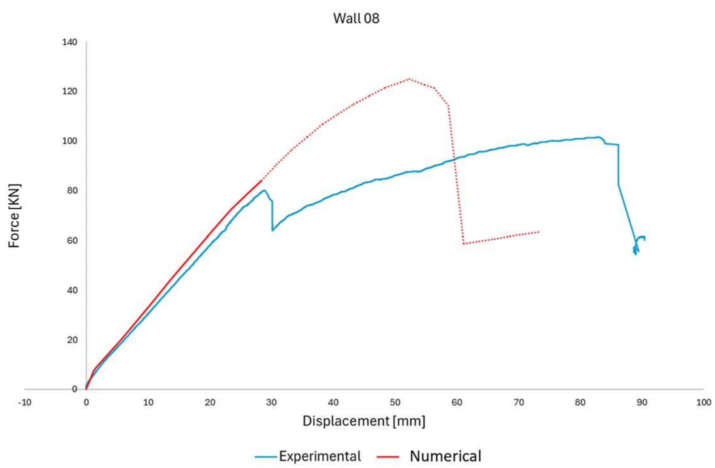

Figure 5.28: *Push-over curves obtained from experimental test compared with FE model for wall 8*

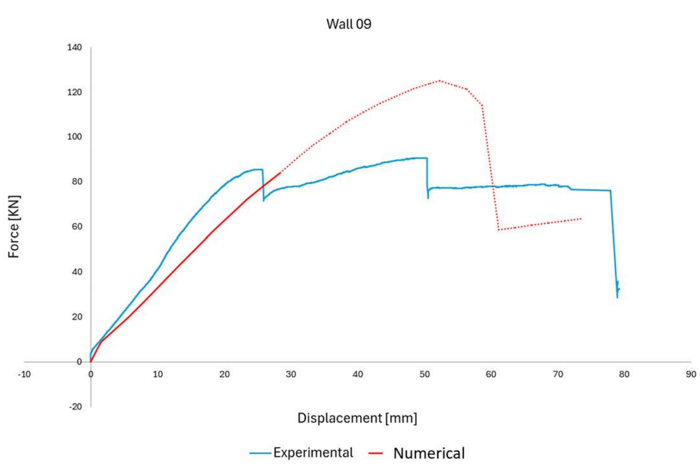

Figure 5.29: *Push-over curves obtained from experimental test compared with FE model for wall 9*

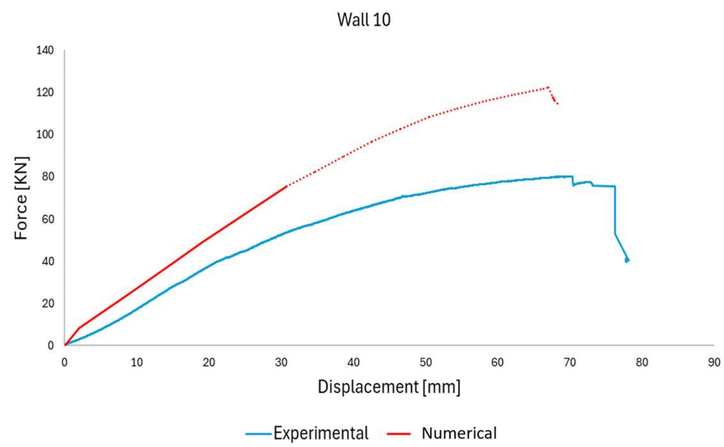

Figure 5.30: *Push-over curves obtained from experimental test compared with FE model for wall 10*

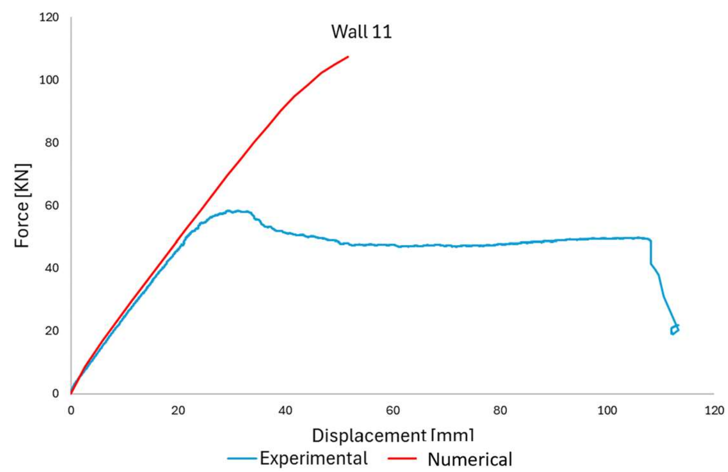

Figure 5.31*: Push-over curves obtained from experimental test compared with FE model for wall 11*

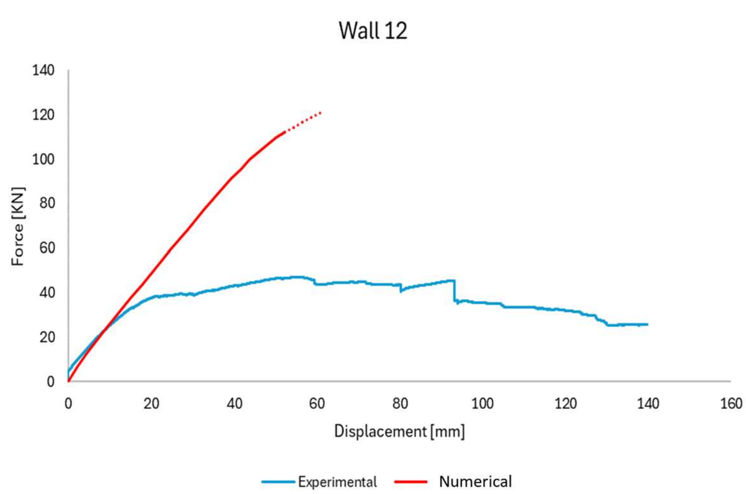

Figure 5.32*: Push-over curves obtained from experimental test compared with FE model for wall 12*

Table 5.7: *Comparison of failure mode and failure force obtained from FEM compared with experimental tests*

Test ID	Opening type	FEM			Experimental test			Divergence	
		Failure mode	Panel failure force [KN]	Hold-down failure force [KN]	Failure mode	Panel failure force [KN]	Hold-down failure force [KN]	Panel failure force	Hold-down failure force
W01	Door	Torsional shear	70.3	100.7	Net Shear	76.1	75.2	1.08	0.75
W02	Door	Torsional shear	50.4	104.6	Net Shear	54.5	61.1	1.08	0.58
W03					Bending	41	63.4	0.81	0.53
W04	Door	Torsional shear	75.1	117	Torsional Shear	63.3	71.4	0.84	0.53
W05	Door	Bending	63.9	102.1	Bending	61.7	62	0.97	0.53
W06	Door	Torsional shear	79.9	119	Torsional Shear	66.7	60.1	0.83	0.51
W07					Torsional Shear	47.9	60.2	0.6	0.51
W08	Door	Torsional shear	84	114.2	Net Shear	80	98.9	0.95	0.87
W09					Net Shear	85.4	76.1	1.02	0.79
W10	Door	Torsional shear	75.3	114	Net Shear	80.2	76.2	1.07	0.67
W11	Window	Hold-down	-	113.2	Torsional Shear	58	48.5	-	0.43
W12	Window	Torsional shear	112.1	120.8	Torsional Shear	46.2	29.7	0.41	0.38

To validate the numerical model developed in this study (chapter 3), the initial in-plane stiffness predicted by the finite-element model was compared with the corresponding values obtained from the laboratory tests on all twelve wall specimens.

The ratio of stiffness obtained from experimental tests to ones from numerical model was calculated for each wall as shown in table 5.8.

The average experimental-to-numerical stiffness ratio is 1.0, confirming that the FE model predicts the walls initial stiffness with perfect accuracy and without any consistent over- or underestimation; this is clearly illustrated in Figures 5.21–5.32, where the FE load–displacement curves almost exactly coincide with the experimental curves throughout the linear range.

Individually, eight specimens deviate by less than ten percent, and ten by less than fifteen percent, demonstrating a consistently high level of predictive accuracy. The only notable discrepancies arise in two door-opening walls W08 and W09 whose measured stiffness exceeds the numerical estimate by approximately sixteen and thirty-four percent, respectively; these larger deviations likely stem from local connection behaviour or material variability that is not fully represented in the current input parameters.

When the results are considered by opening type, the ten door-opening specimens yield an average ratio of 1.01, while the two window-opening specimens yield 0.96, showing that the model reproduces door-wall behaviour almost exactly and overestimates window-wall stiffness only marginally. In summary, these findings confirm that the calibrated FE model provides a reliable and accurate tool for predicting the initial stiffness of CLT shearwalls with both door and window openings, requiring only minor, targeted refinements for a few door-opening specimens.

***Table 5.8**: Comparison of stiffness calculated from FEM compared with experimental tests*

		FEM		Experimental test		Divergence
		Failure mode	Stiffness [KN/mm]	Failure mode	Stiffness [KN/mm]	Ratio
W01	Door	Torsional shear	2.10	Net Shear	2.30	1.1
W02	Door	Torsional shear	1.65	Net Shear	1.34	0.81
W03				Bending	1.4	0.85
W04	Door	Torsional shear	2.10	T. Shear	2.16	1.03
W05	Door	Bending	1.59	Bending	1.36	0.86
W06	Door	Torsional shear	2.08	T. Shear	2.17	1.04
W07				T. Shear	1.98	0.95
W08	Door	Torsional shear	2.88	Net Shear	3.34	1.16
W09				Net Shear	3.87	1.34
W10	Door	Torsional shear	2.39	Net Shear	2.17	0.91
W11	Window	Hold-down	2.33	T. Shear	2.33	1
W12	Window	Torsional shear	2.32	T. Shear	2.14	0.92

Chapter 6: Conclusions

6.1 Purpose and Scope

This chapter consolidates the key findings from three complementary investigations that together underpin the finite-element modelling strategy adopted in this thesis. The numerical FE study of multi-storey CLT shearwalls with openings forms the core of the work; its accuracy is demonstrated through validation against a full-scale experimental campaign on single-storey monolithic CLT shearwalls, while a series of CLT beam tests with vertical outer layers supplied representative mean material properties for the mechanical properties used in the FE model.

6.2 Numerical Analysis of Lintel-Beam and Parapet Effects in Multi-Storey CLT Shearwalls

The current thesis presents the results of an extensive numerical analysis using a validated Finite Element model, with the aim to investigate the influence of the geometrical and mechanical properties of lintel beams and parapets on the stiffness and strength of multi-storey CLT shearwalls with door or window openings. In general, it can be observed that monolithic models, which take into account the interaction between the lintel beam, parapet and the wall segments, resulted in strength and stiffness values that are significantly higher than those obtained in cases where a segmented shearwall was assumed. Despite the fact that this interaction is typically ignored by designers, the analysis clearly shows that when the contributions of these elements are accounted for, it could potentially lead to increased design efficiency. In the vast majority of the investigated cases on shearwalls with window openings, an increase of the peak load of more than 100 % can be observed between monolithic and segmented shearwalls, which was more pronounced when the number of storeys is increased; the increase in peak load reached nearly seven-fold in one of the analysed cases.

The increases in stiffness and peak load values are relatively smaller for shearwalls with door openings, albeit not insignificant. For CLT shearwalls with window openings, changing the height of the lintel beam does not seem to have any significant effect on the failure modes; this is mainly attributed to the role of the parapet, which appears to have a great influence on the failure mechanism even though no structural function is typically associated with it.

For shearwalls with door openings, the lintel height significantly affects the failure mechanism, and a shift in failure mode is observed when the lintel height is changed: at intermediate lintel heights (400mm) failure occurs in the lintel beam; at small lintel heights (200mm) the wall segments behave like two cantilevered walls and failure occurs in the hold-downs; at large lintel heights (800 mm) the shearwalls behave mostly like a single-panel shearwall with no opening and failure occurs in the mechanical anchors. Ratios of peak load from 1.20 to 1.90 and from 1.38 to 2.64 were observed when the lintel height changed from 0.2 m to 0.8 m for two- and six-storey shearwalls respectively, the maximum ratio being 6.44 for a six-storey wall with a lintel width of 0.6 m.

6.3 Full-Scale Experimental Campaign on Monolithic CLT Shearwalls with Cut-Out Openings

The results of an experimental campaign conducted on twelve full-scale monolithic CLT shearwalls with cut-out openings are presented in chapter 5. Differently from previous experimental studies available in the literature, where a very limited number of shearwall specimens involved failure in the CLT panel, all shearwalls tested in this study exhibited crack initiation in the lintel or parapet as an initial failure while the ultimate failure occurred in the hold-down.

Two different scenarios for crack propagation were presented with significant impact on the behaviour of the walls, and multiple and complicated failure mechanisms were observed, making the identification of net shear failure or the distinction between net shear and bending failure challenging.

The numerical prediction was reasonable in terms of load-displacement curves and successfully predicted the location of cracks in the CLT panels prior to hold-down failure. From a quantitative perspective, the discrepancies between the numerical models and experimental tests in terms of maximum load and stiffness were reasonable, while those in terms of displacement at maximum load were significantly less accurate; the influence of variability in material mechanical properties was found to be crucial to the numerical prediction.

6.4 CLT Beams with Vertical Outer Layers

Chapter 4 of this thesis aimed to establish a better understanding of the mechanical behaviour of CLT beams with vertical outer layers, providing valuable information regarding the failure modes and mechanical parameters that can be adopted, particularly in the verification of lintel beams in CLT shearwalls with cut openings.

A total of thirty-six beams consisting of two different lay-ups were tested. An analytical model originally developed for CLT beams with horizontal outer layers was evaluated for adoption to beams with vertical outer layers in order to propose a methodology to determine their resistance and stiffness. Beams with vertical outer laminations designed to fail predominantly in bending consistently achieved that failure mechanism. Torsional and net shear failures were also observed in some beams and were characterised, respectively, by rotation and separation of the outer laminations from the inner layers and by parallel sliding between the outer laminations.

For beams designed to fail in bending, a significant difference was observed between three-ply and five-ply specimens, confirming an inverse correlation between bending strength and lamination thickness that is likely related to the probability of critical defects in larger-dimension lumber. Existing calculation models for bending strength, gross shear strength and net shear strength of CLT beams with horizontal outer laminations can be adopted without adjustment for beams with vertical outer laminations; however, analytical models for torsional strength required adaptation, and the proposed models were successfully verified against data from the current study and the literature.

6.5 Future works

Building on the comparisons presented in Chapter 5 for single-storey monolithic CLT shearwalls with door and window openings, the numerical model has proved highly effective at predicting failure mode, peak load, and initial stiffness.

In the linear range the finite-element response overlaps the test curves almost perfectly; however, once a crack forms and the load begins to drop, the model cannot track the sudden loss of stiffness observed in the experiments. This limitation arises because, although the fastener and hold-down connections are already represented with non-linear spring elements (see Chapter 3), the CLT panels themselves are still treated as linear elastic. Incorporating material non-linearity into the panel formulation is therefore a key next step.

The present FE framework has also been validated only against single-storey walls containing a single opening. Extending the validation to multi-storey configurations and to walls with multi-openings is essential if the model is to be used confidently in full-building design. Additional experimental data at those scales would support calibrating not only the panel non-linearity just noted but also potential interaction effects between storeys and between closely spaced openings.

This extra work will finish the model, letting it accurately predict how any real-world CLT shearwall behaves overall and where damage will start and spread.Collectively, these recommendations aim to inform more robust and reliable design approaches for CLT shearwalls with openings, bridging the gap between current research findings and practical engineering guidelines.

References

Aljuhmani, A. G., Alwashali, H., Ogasawara, A., Atsuzawa, E., Maeda, M., & Seki, M. (2022). *Experimental investigation on the effect of openings on the in-plane shear strength and stiffness of cross-laminated timber panels*. Engineering Structures, 254, 113786. https://doi.org/10.1016/j.engstruct.2021.113786

Andreolli M, Tomasi R (2012). Experimental Investigation on In-Plane Behaviour of Cross-Laminated Timber Elements. International Council for Research and Innovation in Building and Construction. CIB-W18/45-12-4

ANSI/APA PRG 320: Standard for Performance-Rated Cross-Laminated Timber (2019), APA – The Engineered Wood Association

ASTM (2018) E2126-11 - Standard Test Methods for Cyclic (Reversed) Load Test for Shear Resistance of Vertical Elements of the Lateral Force Resisting Systems for Buildings.

Awad V, Giresini L, Koshihara M, Puppio M L, Sassu M (2017) Experimental analysis and numerical models of CLT shear walls under cyclic loading, Intech, March 2017, 10.5772/65024

Bogensperger T, Moosbrugger T, Silly G (2010) Verification of CLT-Plates under loads in plane. WCTE.

Brandner R, Dietsch P, Droscher J, Schulte-Wrede M, Kreuzinger H, Sieder M (2017). Cross laminated timber (CLT) diaphragms under shear: Test configuration, properties and design. Constr Build Mater 2017;147: 312–27.

Casagrande D, Polastri A, Sartori T, Loss C, Chiodega M (2016). Experimental campaign for the mechanical characterization of connection systems in the seismic design of timber buildings. Word conference on timber engineering (WCTE 2016).

Casagrande D, Doudal G, Polastri A (2019) A proposal for the capacity-design at wall- and building-level in light-frame and cross-laminated timber buildings, (2019) Bulletin of Earthquake Engineering, 17 (6), pp. 3139-3167. doi: 10.1007/s10518-019-00578-4.

Casagrande D, Fanti R, Doudak G, Polastrci A (2021a) Experimental and numerical study on the mechanical behaviour of CLT shearwalls with openings, Construction and Building Materials,Volume 298, 6 September 2021, 123858

Casagrande D, Doudak G, Vettori M, Fanti R (2021b) Proposal for an equivalent frame model for the analysis of multi-storey monolithic CLT shearwalls, Engineering Structures, 2021, 245, 112894.

Casagrande, D., Fanti, R., Greco, M., Gavric, I., Polastri, A. (2021c) On the distribution of internal forces in single-storey CLT symmetric shear-walls with openings. Structures, 33, pp. 4718-4742. doi: 10.1016/j.istruc.2021.06.084

Ceccotti A, Lauriola M, Pinna M, Sandhaas C. (2006) SOFIE project – cyclic tests on crosslaminated wooden panels. : Proc World Conf Timber Eng (WCTE), Portland, OR, USA 2006;vol. 1:805–12.

Ceccotti A, Lauriola M P, Pinna M, Sandhaas C (2011) SOFIE project-cyclic tests on cross-laminated wooden panels, the World Conference on Timber Engineering 2006, WCTE 2006, August 6, 2006 - August 10, 2006

Ceccotti A, Sandhaas C, Okabe M, Yasumura M, Minowa C, Kawai N (2013). SOFIE project – 3D shaking table test on a seven-storey full-scale cross-laminated timber building. Earthquake Engineering & Structural Dynamics 42(13) 2013. https://doi.org/10.1002/eqe.2309.

CEN (2005) EN 12512:2001/A1:2005, Timber structures – Test methods –cyclic testing of joints made with mechanical fasteners. Brussels, Belgium: CEN.
CEN (2011) Timber Structures – Test Methods – Racking Strength and Stiffness of Timber Frame Wall Panels, EN 594. . European Committee for Standardization: Brussels, Belgium.

CSA O86-14 (2017) Engineering design in wood. CSA Group, Mississauga

CSI (2017) SAP2000 Integrated Software for Structural Analysis and Design. Berkeley,California: Computers and Structures Inc.

Daneshvar H, Niederwestberg J, Dickof C, Hei Chui Y (2021). Structural behaviour of deep CLT lintels subjected to concentric and eccentric loading. Journal of building Engineering 43 103101. https://doi.org/10.1016/j.jobe.2021.103101.

Danielson H, Serrano E (2018). Cross laminated timber at in-plane beam loading- Predction of shear stress in crossing areas. Engineering Structures 171 (2018) 921-927. https://doi.org/10.1016/j.engstruct.2018.03.018.

Danielsson, H., Pazlar, T., Serrano, E., Azinović, B. (2024) Experimental investigation of the shear force capacity of prismatic cross laminated timber beams (2024) Engineering Structures, 308, art. no. 117889. doi: 10.1016/j.engstruct.2024.117889

D'Arenzo G, Casagrande D, Polastri A, Seim W (2021). CLT Shear Walls Anchored with Shear-Tension Angle Brackets: Experimental Tests and Finite-Element Modeling, Journal of Structural Engineering. Volume 147, Issue 7. July 2021, 10.1061/(ASCE)ST.1943-541X.0003008.

Dujic B, Klobcar S, Zarnic R. (2008) Shear capacity of cross-laminated wooden walls. 10th World Conf Timber Eng 2008 2008;3:1641–8. ISBN: 978-161567088-8.

Dujic B, Klobcar S, Zarnic R (2015) Influence of openings on shear capacity of wooden walls, NZ Timber Design Journal, Volume 16 Issue 1.

EAD 130005-00-0304, Solid wood slab element to be used as a structural element in buildings, EOTA, 2015.

EN 408 (2012). Timber structures Structural timber and glued laminated timber, Determination of some physical and mechanical properties. BS EN 408:2010+A1:2012

EN 12512:2001/A1:2005, Timber structures– Test methods–cyclic testing of joints made with mechanical fasteners. Brussels, Belgium: CEN.

European Technical Assessment ETA-06/0106 (2021) Three-dimensional nailing plate (timber-to-timber/timber-to concrete angle bracket), Simpson Strong-Tie Int. Ltd, ETA-Danmark A/SGöteborg

European Technical Assessment ETA-11/0086 (2015) Three-dimensional nailing plate (Angle brackets and hold-downs for timber-to-timber or timber-to-concrete or steel connections, Rotho Blaas WHT hold downs and angle brackets, ETA-Danmark A/SGöteborg

European Technical Assessment ETA-11/0496 (2014), "RothoBlaas TITAN Angle Brackets," Denmark, 2014.

European Technical Assessment ETA 12/0362 (2020) European Technical Approval: Cross Laminated Timber (CLT) – Solid wood slab elements to be used as structural elements in buildings, Essepi XXL. Eurofins Expert Services Oy, Finland

Flaig M, Blass H J (2013). Shear Strength and Shear Stiffness of CLT-Beams Loaded in Plane. International Council for Research and Innovation in Building and Construction. CIB-W18/46-12-3

Flaig M, Blass H J (2014). Bending Strength of Cross Laminated Timber Beams Loaded in Plane. World Conference on Timber Engineering, Quebec City, Canada.

Flatscher G, Bratulic K, Schickhofer G (2015) Experimental tests on cross-laminated timber joints and walls. Proceedings of the Institution of Civil Engineers – Structures and Buildings 168(11): 868–877, https://doi.org/10.1680/stbu.13.00085.

Gagnon S, Mohammad M, Popovski M (2014). Evaluation of In-Plane Shear Strength of CLT. World Conference on Timber Engineering, Quebec City, Canada.

Gavric I, Fragiacomo M, Ceccotti A (2013) CAPACITY SEISMIC DESIGN OF X-LAM WALL SYSTEMS BASED ON CONNECTION MECHANICAL PROPERTIES, International council for research and innovation in building and construction, Working commission W18-Timber structures. 46th conference, CIB-W18/46-15-2

Gavric I, Fragiacomo M, Ceccotti A (2015a) Cyclic behaviour of typical metal connectors for cross-laminated (CLT) structures. Materials and Structures, Volume 48, 1841-1857, March 2014, 10.1617/s11527-014-0278-7

Gavric I, Fragiacomo M, Ceccotti A (2015b) Cyclic behavior of CLT wall systems: experimental tests and analytical prediction models. American Society of civil engineers. Journal of Structural Engineering, Volume 141 Issue 11, November 2015, 10.1061/(ASCE)ST.1943-541X.0001246.

Hiroshi H, Namba T, Kitamori A, Mori T (2023). Experimental Behavior of L-Shaped and T-Shaped Cross-Laminated Timber to Evaluate Shear Walls with Openings. Journal of Structural Engineering 149(5)-2023. http://dx.doi.org/10.1061/JSENDH.STENG-11474.

Isoda, H., Namba, T., Kitamori, A., Mori, T., Miyake, T., Nakagawa, T., & Tesfamariam, S. (2023). *Experimental behavior of L-shaped and T-shaped cross-laminated timber to evaluate shear walls with openings*. Journal of Structural Engineering, 149(5), 04023035. https://doi.org/10.1061/JSENDH.STENG-11474

Izzi M, Casagrande D, Bezzi S, Pasca D P (2018a) Seismic behaviour of cross-laminated timber structures: a state-of-the-art review, Eng. Struct. 170 (2018) 42–52.

Izzi M, Polastri A, Fragiacomo M (2018b) Investigating the hysteretic behavior of cross-laminated timber wall systems due to connections. Journal of Structural Engineering, Volume 144 Issue 5, May 2018, 10.1061/(ASCE)ST.1943-541X.0002022.

Jeleč M, Danielson H, Rajčic V, Serrano E (2019). Experimental and numerical investigations of cross-laminated timber elements at in-plane beam loading conditions. Construction and Building Materials 206 (2019)329-346. https://doi.org/10.1016/j.conbuildmat.2019.02.068

Jöbstl R A, Bogensperger T, Schickhofer G (2008). In-plane shear strength of cross laminated timber. CIBW18/41-12-3, St. Andrews, Canada

Khajehpour M, Casagrande D, Doudak G (2022). The role of lintels and parapets on the mechanical performance of multi-storey cross laminated timber shearwalls with openings. Engineering Structures, 255 (2022) 113912. https://doi.org/10.1016/j.engstruct.2022.113912

Khajehpour M, Casagrande D, Fanti R, Doudak D. (2025) Experimental investigation of Cross Laminated Timber beams with vertical outer layer. Submitted to Engineering Structures.

Karacabeyli, E, Gagnon, S. (2019) Canadian CLT Handbook 2019 Edition

Li M, Lam F (2015) Lateral behaviour of cross laminated timber shear walls under reversed cyclic loads, Tenth Pacific Conference on Earthquake Engineering, Sydney (Australia)

Li, Z., Wang, X., & He, M. (2022). Experimental and Analytical Investigations into Lateral Performance of Cross-Laminated Timber (CLT) Shear Walls with Different Construction Methods. Journal of Earthquake Engineering, 26(7), 3724–3746. https://doi.org/10.1080/13632469.2020.1815609.

Lium J, Lam F (2018) Experimental test of coupling effect on CLT angle bracket connections, Engineering Structures, Volume 178, January 2019, P586-602.

Masroor, M., Doudak, G., Casagrande, D.Experimental investigation of dissipative connections in cross-laminated timber shearwalls (2024) Construction and Building Materials, 413, art. no. 134828. doi: 10.1016/j.conbuildmat.2023.134828

Mestar M, Doudak G, Caola M, Casagrande D (2020) Equivalent-Frame Model for Elastic Behaviour of Cross-Laminated Timber Walls with Opening. Constuction and Building Materials, Volume 298, September 2021, 123858

Mestar M, Doudak G, Polastri A, Casagrande D (2021). Investigate the kinematic modes of CLT shear-walls with openings. Engineering Structures, Volume 228, February 2021, 111475.

Moosbrugger T, Guggenberger W, Bogensperger T (2006) Cross-laminated timber wall segments under homogeneous shear - With and without openings. 9th world conference on timber engineering 2006, WCTE 2006, August 6, 2006 - August 10, 2006. Portland, OR, United states: Oregon State University Conference Services; 2006. p. 219–28

Nolet V, Casagrande D, Doudak G (2019) Multipanel CLT shearwalls: an analytical methodology to predict the elastic-plastic behaviour, Engineering Structures, 179, pp. 640-654. doi: 10.1016/j.engstruct.2018.11.017

NS-GT6 (2020) Nordic x-lam technical guide, https://www.nordic.ca/en/documentation/technical-documents/ns-gt6-ca.

Pai S G, Lam F, Haukaas T (2016) Force Transfer Around Openings in Cross-Laminated Timber Shear Walls. Journal of Structural Engineering, Volume 143, Issue 4, April 2017, 10.1061/(ASCE)ST.1943-541X.0001674.

Pei S, Van de Lindt, J-WG, Popovski M, Berman JW, Dolan JD, Ricles J, Sause R, Blomgren H, Rammer D R (2016) Cross Laminated Timber for seismic regions: progress and challenges for research and implementation. Journal of Structural Engineering, Volume 142 Issue 4, April 2016, 10.1061/(ASCE)ST 1943-541X.0001192.

Popovski M, Schneider J, Schweinsteiger M. (2010) Lateral load resistance of cross-laminated wood panels. In: World Conference on Timber Engineering (WCTE), Riva delGarda, Italy; 2010.
Popovski, M., Gavric, I. (2016) Performance of a 2-Story CLT House Subjected to Lateral Loads (2016) Journal of Structural Engineering (United States), 142 (4), doi: 10.1061/(ASCE)ST.1943-541X.0001315

Ruggeri, E. M., D’Arenzo, G., & Fossetti, M. (2023). *Investigating the effect of the structural interactions due to floors and lintels on the lateral response of multi-storey cross-laminated timber shear walls*. Engineering Structures, 290, 116327.

https://doi.org/10.1016/j.engstruct.2023.116327

Sciomenta, M., Fanti, R., Doudak, G., Polastri, A., & Casagrande, D. (2024). *Predicting the non-linear behaviour of cross-laminated timber shearwalls with cut-out openings*. Structures, 68, 107138. https://doi.org/10.1016/j.istruc.2024.107138

Shahnewaz Md, Shahria Alam M, Tannert T, Popovski M (2017a) Capacity-Based Design for Cross-Laminated Timber Buildings. Structures Congress 2017(ASCE), P.400-410. ISBN 0784480427

Shahnewaz M, Tannert T, Alam M S, Popovski M (2017b) In-plane stiffness of cross-laminated timber panels with openings (2017) Structural Engineering International, 27 (2), pp. 217-223. doi: 10.2749/101686617X14881932436131

Shen, Y L, Schneider J, Tesfamariam S, Stiemer S F, Mu Z G (2013) Hysteresis behaviour of bracket connection in cross-laminated-timber shear walls. Construction and Building materials, Volume 48, P.980-991, November 2013, 2013.07.050.

Sikora K s, Mcpolin D o, Harte A m (2016). Effects of the thickness of cross-laminated timber (CLT) panels made from Irish Sitka spruce on mechanical performance in bending and shear. Construction and Building Materials 116(2):141-150. https://doi.org/10.1016/j.conbuildmat.2016.04.145

Tannert T, Follesa M, Fragiacomo M, Gonzalez P, Isoda H, Moroder D, Xiong H (2018). Seismic Design of Cross-Laminated Timber Buildings. Wood and Gober Science, Volume 50, 2018.

Tomasi R, Smith I (2015) Experimental characterization of monotonic and cyclic loading responses of CLT Panel-To-Foundation Angle Bracket Connections (2015) Journal of Materials in Civil Engineering, 27 (6), art. no. 04014189. doi: 10.1061/(ASCE)MT.1943-5533.0001144

Yamagata K, Inoue R, Mori T, Nakashima S, Araki Y, Nakagawa T, Isoda H (2023). Effects of shear performance by shear span and stress direction in cross laminated timber. THE 6TH INTERNATIONAL CONFERENCE ON SCIENCE AND TECHNOLOGY (ICST21), Mataram, Indonesia. Volume 2609, Issue 1. https://doi.org/10.1063/5.0124014

Yasumura M, Kobayashi K, Okabe M, Miyake T, Matsumoto K (2015) Full-scale tests and numerical analysis of low-rise CLT structures under lateral loading. Journal of Structural

Engineering (New York,N.Y.), Volume 142 (4), April 2016, 10.1061/(ASCE)ST.1943-541X.0001348.

Yinlan S, Schneider J, Stiemer S F, Xueyong R (2019) Failure Modes and Mechanical Properties of Bracket Anchor Connections for Cross-Laminated-Timber. MATEC Web of Conferences 275,01011, ACEM2018 and SBMSI.

Zarnani P, Quenneville P, (2015) New design approach for controlling brittle failure modes of small-dowel-type connections in Cross-laminated Timber (CLT). Construction and Building Materials, Volume 100, December 2015, Pages 172-182, 2015.09.049.

Zhang X. et al. (2021a) “Seismic Performance of Three-Story Cross-Laminated Timber Structures in Japan,” *Journal of Structural Engineering*, ASCE, 147(2): 04020319.

Zhang, D., Shen, L., Zhu, X., Zhang, S., and Gong, M. (2021b). "The influence of the opening size on the shear performance of the cross-laminated timber (CLT) walls," BioResources 16(4), 7071-7085.